Verification of an independent monitor unit calculation program for IMRT quality assurance

Michael Peter Currie
University of Wollongong

VERIFICATION OF AN INDEPENDENT MONITOR UNIT CALCULATION PROGRAM FOR IMRT QUALITY ASSURANCE

A thesis submitted in fulfilment of the requirements for the award of the degree

Master of Science - Research

from

UNIVERSITY OF WOLLONGONG

by

Michael Peter Currie, B Med Rad Phys (Honours)

Department of Engineering Physics

2007

Certification

I, Michael Peter Currie, declare that this thesis, submitted in partial fulfilment of the requirements for the award of Master of Science - Research, in the Department of Engineering Physics, University of Wollongong, is wholly my own work unless otherwise referenced or acknowledged. The document has not been submitted for qualifications at any other academic institution.

Michael Peter Currie
16/02/07

Acknowledgements

I would like to thank my supervisor, Professor Peter Metcalfe, as well as Dr Matthew Williams for their support and assistance in this project, as well as many useful discussions and helpful advice. I would also like to thank Professor Anatoly Rosenfeld for providing general assistance during the project and my previous years at UOW, the physics staff at ICCC for their assistance, and my family and my wife, Mindy, for their support and encouragement.

Contents

List of Figures

List of Tables

Abbreviations

ρ – density

AAPM – American Association of Physicists in Medicine

BCF – block correction factor

BF – boundary factor

CF – calibration factor

CT – computed tomography

D_{max} – maximum dose, typically on central axis

d_{max} – depth of maximum dose on central axis

DVH – dose volume histogram

FTP – file transfer protocol

Gy – Gray

IAEA – International Atomic Energy Agency

ICCC – Illawarra Cancer Care Centre

ICF – inhomogeneity correction factor

IMRT – intensity modulated radiation therapy

ISF – inverse square law factor

Linac – linear accelerator

MCI – modified Clarkson integral

MF – Mayneord factor

MLC – multileaf collimator

MU – monitor units

NSW – New South Wales

OAD – off axis distance

OAR – off axis ratio

PDD – percentage depth dose

POCR – primary off centre ratio

QA – quality assurance

RFO – radiation field offset

SAD – source to axis distance

S_c – collimator scatter factor

SCD – source to calibration point distance

SMR – scatter maximum ratio

S_p – phantom scatter factor

SSD – source to surface distance

SSDF – SSD factor

TERMA – total energy release per unit mass

TMR – tissue maximum ratio

TPR – tissue phantom ratio

TPS – treatment planning system

Abstract

Independent monitor unit (MU) calculations are a vital part of radiotherapy treatment planning quality assurance. In the case of complex treatment planning methods, such as intensity modulated radiotherapy (IMRT), traditional independent monitor unit calculations using tables of beam data and manual calculations are inadequate. Recently, computer programs have been developed that can perform independent monitor unit calculations for IMRT treatment plans using scatter summation methods. One such program is RadCalc, produced by Lifeline Software Inc. The purpose of this project was to test RadCalc, and determine whether it is suitable for routine use in IMRT treatment planning quality assurance.

Once the software was installed, beam data measured on the treatment linear accelerator (linac) was imported into RadCalc, to be used in MU calculations. RadCalc was tested for data integrity to ensure that the correct data was accessed for its calculations. The interface between RadCalc and the treatment planning system, Pinnacle^3, was set up so that treatment plan data could be imported directly from Pinnacle^3 into RadCalc. Test plans were imported into RadCalc to ensure the Pinnacle^3-RadCalc interface was working correctly.

Test plans were created with open, blocked, segmented and IMRT fields, and delivered to a phantom on the linac to test RadCalc's block correction algorithm. Doses were measured using a thimble ionisation chamber, and compared to the doses calculated by RadCalc and Pinnacle^3. The agreement between RadCalc and measured doses for most situations was comparable to the agreement between Pinnacle^3 and measured doses. However, a systematic difference between RadCalc and measured dose was shown to occur for asymmetric fields. In addition to this, an increase in the level of blocking of the calculation point for segmented and IMRT fields appeared to increase the difference between RadCalc and measured dose.

Thirty-two patient IMRT plans at the Illawarra Cancer Care Centre (ICCC) were verified by reproducing the plan using a phantom CT dataset, and then delivering the fields to the phantom and measuring the delivered dose. This data was compared to the doses calculated by RadCalc and Pinnacle^3. The doses calculated by RadCalc and

Pinnacle^3 for the plans created on patient CT datasets were also compared. In analysing the data, a systematic difference between RadCalc and measured dose was detected. Improved agreement was achieved by adjusting the MLC transmission parameter in RadCalc. The average percentage difference per field for the phantom plans between RadCalc and measured dose was 0.1% with a standard deviation 5.3%, while the average percentage difference between Pinnacle^3 and measured dose was -0.2% with a standard deviation of 4.2%. The average percentage difference for total plan dose for the phantom plans between RadCalc and measured dose was 0.0% with a standard deviation 1.7%, while the average percentage difference between Pinnacle^3 and measured dose was -0.3% with a standard deviation of 1.1%. For the patient plans, the average percentage difference per field between RadCalc and Pinnacle^3 was 0.8% with a standard deviation of 5.6%, while the average percentage difference per plan was 1.1% with a standard deviation of 1.1%.

The final recommendation is that RadCalc is accurate enough for routine IMRT treatment planning quality assurance. A physical measurement should accompany the RadCalc check to verify the transfer of data to the record and verify system and the dose delivery process.

Chapter 1: Introduction

In New South Wales (NSW) in 2004, 34,092 people were diagnosed with cancer and 12,686 died of the disease[1]. According to the Australian Institute of Health and Welfare, "the current risk of a diagnosis of cancer in Australia by age 75 years is 1 in 3 for males and 1 in 4 for females"[2]. The Cancer Institute of NSW states that "around 63% of cancer patients in NSW are alive 5 years after the diagnosis with many cured of their disease"[3]. Radiotherapy has the ability to provide local control by destroying the primary tumour and surrounding microscopic disease. Cancer cells are killed due to DNA damage sustained directly or indirectly from the ionising radiation. The Cancer Institute of NSW estimates that 50 to 52% of new cancer patients require radiotherapy[4].

The goal of curative radiotherapy is to deliver a curative radiation dose to the target volume, while sparing normal tissue. Since the amount of dose delivered to the target is often limited by the tolerance dose of surrounding normal tissues, and small changes in dose to the target can have a large impact on the clinical outcome, it is vitally important that radiotherapy be planned and treated accurately. Treatment plan reviews are an essential part of treatment planning quality assurance. Both the American Association of Physicists in Medicine (AAPM)[5] and the International Atomic Energy Agency (IAEA)[6] recommend that all graphical treatment plans be reviewed by a radiation oncology physicist, preferably before treatment, or before 10% of the total dose has been delivered. In addition to checking treatment parameters, patient set-up, the quality of the plan and the presence of all required signatures, an independent dose calculation for one point in the plan is performed. According to AAPM and IAEA, if the calculation differs by more than ±5%, the cause of the difference should be resolved before treatment is to commence or continue[5,6].

Originally, the treatment Monitor Units (MUs), which determine the amount of dose delivered by the treatment machine, were calculated manually. These calculations used depth dose curves, beam profiles, output factors, and other correction factors, either from published tables, or from data measured directly on the treatment machine being used. Because the calculations were relatively simple, MU checks were simply a

secondary check of the original calculation, to ensure the correct factors had been used, and that the calculation was performed correctly.

As computer technology has advanced and become increasingly available and affordable, the task of MU calculations has been gradually taken over by Treatment Planning Systems (TPSs). These systems are capable of performing more sophisticated calculations than is practical with manual methods. A modern Treatment Planning System is a computer system and software package designed to use a virtual linear accelerator to create a plan on a virtual patient. This virtual patient is typically a CT dataset of the patient provided by a CT scanner or a simulator. The virtual linear accelerator is created by entering required physical parameters of the machine into the TPS, and either using measured beam data (depth doses, output factors, beam profiles etc) directly, or a beam model to compute doses closely matching those delivered by the treatment machine. The plan created on the TPS determines the beam angles, field sizes, blocking, wedges, beam weightings, MUs and other treatment parameters that will ultimately be used to treat the patient. A 3D dose grid is defined which determines the volume and resolution at which the dose is calculated. The dose deposited at every voxel in the dose grid is calculated for each beam. The dose distributions are usually visualised in 2D (axial, coronal and sagittal planes) using isodose curves. Dose Volume Histograms (DVHs) are a commonly used tool for 3D dose volume analysis, although other 3D dose visualisation tools are available. The dose calculation takes into account complicated effects due to factors such as tissue inhomogeneities, patient contours and blocked fields.

Despite the fact that modern TPS calculations are more sophisticated than manual monitor unit calculations, software faults and improper use can still result in radiation accidents occurring[7]. Such incidents have highlighted the importance of performing an independent MU check. For each beam, the MUs required to deliver the planned dose to a single point are calculated, and compared to the dose given by the TPS. The purpose of this check is to ensure that the TPS is using the correct data and that the TPS has performed the dose and MU calculation properly. Independent MU calculations were historically performed with a pocket calculator, usually termed a “manual calculation check”. Spreadsheets or specially designed MU calculation software are now more commonly employed. These use measured beam data to calculate dose or MUs. With

the introduction of more complex treatment methods such as Intensity Modulated Radiotherapy (IMRT), using manual verification calculations is not feasible[8]. Instead, the accuracy of such treatments is often verified by performing ion chamber measurements in a phantom, which can be time consuming.

New monitor unit calculation software packages such as RadCalc produced by Lifeline Software Inc, claim to be capable of accurately calculating monitor units for IMRT plans. The aim of this research is to determine the accuracy of RadCalc, to determine the strengths and weaknesses of the program, and to determine whether it can be used to perform IMRT plan quality assurance.

Chapter 2: Literature Review

2.1 Manual MU Calculations

Monitor units can be calculated manually using one of two commonly used methods: the fixed SSD method, or the isocentric Method. The formula for the fixed SSD method, based on the method described by Khan[9] is given in Equation (1):

$$\mathrm{MU} = \frac{\mathrm{Dose} \times 100}{\mathrm{CF} \times \mathrm{PDD} \times S_c \times S_p \times \mathrm{OAR} \times \mathrm{ICF} \times \mathrm{BCF} \times \mathrm{SSDF} \times \mathrm{MF}} \quad (1)$$

The formula for the isocentric method is given in Equation (2):

$$\mathrm{MU} = \frac{\mathrm{Dose} \times 100}{\mathrm{CF} \times \mathrm{TPR} \times S_c \times S_p \times \mathrm{OAR} \times \mathrm{ICF} \times \mathrm{BCF} \times \mathrm{ISF}} \quad (2)$$

Where Dose is energy absorbed per unit mass (typically given in units of cGy), CF is the Calibration Factor [dose (in cGy) per monitor unit in reference conditions (reference depth, field size and SSD)], PDD is the Percentage Depth Dose, TPR is the Tissue Phantom Ratio, S_c is the Collimator Scatter Factor, S_p is the Phantom Scatter Factor, OAR is the Off Axis Ratio, ICF is the Inhomogeneity Correction Factor, BCF is the Block Correction Factor, SSDF is the SSD factor, MF is the Mayneord Factor, and ISF is the Inverse Square Law Factor. The factor of 100 is introduced where PDDs or TPRs are given as percentages normalised to 100%.

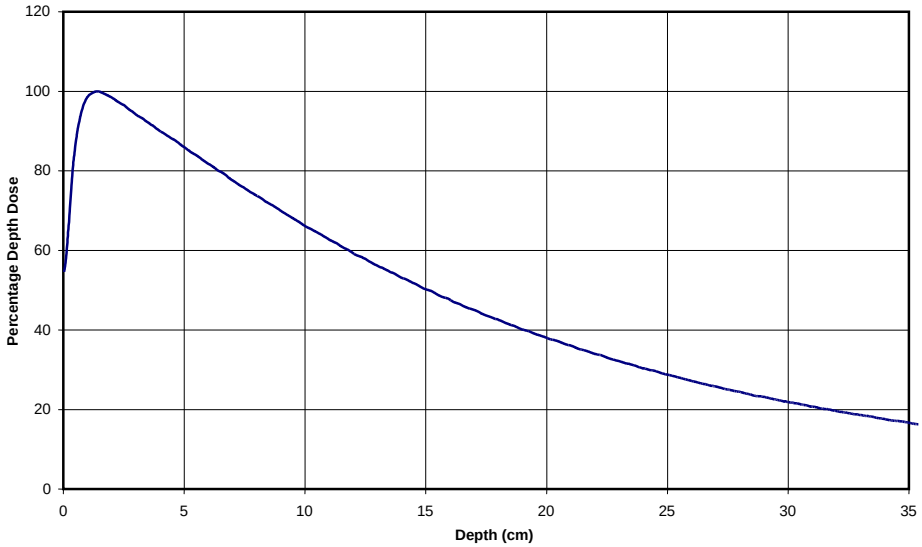

Figure 2-1. An example of a percentage depth dose curve. This curve was measured using a 6MV, 10 x 10cm open field, at 100cm SSD, on a Varian 21EX linac.

Percentage depth dose is a method for characterising the central axis dose distribution as it varies with depth. For a fixed SSD, the dose at any point on central axis is normalised to the dose at a reference depth, often the depth of maximum absorbed dose (D_{max}). This is expressed in Equation (3):

$$\text{PDD} = \frac{D_d}{D_{d_{\text{ref}}}} \times 100 \qquad (3)$$

Where D_d is the dose at any depth d, and $D_{d_{\text{ref}}}$ is the dose at the reference depth. Percentage depth dose is used in fixed SSD calculations to account for the variation of dose with depth. The shape of PDD curves is dependent on beam energy, field size and SSD. A typical PDD curve is shown in Figure 2-1. Percentage depth dose curves used as one parameter in MU calculations are typically measured on the treatment machine, in a water phantom, for each energy available, and for a variety of field sizes. A diagram illustrating the setup for measurement of PDD is shown in Figure 2-2.

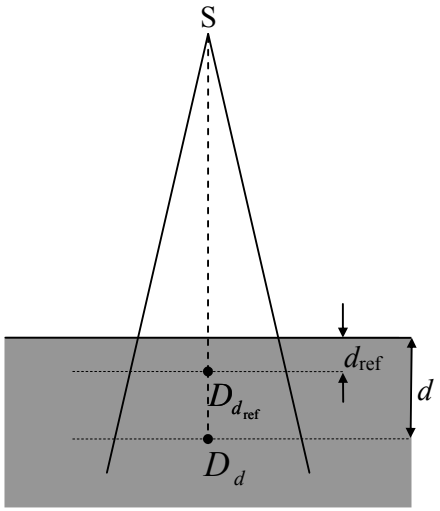

Figure 2-2. A diagram of the setup used for measuring percentage depth doses. The PDD at depth d for a given beam arrangement, is given by dividing the dose at that point, D_d, by the dose at the reference depth, $D_{d_{\text{ref}}}$, for a fixed SSD.

Another common method for accounting for the variation in dose with depth is to use Tissue Phantom Ratios (TPRs). TPR is similar to PDD, except that instead of a fixed SSD, the Source to Axis Distance (SAD) is fixed. The dose at any depth, at a fixed SAD, is normalised to the dose at a reference depth. With reference to Figure 2-3, this is expressed in the formula:

$$\text{TPR} = \frac{D_d}{D_{d_{\text{ref}}}} \times 100 \qquad (4)$$

Tissue phantom ratios are especially useful in MU calculations for isocentric fields, where the SSD may vary, but the SAD remains constant, as they are independent of SSD. As with PDD curves, TPR curves are dependent on beam energy and field size. A special case of TPR is the Tissue Maximum Ratio (TMR), where the doses are normalised to the dose at the depth of maximum dose. Figure 2-3 shows the setup used to measure TPRs.

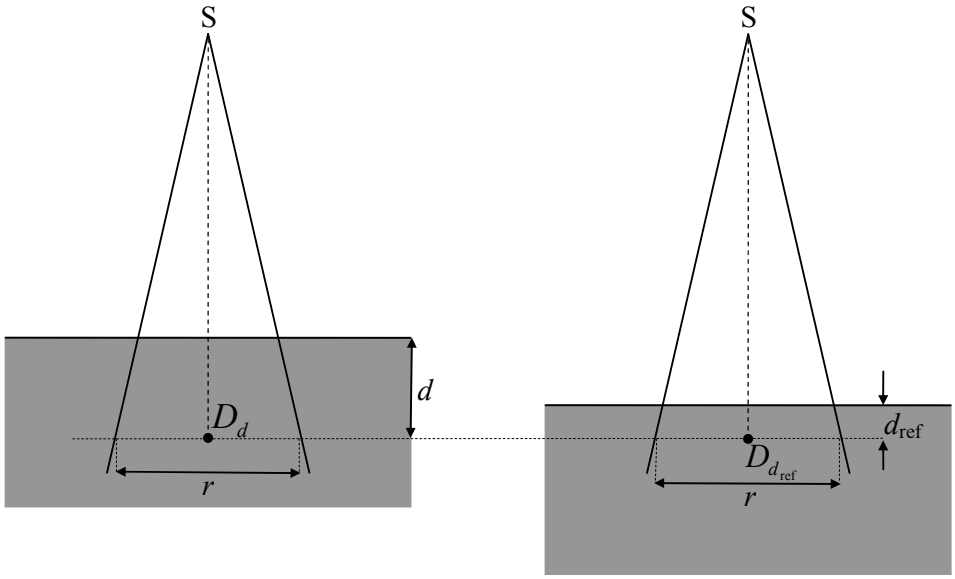

Figure 2-3. A diagram of the setup used for measuring tissue phantom ratios. The TPR at depth *d* for a given beam arrangement, is given by dividing the dose at that point, D_d, by the dose at the reference depth, $D_{d_{\text{ref}}}$, for a fixed SAD.

Collimator scatter factors correct for scatter effects external to the phantom, which influence beam output. These effects include the increase in scatter contribution to the primary beam from the jaws (collimators) as the field size increases, due to the larger surface area of jaw face exposed to the primary beam, the increase in scatter from the flattening filter as field size increases, and reduced backscatter from the top surface of the jaws into the monitor unit chambers as field size increases[10]. S_c is defined as the ratio of the output in air for a given field to that for a reference field (e.g. 10x10cm). Collimator scatter factors are usually measured either in a build up cap[11], or in a mini-phantom[12] as shown in Figure 2-4. The mini-phantom places the chamber at depth, removing any effects due to contamination electrons.

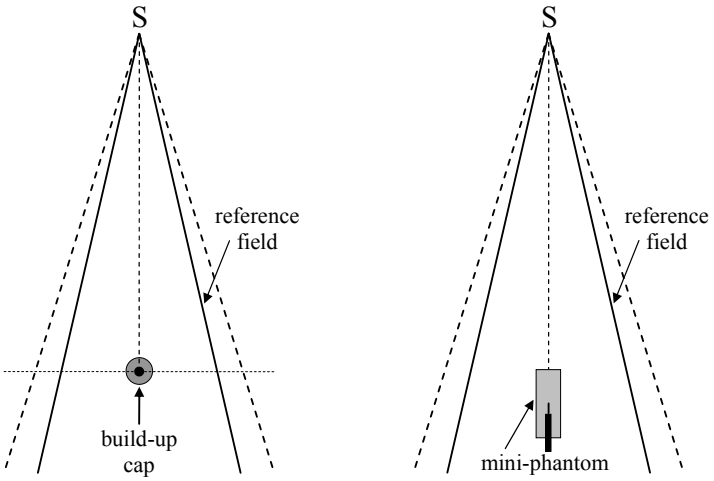

Figure 2-4. A diagram illustrating the different methods of measuring S_c. Measurements are usually performed in air at a fixed SAD using an ion chamber placed inside either a build-up cap (left), or a mini-phantom (right), which places the chamber at depth, removing any effects from contamination electrons. The S_c is given by dividing the dose for a given field size by the dose at the reference field size.

Phantom Scatter factors are used in conjunction with collimator scatter factors, and account for the increase in scattered radiation produced in the phantom caused by an increase in field size. S_p is defined as the ratio of the scattered dose at a reference depth for a given field size to the scattered dose at the same depth for a reference field size (e.g. 10x10cm), with the same collimator opening[9]. To measure S_p directly, the primary component of the radiation beam must be removed, which is very difficult to achieve. Instead, the total scatter correction factor ($S_{c,p}$), can be used. $S_{c,p}$ is defined as the ratio of the dose for a given field at a given depth and the dose for the reference field size at the same point and depth, and was traditionally referred to as the field size factor. The setup for measurement of $S_{c,p}$ is shown in Figure 2-5. Since this is easier to measure, and since $S_{c,p}$ is equal to the product of S_c and S_p, S_p is often determined using the following equation:

$$S_p = \frac{S_{c,p}}{S_c} \tag{5}$$

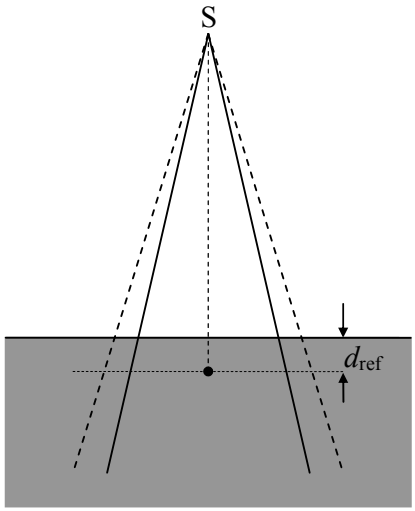

Figure 2-5. A diagram illustrating the setup for measuring $S_{c,p}$. Measurements are performed in a phantom at a fixed depth and SSD. The $S_{c,p}$ is given by dividing the dose for a given field size by the dose at the reference field size.

Off Axis Ratios are used to account for the variations in dose for points that are not on central axis, such as in Figure 2-6, and are calculated by taking the ratio of the dose at the off-axis distance x, and the dose on central axis at the same depth:

$$\text{OAR} = \frac{D_x}{D_0} \tag{6}$$

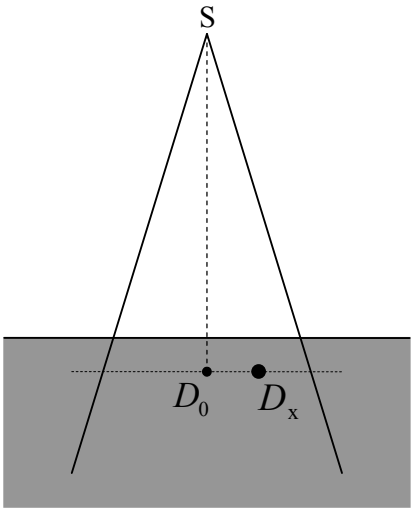

Figure 2-6. A diagram illustrating the setup for measuring off axis ratios. Measurements are usually performed in a phantom at a fixed depth and SSD. The OAR is given by dividing the dose at a distance, *x*, from central axis, by the dose on central axis.

In MU calculations, TPR/PDDs and other factors that are used assume that the calculation point is in a perfectly homogeneous medium. In cases such as that depicted in Figure 2-7, where the calculation point is in or behind an inhomogeneous region such as bone or lung tissue, the attenuation of the primary beam, and the scattered dose deposited at the calculation point will not be the same as for a homogeneous phantom. Two methods commonly used to account for tissue inhomogeneity effects in manual monitor unit calculations are the "Equivalent Path Length Method" and the "Batho Power Law Method".

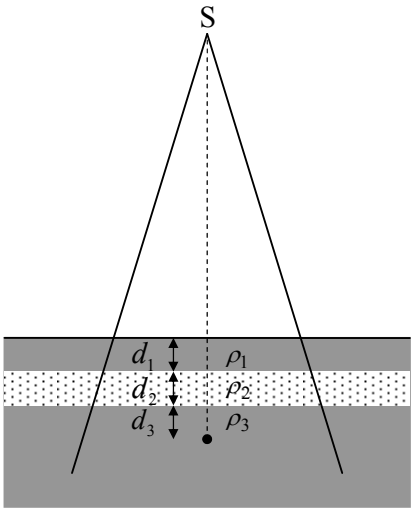

Figure 2-7. Diagram of a simple phantom containing slabs of different density, illustrating the concept of equivalent path length. The first slab has density ρ_1 and thickness d_1. The second slab has density ρ_2 and thickness d_2. The third slab has density ρ_3 and the distance to the measurement point is d_3. The equivalent path length is determined by scaling the distance through each structure by its density relative to water.

The Equivalent Path Length Method[13] calculates a new path length, d_{equiv}, based on the densities of structures between the phantom surface and the measurement point.

$$d_{\text{equiv}} = \rho_1 d_1 + \rho_2 d_2 + \rho_3 d_3 \ldots\text{etc} \tag{7}$$

Where, $d_{1,2,3}$ is the path length through region 1,2,3 etc, and $\rho_{1,2,3}$ is the density of material in region 1,2,3 etc.

The original equivalent path length correction method used a ratio of infinite percentage depth dose data. Using standard percentage depth dose data, the inhomogeneity correction factor is given by:

$$\text{ICF} = \frac{\text{PDD}(d_{\text{equiv}}, r)}{\text{PDD}(d_{\text{phys}}, r)} \cdot \left(\frac{\text{SSD} + d_{\text{equiv}}}{\text{SSD} + d_{\text{phys}}} \right)^2 \tag{8}$$

Where d_{equiv} is the equivalent path length and d_{phys} is the physical path length. This is approximately equivalent to the inhomogeneity correction factor used by RadCalc,

which is calculated by taking a ratio of the TPR for the new equivalent depth and field size r, with the TPR for the physical depth and field size r:

$$\mathrm{ICF} = \frac{\mathrm{TPR}(d_{\mathrm{equiv}}, r)}{\mathrm{TPR}(d_{\mathrm{phys}}, r)} \tag{9}$$

This method only takes into account changes in the attenuation of the primary beam, and does not account for changes in scatter conditions, or the position of the inhomogeneity relative to the calculation point.

The Batho Power Law Method, proposed by Batho[14] and later refined into a more general form by Sontag and Cunningham[15], uses the following equation:

$$\mathrm{ICF} = \frac{\mathrm{TPR}(d_3, r)^{\rho_3 - \rho_2}}{\mathrm{TPR}(d_2 + d_3, r)^{1-\rho_2}} \tag{10}$$

This method takes into account the position of the inhomogeneity relative to the calculation point, and can also correct for calculation points within an inhomogeneity. However, as with the equivalent path length method, the Batho power law method assumes that each homogeneous and inhomogeneous region is infinite in the lateral plane. The specific shape of each region is not taken into account. The Batho method and the equivalent path length method were compared by Tang et al, using a phantom with low density (0.25g/cm^3) inhomogeneities. For beam energies greater than 10MV, the Batho method was found to perform better than the equivalent path length method[16].

For PDD calculations where a non-standard SSD is used, the inverse square change in fluence at the calibration point is taken into account using an SSD factor:

$$\mathrm{SSDF} = \left(\frac{\mathrm{SSD}_{\mathrm{ref}} + d_{\mathrm{ref}}}{\mathrm{SSD}_{\mathrm{calc}} + d_{\mathrm{ref}}} \right)^2 \tag{11}$$

Where $\mathrm{SSD}_{\mathrm{ref}}$ is the reference SSD, d_{ref} is the reference depth, and SSD_{calc} is the SSD at the calculation point.

A change in SSD also results in a change in PDD at depth, due to inverse square effects. An approximate method for accounting for this effect is called the Mayneord factor:

$$\mathrm{MF} = \left(\frac{\mathrm{SSD}_{\mathrm{calc}} + d_{\mathrm{ref}}}{\mathrm{SSD}_{\mathrm{ref}} + d_{\mathrm{ref}}} \right)^2 \cdot \left(\frac{\mathrm{SSD}_{\mathrm{ref}} + d_{\mathrm{calc}}}{\mathrm{SSD}_{\mathrm{calc}} + d_{\mathrm{calc}}} \right)^2 \tag{12}$$

For TPR calculations where the calculation point is at a non-standard SAD, an Inverse Square Law Factor may be used to account for the inverse square change in photon fluence. The ISF is given by the following equation:

$$\mathrm{ISF} = \left(\frac{\mathrm{SCD}}{\mathrm{SPD}_{\perp}} \right)^2 \tag{13}$$

Where SCD is the source to calibration point distance, and $\mathrm{SPD}_{\perp}$ is the source to point distance along central axis. The change in scatter conditions at the calculation point can be accounted for by using the phantom scatter factor for the field size at the new SAD. Unlike PDDs, which are influenced by both attenuation and distance from the source, TPRs are primarily influenced by attenuation and are approximately independent of the distance from the source and do not require any correction.

When blocks or Multileaf Collimators (MLCs) are used to create irregularly shaped fields, a correction to monitor unit calculations must be applied to account for the difference in TPR (or PDD) and phantom scatter between the irregular fields and the rectangular fields for which data is tabulated or has been measured. The simplest method for accounting for field blocking is the Percentage Blocked Method. Using this method, the proportion of the beam that is left unblocked is calculated, and used to determine a new equivalent square that represents the area of the blocked field (r_{blocked}). The BCF is given by the following equation:

$$\mathrm{BCF} = \frac{\mathrm{TPR}(d, r_{\mathrm{blocked}})}{\mathrm{TPR}(d, r_{\mathrm{open}})} \times \frac{S_p(r_{\mathrm{blocked}})}{S_p(r_{\mathrm{open}})} \tag{14}$$

This method does not take into account the specific shape of the block and assumes that the TPR and S_p will be the same for the irregular field as for a square field of equivalent size.

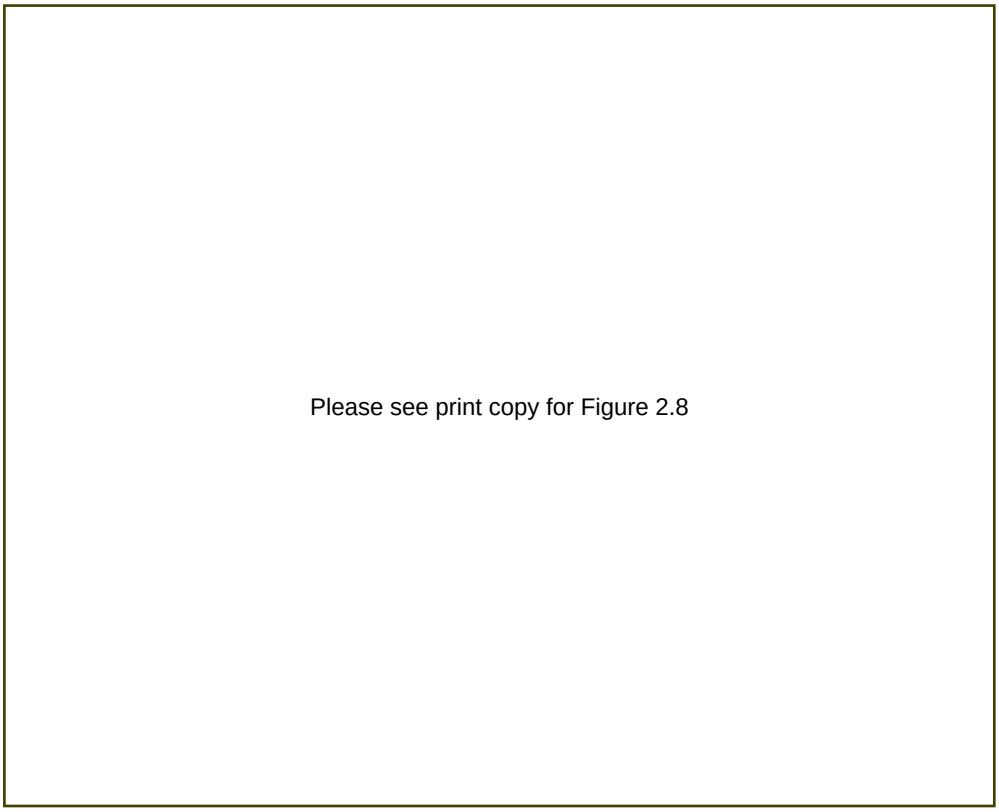

Figure 2-8. Diagram illustrating the Clarkson method of block correction for a mantle field. The field is divided into sectors, and the scatter contribution from each sector is determined based on the sector angle and radius drawn through the centre of each sector from the calculation point to the field edge. (courtesy of IAEA[17]).

An alternative method was proposed by Clarkson[18] and later refined by Cunningham[19,20]. The Clarkson Method is based on the principle that the scattered component of dose delivered to a point, which is dependent on field size and shape, can be calculated separately to the primary component, which is independent of field size and shape. As shown in Figure 2-8, radii are drawn out on the field cross-section from the calculation point to the field edge. These radii divide the field into pie shaped sectors, each characterised by its radius and angle. For example, if the field is divided into 36 sectors, each with an angle of 10 degrees, then a single sector will contribute 1/36 the amount of scatter of a full circular field of same radius and centred on the calculation point. Therefore, using a table of Scatter-Maximum Ratios (SMRs) for

circular fields, SMR values for each segment are summed to give the average scatter-maximum ratio ($\overline{\text{SMR}}$).

$$\overline{\text{SMR}}(d,r_d) = \frac{1}{n}\sum_{i=1}^{n}\text{SMR}(d,r_i) \tag{15}$$

Scatter Maximum Ratio is defined as the ratio of the scattered dose at a given point in a phantom to the effective primary dose at the same point at the reference depth of maximum dose[9]. This is expressed in the following equation:

$$\text{SMR}\ (d,\ r_d) = \text{TMR}\ (d,\ r_d)\left(\frac{S_p(r_d)}{S_p(0)}\right) - \text{TMR}\ (d,\ 0) \tag{16}$$

If a part of a segment is blocked as shown in segment 7 in Figure 2-8, then the contribution from that segment is calculated by subtracting the scatter contribution from the blocked area.

$$(\text{SMR}_{QA})_{net} = \text{SMR}_{QA} - \text{SMR}_{QB} + \text{SMR}_{QC} \tag{17}$$

The $\overline{\text{SMR}}$ is converted into average tissue-maximum ratio ($\overline{\text{TMR}}$) by the equation:

$$\overline{\text{TMR}} = [\text{OAR}\cdot\text{TMR}(d,0) + \overline{\text{SMR}}(d,r_d)]\times\frac{S_p(0)}{\overline{S}_p(r_d)} \tag{18}$$

Where OAR is the off axis ratio, TMR(d,0) is the TMR for a 0x0 field, $S_p(0)$ is the phantom scatter factor for a 0x0cm field size and $\overline{S}_p(r_d)$ is the average phantom scatter factor for the irregular field

2.2 Convolution-Superposition Dose Calculation Method

An alternative to the correction based dose calculation method described above is to calculate the dose distribution from first principles, from the physics of photon and electron transport[21]. Unlike correction based methods, methods such as Monte Carlo and Convolution/Superposition do not use measured data in dose calculations, although measured data may be used to test and optimise the model. Because they calculate dose from first principles, they have the potential to be more accurate than correction based methods for patient situations. By accounting for electron transport, the accuracy of dose calculations can be improved for situations involving complex heterogeneities and regions of high or low density. Although these methods are based on photon-electron beam interactions, some approximations are applied to simplify and speed up calculations.

The plans studied in this thesis have been planned on a Phillips Pinnacle[3] treatment planning system. This system was the first commercial systems to implement a model based convolution-superposition calculation method. Convolution-superposition was first established by Mackie et al[22], and formalised mathematically by Boyer and Mok[23]. The method is sometimes referred to as a "Differential Pencil Beam" calculation[24]. Pinnacle uses a beam model and a form of collapsed cone convolution (developed by Ahnesjö[25]) to calculate dose from first principles (using some approximations). The dose is calculated from the primary fluence, the total energy released per unit mass (TERMA) at each point, and dose kernels, which describe the distribution of dose around an interaction site due to primary photon interactions.

Before the actual convolution-superposition process begins, a number of steps must first take place. Firstly, a dose-grid must be defined. This is a 3 dimensional array of voxels, each with its own density value. This is usually derived from a patient's CT dataset, and defines the volume over which the dose is to be calculated. CT numbers were originally characterised in terms of linear attenuation coefficient[26]. If the beam energy and the atomic composition of the scanned material are known, the relationship between CT number and relative electron density can be calculated[27]. However, a more practical approach is to establish an experimental relationship by CT scanning a phantom containing samples of known density[28]. The majority of treatment planning systems

require the input of electron density values as electron density scaling has been shown to be more accurate than mass density scaling for radiotherapy treatment planning. This is due to the dominance of Compton and electron interactions at typical linac energies[29]. However, Pinnacle[3] requires the input of physical density, since its TERMA calculation relies on mass attenuation coefficients, which are referenced by the physical density of each material[30]. Shown in Figure 2-9 is a phantom used to characterise the relationship between CT number and physical or electron density, as well as an example of a graph of CT vs. physical density.

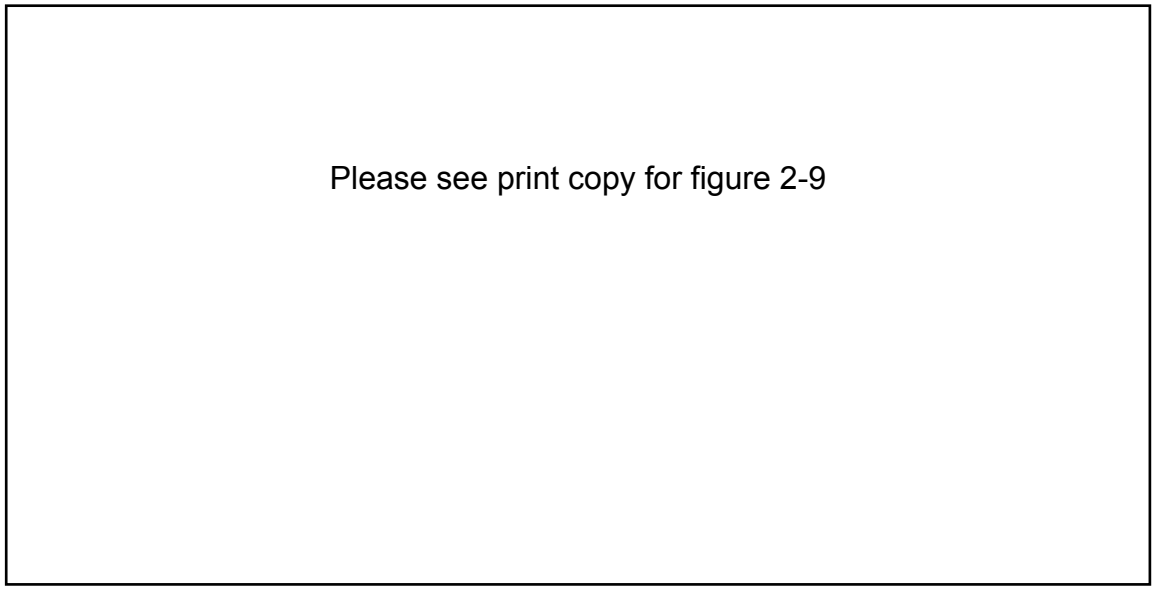

Next, the radiological depth (relative to the radiation source) of each voxel in the dose grid is calculated using ray-tracing methods. Ray tracing works by tracing a line from the source to the voxel in question and multiplying each increment in length by its corresponding electron density. They are summed together from the first voxel with density greater than that of air to the voxel in question to calculate its radiological depth.

This data is then used to calculate the TERMA for each voxel. This represents the total energy lost from the primary beam in a given unit of mass, including the energy given to secondary particles, and the energy retained by scattered photons. In addition to radiological depth, TERMA calculations must account for beam divergence, beam attenuation, the polyenergetic nature of the beam, and the density of the voxel for which

the TERMA is being calculated. A 3D array of TERMA values is required before superposition can begin.

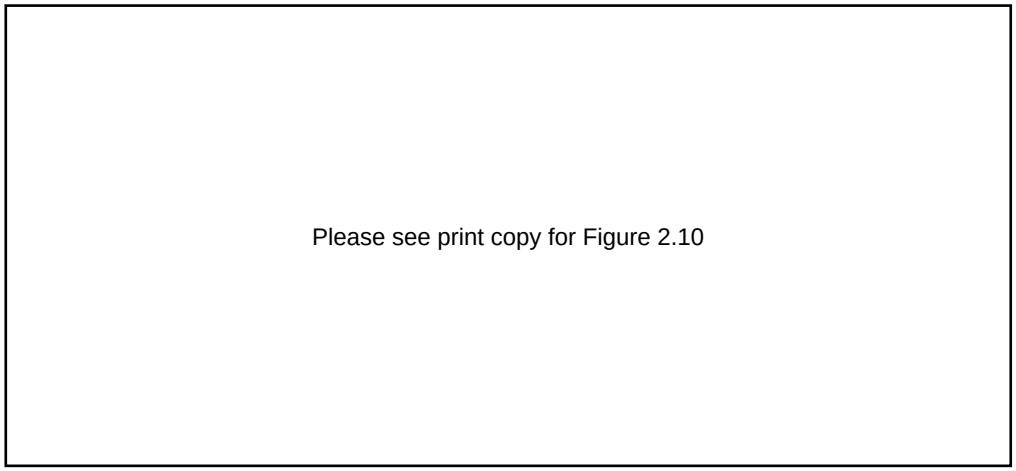

Figure 2-10. Diagrams demonstrating the Deposition (left) and Interaction (right) points of view, used during the superposition of dose kernels. The deposition point of view method determines the dose at each point in the dose grid by summing the dose contribution from each interaction point. The interaction point of view method sums the dose contribution to the surrounding voxels of each interaction point. (courtesy of Metcalfe et al[32])

Using the original method of Mackie et al[22], the actual dose distribution is calculated by the superposition of Monte Carlo derived dose kernels. A kernel is a 3 dimensional array describing the dose delivered to the voxels surrounding the interaction site resulting from primary photon interactions. The actual superposition of these kernels is usually performed using one of two methods shown in Figure 2-10. The first is known as "the deposition point of view" (Figure 2-10 (left)). In this method, the dose at each voxel is calculated by summing the dose contributed to the deposition voxel from each interaction site. This is done by multiplying the TERMA at each voxel by the dose kernel value for the deposition voxel. The second method is termed "the interaction point of view" (Figure 2-10 (right)). In this method, the dose contribution to the surrounding voxels, due to the TERMA at each interaction voxel is calculated and summed to give the total dose distribution. Pinnacle uses the deposition point of view method[33].

Dose kernels were first derived using Monte Carlo techniques. Monte Carlo methods determine the "histories" of incident primary photons. This refers to the transport of the primary photon, as well as the secondary particles it sets in motion. The fate of each

particle is determined by taking into account factors such as the energy of the particle, the atomic composition and density of the medium it is travelling in, and the probability distribution of each possible interaction. Random number generators are used to determine where, when and how interactions take place.[32]

To derive a dose kernel, firstly a 3D, uniform, homogeneous phantom is defined. This phantom is partitioned into an array. A voxel in the array is chosen to be the interaction site. Photons from a given angle of incidence are forced to interact in that voxel. Photon histories are generated using Monte Carlo techniques. For each history, the dose deposited in each voxel of the array is recorded. Separate dose kernels are usually derived called the primary kernel and the scatter kernel. The scatter kernel is sometimes also separated into the first scatter kernel and the multiple scatter kernel. The primary kernel is derived by recording the dose delivered to each voxel due to secondary particles produced by the primary photon interaction. The scatter kernel is derived by recording the dose delivered to each voxel due to secondary particles produced by interactions of scattered photons. Millions of photon histories are used to derive dose kernels to ensure very low uncertainty in the dose distribution. The end result is a 3 dimensional array of values that correspond to the fractional energy deposited in each voxel due the incident photons. This array is called a "dose spread array"[22]. A number of monoenergetic dose kernels are shown in Figure 2-11.

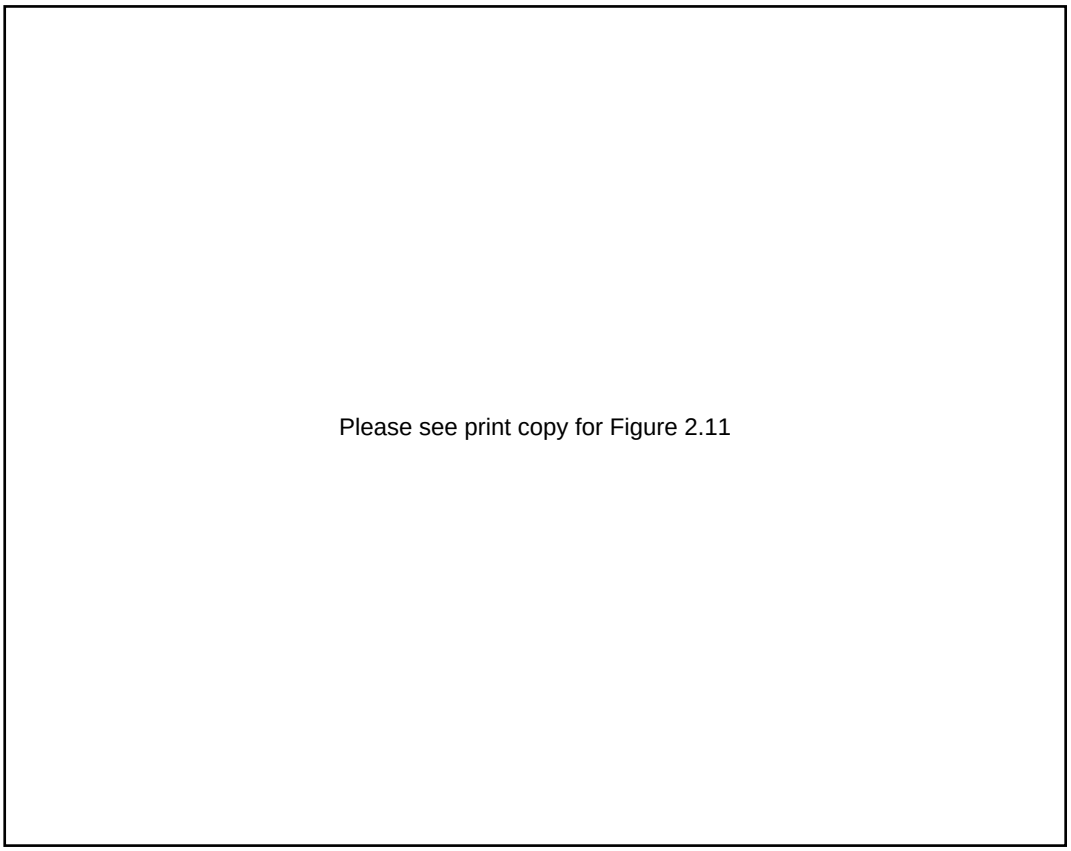

Figure 2-11. Diagram representing dose kernels for various photon energies. Dose kernels are generated using monte carlo techniques to calculated the dose distribution due to photons interacting in a particular voxel. The diagram shows the difference in dose distribution due to photon energy, with higher energy dose kernels more forward focussed than lower energy dose kernels. (courtesy of Ahnesjö et al[34]).

Monoenergetic dose kernels are not particularly useful in radiation therapy planning, as the photon beams most commonly used are polyenergetic. To calculate dose for a polyenergetic beam, a separate convolution would have to be performed for each component of the polyenergetic spectrum of the photon beam, weighted by the spectral contribution. This would be a long process. Therefore, polyenergetic dose kernels are derived in one of two ways. First, separate dose kernels can be derived for each energy component in the spectrum of the beam being modelled. The kernel for each energy in the beam spectrum is then scaled according to its relative intensity, and combined to form a single polyenergetic dose kernel. The alternative is to use a polyenergetic spectrum of incident photons to derive the kernel.[35]

In principle, dose kernels can be derived experimentally, by deconvolving a measured beam profile[36]. However, this method is difficult, and is not commonly used. Monte Carlo methods are favoured as they determine kernels from first principles, they are

simpler to derive (provided sufficient computer power is available) using computer simulation rather than difficult experiments, they are more flexible and their accuracy has been proven and is well documented.

Dose can be accurately calculated using standard convolution/superposition methods. However, as the dose deposited at each voxel must be calculated from interactions in every other voxel in the dose grid, calculations require a large amount of computation time. To overcome this problem, some convolution based treatment planning systems use "Collapsed Cone Convolution". Collapsed cone convolution is an efficient convolution/superposition method originally proposed by Ahnesjö[25]. Instead of being expressed in cartesian arrays, polyenergetic dose kernels are represented analytically in polar coordinates. These are then divided into coaxial cones, such that the total solid angle of the cones for each kernel is equal to 4π. The collapsed cone convolution approximation is that for each cone the dose that would have been delivered throughout the whole solid angle of the cone is rectilinearly transported, attenuated and deposited in elements along its axis[25]. The name "collapsed cone convolution" comes from the way the dose distributed throughout the cone is effectively collapsed onto its axis.

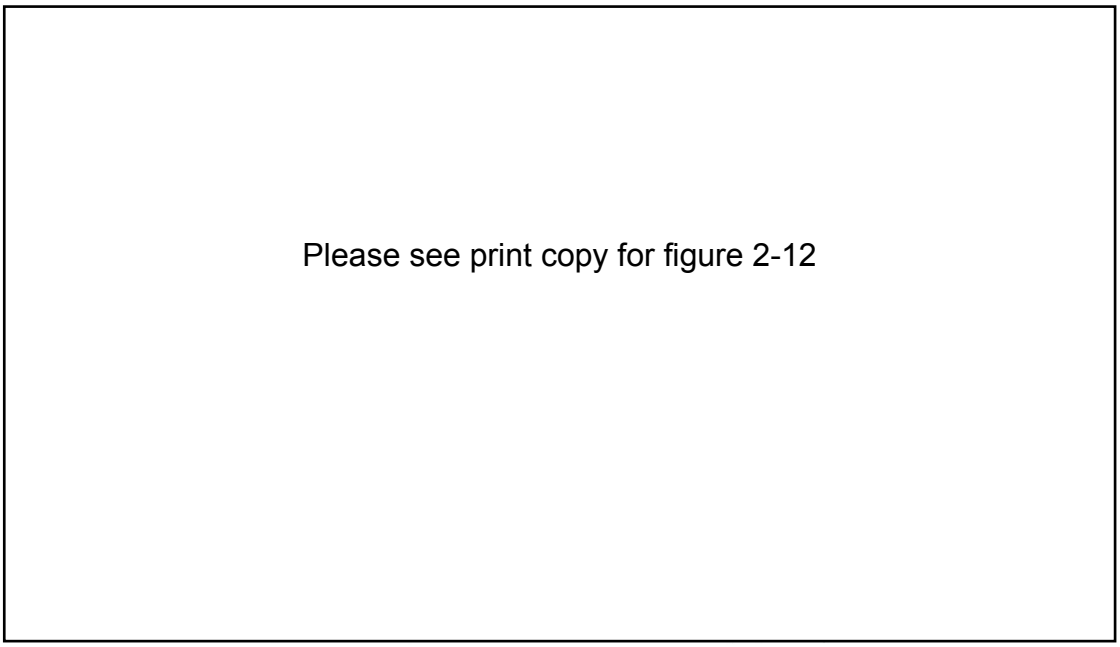

Figure 2-12. Left: Diagram demonstrating errors that result from collapsing the dose in the cone onto its axis. The dose at point B' from interactions in point A is now deposited at point B. This is compensated for to some extent by the dose at point B from interactions at point A being deposited at point B'. Right: Diagram showing a lattice of cone directions intersecting each voxel. Using collapsed cone convolution, the dose from interactions in each voxel that would have been deposited throughout the volume is approximated to be only transported, attenuated and deposited along the centre of these cones (courtesy of Ahnesjö et al[37]).

As shown in Figure 2-12(right), a lattice of lines representing cone axis directions is constructed. This lattice is optimised so that each direction intersects each voxel in the calculation grid once. In normal convolution/superposition methods, for each interaction/deposition point, the dose contribution to/from every deposition/interaction point must be calculated and summed together to form the final dose distribution. In collapsed cone convolution, using the interaction point of view, for every interaction point, only the dose at each point on the lines representing the cone axes is calculated. This results in a dramatic reduction in the number of calculation points and saves a great deal of computational time.

There are errors associated with this method, however. As shown in Figure 2-12(left), the dose that should have been deposited in voxel B' from interactions in voxel A are now deposited in voxel B. This is compensated for in a limited way by the fact the dose that should have been delivered to voxel B from interactions in voxel A' will be deposited in voxel B'. But this exchange will not always be perfect in a heterogeneous medium. Errors due to the collapsed convolution approximation increase as the distance

from the interaction voxel increases. However, as most of the dose is delivered to voxels close to the interaction site where the error is small, the dose delivered to voxels further from the interaction site is so low that these "displacement errors", as they are called, have an acceptably low impact on the final dose calculation. The conservation of the total energy deposited is more important than the precise deposition of small amounts of dose at large displacements from the interaction site. Collapsed cone convolution methods have been tested against Monte Carlo simulations, and have demonstrated very good results[37].

Probably the most significant advantage of the collapsed cone convolution method is the dramatic reduction in computation time required, compared to that of normal convolution/superposition methods. In normal convolution/superposition methods, for a 3D array of N x N x N (N^3) voxels, for each of the N^3 interaction voxels (taking the interaction point of view), the dose to each of the N^3 deposition voxels must be calculated. This means that the total number of operations required to calculate the dose is proportional to N^3 x N^3, or N^6. In contrast, in the collapsed cone convolution approximation, the dose is delivered along a number of lines corresponding to the direction of cone axes radiating out from the interaction point. Therefore, if M cone directions are used, at each interaction point the dose must be calculated for a number of deposition points proportional to M x N, since the number of deposition points along each directional line will be proportional to N. Since there N^3 are interaction points, the total number of operations required to calculate the dose will be proportional to M x N x N^3, or MN^4. According to Ahnesjö[37], if the dose is calculated in one sequence for a bulk of N^3 points, the total number of operations needed in a heterogeneous medium is proportional to MN^3.

Tissue heterogeneities are partially accounted for in the TERMA calculation. Ray tracing[38] is used to determine the average density between the surface and the interaction site, which allows the calculation of the attenuation of the primary beam's energy fluence. Voxel density is then taken into account in the TERMA calculation, as it determines the likelihood of a primary photon interaction. More difficult to account for, however, is the effect of density variations between the interaction site and the energy deposition site.

The most commonly used heterogeneity correction method, and that used by Pinnacle[3] Treatment Planning System[33] uses a ray tracing technique, similar to that used to calculate the beam energy fluence at an interaction voxel. The average density of the voxels between the interaction site and the deposition site is calculated and used to scale the dose kernel value at the deposition site. This method assumes that electrons deposit their energy along a linear track, which is not the case. Electron tracks are far more random and curved. While more complex methods of accounting for non-linear electron tracks have been developed[39,40], this method of density scaling has been found to be a reasonable approximation, as at large distances and for multiple scattered photons where the error is greatest, the dose is much lower, so it has a low effect on the overall accuracy of the calculated dose distribution.

2.3 Intensity Modulated Radiation Therapy

In modern linac based radiotherapy, Intensity Modulated Radiotherapy (IMRT) refers to a technique that involves varying the fluence across individual fields. The purpose is usually to conform a uniform dose distribution to a specific target and/or spare dose to critical structures. Intensity modulation can be achieved using physical wedges, dynamic wedges and compensators. However, modern linacs most commonly achieve intensity modulation for IMRT treatments using MLCs[41].

The two main methods by which MLCs are used for IMRT are "Dynamic IMRT" and "Step and Shoot IMRT". In Dynamic IMRT, the MLCs are moved across the field, usually in a sliding window delivery pattern while the beam is on. In Step and Shoot IMRT, each field is made up of a number of different static MLC shapes called "segments", with a fraction of the total MUs for the field delivered by each segment as determined by the segment weight.

3D conformal treatments are forward planned. Starting with a set of conformal beams, internal apertures, wedges and even additional beam directions are added to modify the isodose distribution until it is satisfactory. Fields with up to 3 segments can generally be forward planned. For more complex volumes requiring a greater number of segments, forward planning becomes impossible. Therefore a relatively new approach known as inverse planning is frequently used for IMRT treatment planning, where more complex dose distributions are desired.

In inverse planning the dose objectives are defined by the user and the delivery parameters required to achieve those objectives are iteratively derived through computer based optimisation. In Pinnacle, dose-volume objectives and constraints are defined for various volumes of interest. Objectives are the desired goals, and are assigned weighting based on their importance, whilst constraints are goals that must be met by the software. The user specifies the beam energy, field size and field angles. The software calculates an ideal Opening Density Matrix (ODM) for each treatment field. The ODM is a transmission array expressed as the relative intensity between the intensity-modulated field and the open field. Pinnacle optimises the intensity of each element of the ODM using a sequential quadratic programming algorithm for solving

non-linear optimisation problems (NPSOL). This algorithm iteratively changes the ODM for each beam, recalculates dose, and scores the plan based on how successfully it meets the objectives. The score, or objectives function, is the weighted sum of the squared difference between the required dose and the actual dose calculated for each structures.[42,43]

The conversion of the ODM into a deliverable sequence of MLC segments occurs via a two stage process[44]. Firstly, a clustering algorithm transforms the quasi-continuous distribution of the ODM into a clustered ODM, containing a smaller number of discrete levels. Then a segment extraction algorithm is used to convert the clustered ODM into step-and-shoot MLC segments. The level of agreement between the deliverable ODM and ideal ODM is controlled by a user specified parameter. The final dose calculation is based on the deliverable sequence of MLC segments. Direct aperture optimisation (DAO) has recently been introduced as an additional IMRT option in Pinnacle[45]. In DAO the conversion of the ODM into a deliverable MLC sequence takes place during the optimisation, hence any detrimental impact of the MLC delivery constraints on plan objectives can be accounted for during the optimisation.

Due to the complexity of IMRT treatments, standard MU verification calculations and QA measures are not adequate. According to Ezzell et al[41], a comprehensive IMRT QA program should verify the accuracy of each of the following elements of the treatment process: 1) Dose and MU calculation; 2) Information transfer from planning system to record and verify system to delivery system; and 3) dose delivery. Typically, this will involve an independent MU calculation using specialised software to verify the dose and MU calculation, a phantom measurement to verify the data transfer and delivery and various other tests and inspections to ensure the accuracy of the delivered plan. While there is no formal recommendation on the level of agreement between calculated dose and measurement, Ezzell states that "there is a developing consensus that ion chamber measurements in high dose, low gradient regions should agree with the plan to within 3% to 4%". It is reasonable that a similar level of agreement between independent MU calculations and planning calculations would be acceptable. In addition to this, QA should be regularly performed on the treatment machine to verify factors such as MLC leaf positioning accuracy and linac performance.

2.4 Modified Clarkson Integral

As mentioned previously, although modern planning systems such as Pinnacle[3] are very accurate in calculating patient doses, independent MU calculations are still required to verify the accuracy of treatment plans, and are mandatory in all NSW public hospitals according to Department of Health policy[46]. For IMRT plans, a number of independent MU checking methods have been proposed. One option is to use a separate IMRT treatment planning system to verify IMRT plans[47]. However, for most radiotherapy departments this would be impractical due to the cost of a second IMRT treatment planning system as well as the extra time required to create the verification plan. Others have proposed using Monte Carlo techniques to verify IMRT plans. While Monte Carlo methods have the potential to be very accurate, in the past, the high level of computing power, long calculation times, and technical knowledge required have prohibited them from being routinely used. However, due to improvements in computer power and algorithm efficiency, methods such as that developed by Fan et al (2006)[48] may become more feasible for routine use.

A concept called Modified Clarkson Integral, based on the Clarkson Method has been introduced by Kung et al[49], which is capable of calculating monitor units for intensity modulated fields. For a step and shoot IMRT field, firstly the contributions from each segment, weighted by the fraction of total MU delivered, are summed to produce the total fluence map MU(x,y). MLC transmission is also taken into account, contributing a fixed percentage of segment MUs as transmission fluence. Varian's rounded leaf ends are taken into account by the Radiation Field Offset (RFO), which is the difference between the 50% dose level of the radiation field and the projected light field at the source to axis distance. Therefore, the RFO (~0.7mm for 6MV) is applied to digital MLC positions during reconstruction of fluence map.

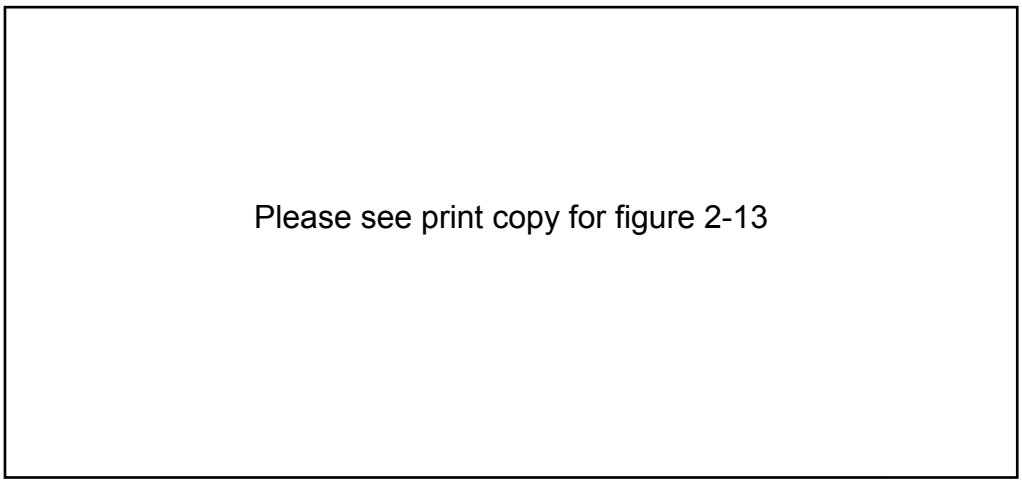

Figure 2-13. Diagram showing conversion of fluence map converted into annular sectors. Assuming radial symmetry of scattered dose to the calculation point, the fluence map, MU (x, y), is replaced by annular sectors representing the average fluence at a given radius, MU(r). (courtesy of Kung et al[49]).

Next, it is assumed that for identical MU, the scatter from any point on a fixed radius will contribute equally to scattered dose at central axis. Therefore, fluence MU(x,y) is replaced by an azimuthal average at each radius MU(r), producing a series of uniform annular sectors as shown in Figure 2-13. The dose at central axis will be equal to the primary dose, plus the sum of the scattered dose due to the annular sectors. Scattered dose is calculated by assuming that the scattered dose from an annular ring is equal to the dose from a circular field with radius equal to the outer radius of the annular sector, subtracted by the dose from a circular field with radius equal to the inner radius of the annular sector, as expressed in Equation (19). This concept is illustrated in Figure 2-14.

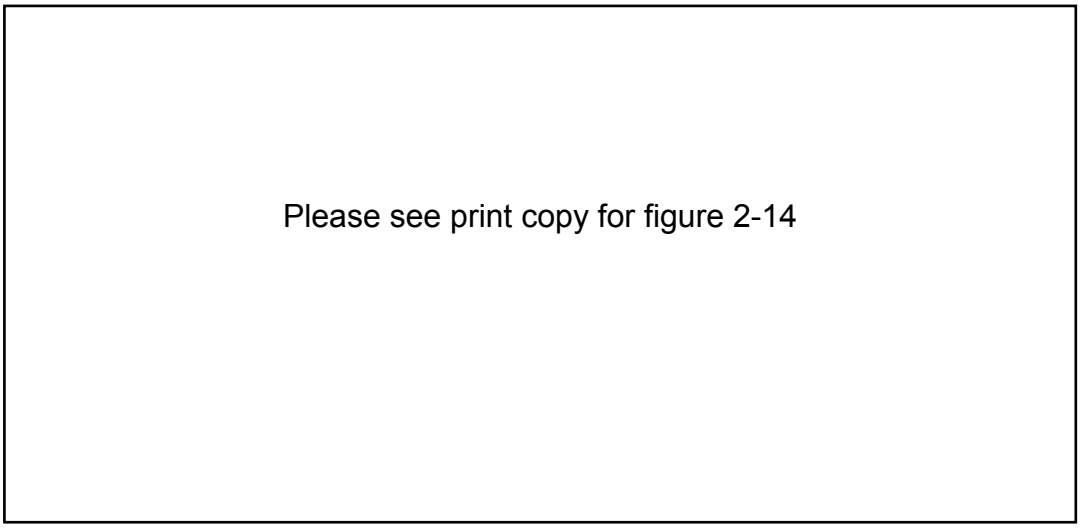

Figure 2-14. Diagram demonstrating the calculation of dose contribution from an annular sector. The scattered dose deposited at the calculation point from an annular sector of thickness ΔR is approximated as the scattered dose from the circular field with radius $R+\Delta R$ subtracted by the scattered dose from the circular field with radius R. (courtesy of Kung et al[49]).

A similar integration to Clarkson Integration is then performed to calculate the total scatter contribution, using annular sectors instead of the pie shaped sectors used in the Clarkson method. This is expressed in the following formula:

$$\begin{aligned} D(d) &= D(d,\text{primary}) + \sum_{annulus} D(d,\text{annulus}) \\ &= \text{CF}\cdot\text{ISF}\cdot S_c\left[\text{MU}(0)S_p(0)\text{TPR}(0) + \sum_r \text{MU}(r)\left[S_p(r+\Delta r)\text{TPR}(r+\Delta r) - S_p(r)\text{TPR}(r)\right]\right] \end{aligned} \quad (20)$$

The advantages of this method are that it relies on readily obtained measured data and a relatively simple algorithm, resulting in very short computation times.

RadCalc, the commercial monitor unit calculation software that is tested in this thesis, uses MCI in its IMRT calculations. The full monitor unit calculation formula used by RadCalc is as follows:

$$\text{MU} = \frac{\text{Dose}}{\text{CF}\times\text{ISF}\times\text{ICF}\times\sum_{\text{ControlPts}} S_c\times(\text{Primary}\times\text{POCR}+\text{Scatter})} \quad (21)$$

Where

$$\text{Primary} = \overline{\text{MU}(r=\min)}\cdot\text{TPR}(d,\ r=\min)\cdot S_p(r=\min) \quad (22)$$

and

$$\text{Scatter} = \sum_{r=\min}^{\text{Max}} \overline{\text{MU}(r\to(r+\Delta r))}\cdot\begin{bmatrix}(\text{TPR}(d,r+\Delta r)\cdot S_p(d,r+\Delta r))\\ -(\text{TPR}(d,r)\cdot S_p(d,r))\end{bmatrix} \quad (23)$$

$\overline{\text{MU}(r=\min)}$ is the average MU over the minimum radius (between 0 and 1cm). $\overline{\text{MU}(r\to(r+\Delta r))}$ is the average MU fraction from an annular ring with inner radius r and outer radius $(r+\Delta r)$. POCR is the primary off-centre ratio. To calculate OARs RadCalc uses the method given by Chui et al[50,51], which separates the OAR into the Primary Off Centre Ratio (POCR) and the Boundary Factor (BF). The POCR is defined as the ratio of the dose at a point off central axis to the dose of the corresponding point

on central axis, for an infinite field. The BF accounts for the shape of the beam profile 5cm or closer to the field edge. While the BF is included in non-segmented beam calculations, it appears that only POCR is taken into account in calculations for segmented beams.

Chapter 3: Materials

The linac used in this study was a Varian 2100EX, as shown in Figure 3-1. This machine is a dual photon energy machine, with energies 6MV and 10MV. It is also capable of producing electron beams with energy 6MeV, 9MeV, 12MeV, 16MeV and 20MeV. The linac is equipped with the Varian Millennium^{TM} MLC-120 multi-leaf collimator system. The leaf width for the inner 80 leaves is 0.5cm, and 1cm for the outer 40 leaves. Although the linac is capable of producing a 10MV beam, only the 6MV beam is considered in this thesis, as it is the only energy used for IMRT at ICCC.

Figure 3-1. Varian 2100EX linear accelerator used for all measurements in this project. The linac is capable of producing both 6MV and 10MV photon beams (although only 6MV was used in this project), as well as multiple electron beam energies. It is equipped with the Varian Millennium^{TM} MLC-120 multi-leaf collimator system.

Two vented air ionisation chambers, shown in Figure 3-2, were used for dose measurements. The first was a NE Technology 2571 Farmer chamber. It has a sensitive volume of 0.69cm^3. It has an outer diameter of 6.3mm, a wall thickness of 0.36mm and

a length of 24.1mm. The outer wall is composed of high purity graphite, while the inner electrode is composed of pure aluminium. The second chamber used was a Scanditronix- Wellhöfer CC13 chamber. The chamber is vented through a waterproof silicon sleeve, making it convenient for water measurements. It has a relatively small volume of 0.13cm^3. It has an outer diameter of 6.8mm, a wall thickness of 0.4mm and a total active length of 5.8mm. Both the outer wall and inner electrode are composed of an air equivalent plastic called Shonka C552. The recommended polarising voltage is ±300V. The leakage current is < ± 4x10^{-15} A. Its sensitivity is 3.8x10^{-9} C/Gy. These chambers were connected to a NE Farmer 2570/1 electrometer, shown in Figure 3-3, for dose measurements.

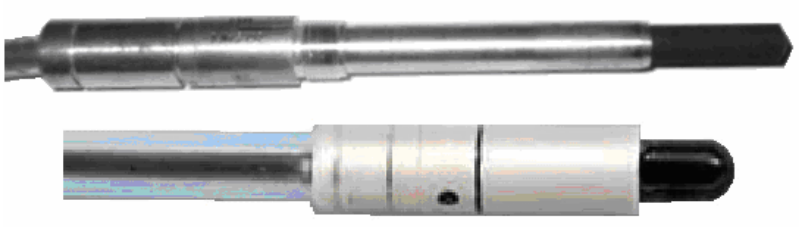

Figure 3-2. NE Technology Farmer 2571 (above) and Scanditronix-Wellhöfer CC13 (below) ionisation chambers used for dose measurements in this project (not to scale).

Figure 3-3. NE Technology 2570/1 electrometer used for all dose measurements in this project.

The main phantom used was a Scanditronix-Wellhöfer I'mRT phantom, shown fully assembled in Figure 3-4. The phantom is made of RW3, a water-equivalent polystyrene material (%2 titanium oxide) with density 1.045g/cm^3. The phantom is composed of a torso phantom, a cubic head and neck phantom, and lateral scattering bodies. It is designed so that an ion chamber and films can be inserted in the coronal plane at one end, and films placed in the axial plane at the other end at the same time. The torso

phantom consists of 15 36cm x 18cm x 1cm thick slabs. Films can be placed in between the slabs to give transverse dose distributions. The outer dimensions of the head and neck cube are 18cm x 18cm x 18cm. Standard inserts of 16 x 16 x 1cm can be inserted into the cube, as well as compensating inserts of different lengths, heights and widths, films, and inserts for different ionisation chambers. Using the standard, chamber and compensating inserts, a chamber such as the CC13 can be placed at any point in the cube within a 1cm grid. Lateral scattering bodies attach either side of the head and neck cube. The torso phantom slabs and lateral scattering bodies are held together by two threaded nylon rods that run through the phantom and are fixed by bolts at either end. The head and neck cube was not considered suitable due to the sharp contours present when the lateral scattering bodies were removed. In addition, removal of the lateral scattering bodies would prohibit axial film measurements. Hence, the fully constructed torso phantom was used in all IMRT validation experiments.

Figure 3-4. Scanditronix-Wellhöfer I'mRT phantom used for IMRT verification measurements, shown with the head and neck cube towards the front, with lateral scattering bodies in place, and the torso phantom at the rear. The phantom is also shown with a CC13 chamber and film inserted.

In addition to the I'mRT phantom, a phantom constructed out of 30cm x 30cm slabs of Solid Water of varying thickness, such as that shown in Figure 3-5, was also used for dose measurements. The Solid Water used was RMI-457 (Gammex RMI, Wisconsin,

USA). It has a density of 1.03 g/cm^3, and an effective atomic number of 5.96 (compared to 6.6 for water).

Figure 3-5. Gammex RMI-457 Solid Water slabs used for phantom measurements

Percentage depth dose curves and beam profile data used in RadCalc for dose calculation was previously collected using a Scanditronix-Wellhöfer 3D water phantom (Blue Phantom), shown in Figure 3-6 and accompanying computer program OmniPro-Accept Version 6.2A. Two CC13 ion chambers (S/N 5652 & 5653) were used interchangeably, one as a field instrument and the other as a reference. For field sizes less than 4x4 cm, a 0.01cm^3 volume CC01 chamber was used for PDD, beam profile and output factor measurements. The PDD curves were measured for a range of symmetric field sizes (1x1cm-40x40cm). Beam profiles were measured for a range of field sizes (1x1cm-40x40cm) at a range of depths (0cm-20cm). These curves were imported directly into RadCalc from the Scanditronix/Wellhöfer water tank software. PDD were converted into TPR using the RadCalc software. Beam profiles were used in OAR calculations.

Figure 3-6. Scanditronix-Wellhöfer 3D water phantom (Blue Phantom) used to collect depth doses and beam profiles used in RadCalc calculations.

S_c factors were measured in a polystyrene mini-phantom[12] at 100cm SSD, for a range of square field sizes (4x4cm-40x40cm), using an NE 2571 Farmer chamber and an NE Farmer 2570/1 electrometer. Due to the physical limitations of the phantom used for S_c measurements, field sizes 3x3cm and smaller could not be measured. The S_c value is based on the jaw settings and it is not anticipated that field sizes smaller than a 4x4cm jaw setting would be used in IMRT. However, the S_p value is based on the blocked equivalent square and blocked field sizes smaller than 4x4cm may be involved in IMRT plans. Hence S_p values smaller than 4x4cm were required. These values were determined by measuring $S_{c,p}$ for field sizes 1x1cm up to 40x40cm and dividing out the S_c contribution. $S_{c,p}$ factors were measured in a Scanditronix-Wellhöfer 3D water phantom at 100cm SSD, using a CC13 ion chamber and a N/E Farmer 2570/1 electrometer. For field sizes smaller than 4x4cm, extrapolated S_c values were used based on a 3rd order polynomial fit of the measured data. If no factors are entered for small field sizes in RadCalc, factors are extrapolated based on the method described by P Nizin et al[52]. However, it was decided that factors based on measured output factors would more closely represent the true values. A number of IMRT plan calculations were

performed using both RadCalc calculated and manually calculated S_c and S_p values. The results showed a difference of less than 1% in total plan dose.

The manually calculated factors were manually entered into the RadCalc software. Although factors were measured for a range of symmetric and asymmetric field sizes, RadCalc only allows the entry of factors for symmetric field sizes. For rectangular, asymmetric and blocked fields, S_c factors are calculated by RadCalc using a field-mapping technique[53]. Essentially, a detector's eye view is used to determine the composite field at the source plane. A Clarkson type integration is then performed on the head scatter.

The monitor unit calculation software tested in this study was RadCalc, produced by Lifeline Software Inc. RadCalc uses measured depth dose curves or TPRs, beam profiles, output factors, wedge factors etc to calculate the MUs required to deliver a given dose. The treatment plan data may either be entered into RadCalc manually or can be imported directly from a treatment planning system. RadCalc is capable of performing MU calculations for photon fields involving physical wedges, dynamic wedges, off-axis calculation points, asymmetric fields, tissue inhomogeneities, blocking and intensity modulation, as well as performing MU calculations for electron beams.

When a patient plan is opened, the plan data is displayed in 5 separate screens: Prescription, Photon Beams, Inhomogeneity Corrections, MLC Data and Points and Off Axis Assistance. These screens are shown for a sample patient in Figure 3-7, Figure 3-8, Figure 3-9, Figure 3-10 and Figure 3-11. By opening each of these screens, the planning/treatment data can be viewed, verified and edited.

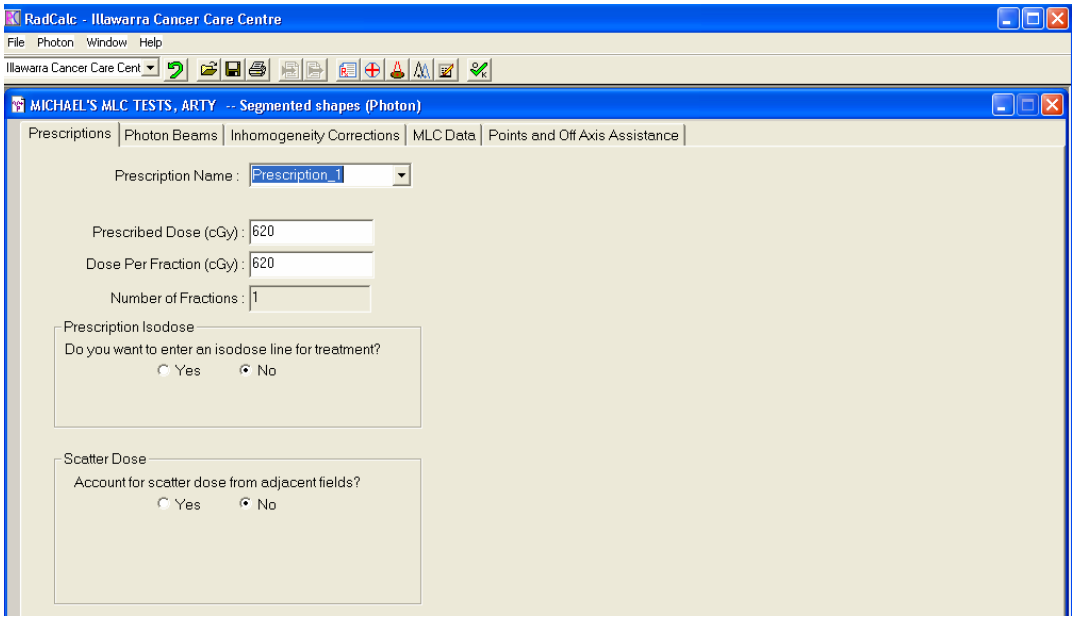

Figure 3-7. Screenshot of RadCalc Prescription window. This window allows the user to view and edit the plan prescription.

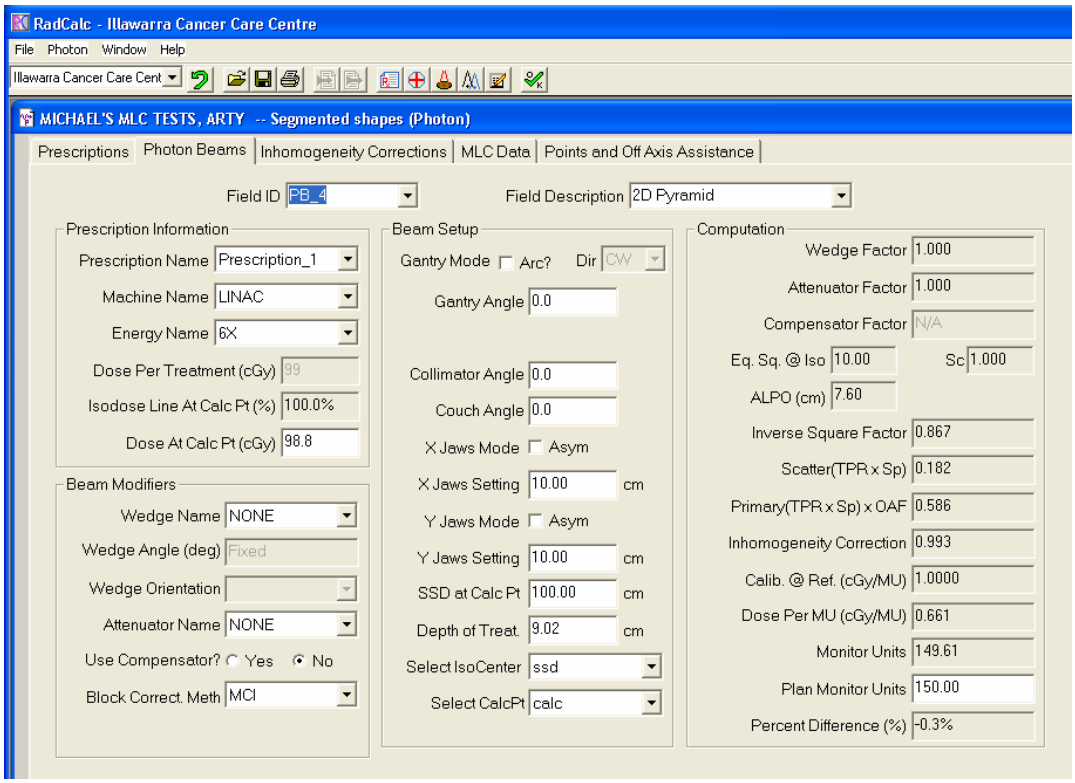

Figure 3-8. Screenshot of RadCalc Photon Beam window. This window allows the user to edit the beam parameters of each field, such as beam dose, wedges, field size and orientation, SSD, depth, as well as enter the calculated monitor units.

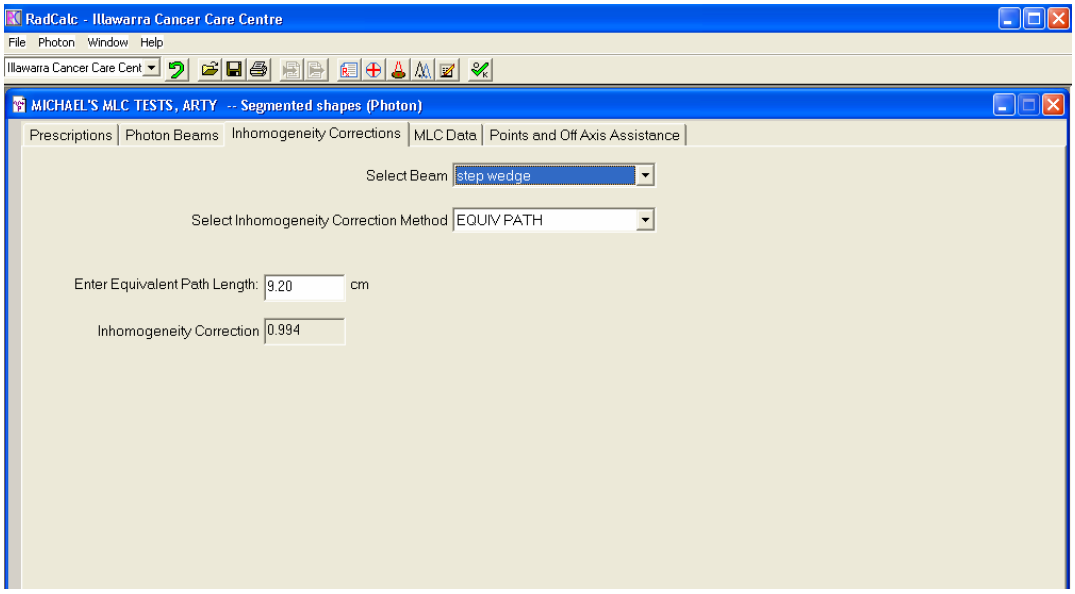

Figure 3-9. Screenshot of RadCalc Inhomogeneity Corrections window. This window allows the user to determine the inhomogeneity correction method used for each beam. The user can select between no correction, manually entering a correction factor, equivalent path length and Batho power law correction.

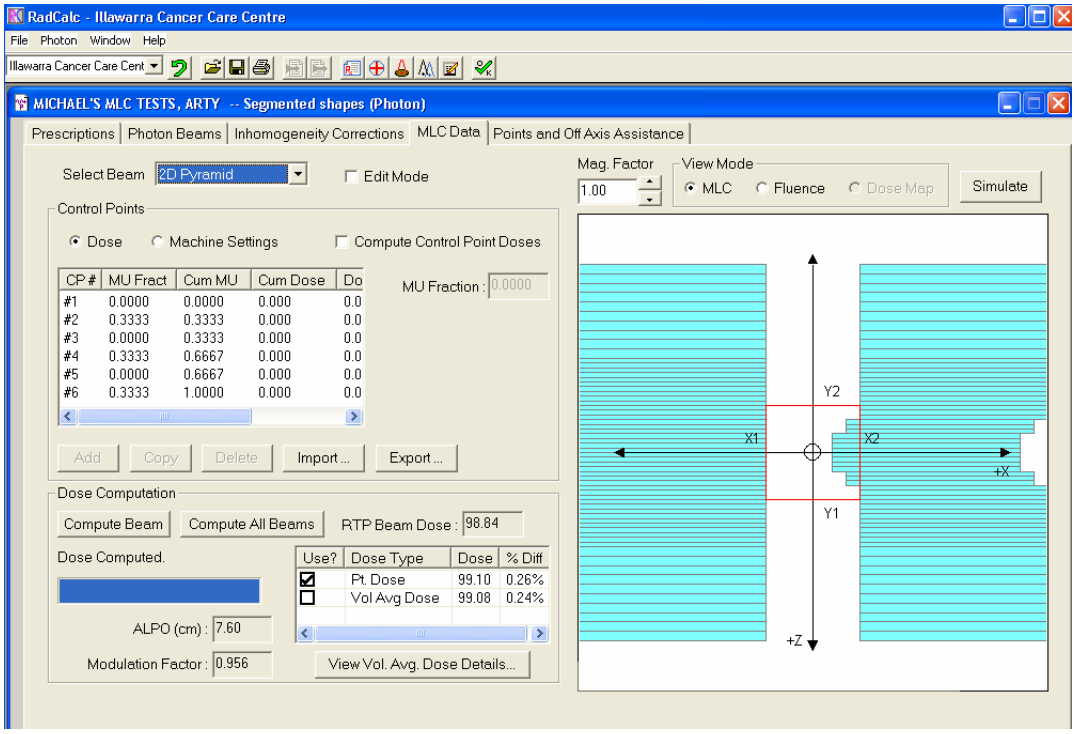

Figure 3-10. Screenshot of RadCalc MLC Data window. This window allows the user to view and edit MLC segment shapes and weightings, and display the fluence for each beam.

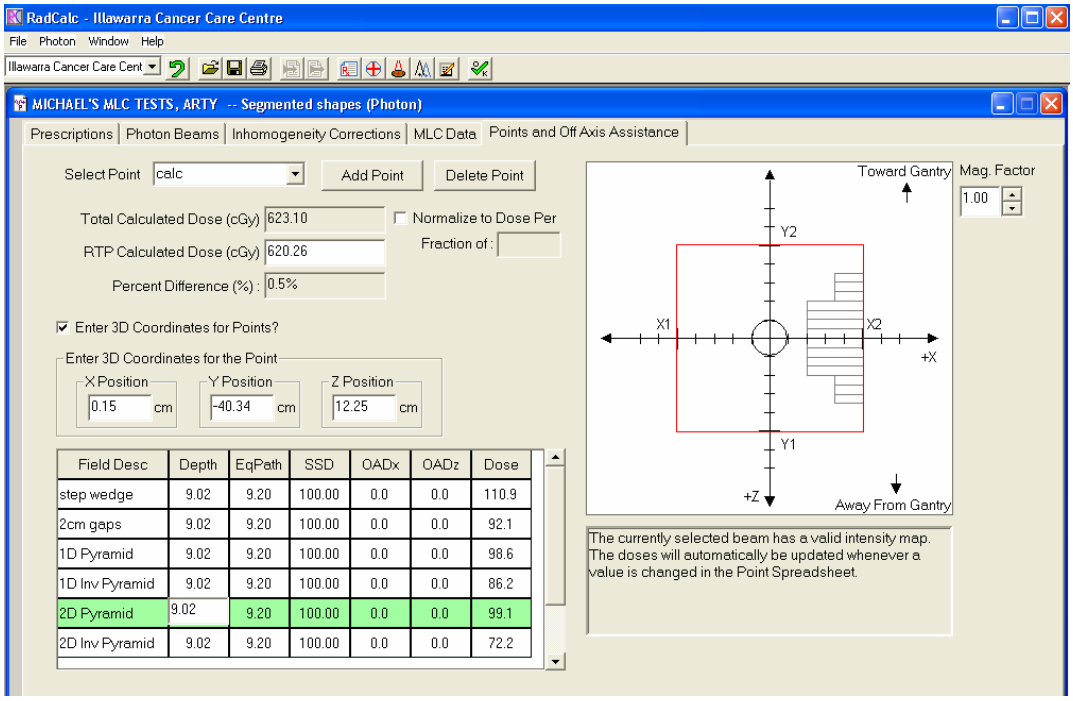

Figure 3-11. Screenshot of RadCalc Points and Off Axis Assistance window. This window allows the users to view a beams eye view of each beam, showing the position of the calc point. The user can also view the total treatment dose, as well as the dose for each field.

RadCalc is capable of importing plans with multiple prescriptions, which can be viewed and edited in the Prescriptions window (Figure 3-7). The Photon Beams window (Figure 3-8) allows the user to verify the data imported from the TPS for each field, make any additions or changes necessary, select block correction method and then view the calculated monitor units. While the dose for each field is directly imported from the TPS, the planned monitor units must be entered manually. Once this has been done, the percentage difference between planned monitor units and the RadCalc calculated monitor units is displayed. The Inhomogeneity Corrections window (Figure 3-9) allows the user to choose between different inhomogeneity correction methods: no correction, manually entered correction factor, equivalent path length and Batho power-law. Batho-power law may not be used for IMRT fields, so equivalent path length is used instead. The user can view and edit MLC segments by opening the MLC Data window (Figure 3-10). Fluence maps calculated by RadCalc can also be displayed in this window. For segmented and IMRT fields requiring a modified Clarkson integral block correction calculation, this window must be accessed to initiate the dose computation. In the Points and Off Axis Assistance window (Figure 3-11), points of interest may be added or deleted, and their 3D coordinates viewed or edited. By scrolling through each point, the

total dose delivered at that point for all fields as calculated by RadCalc and the TPS may be viewed, as well as the percentage difference. The RadCalc dose for each field, calculated using the planned monitor units, is also displayed. A beams eye view is displayed including MLC shapes and the selected point of interest. Once a MU calculation has been performed, the calculation is saved in a database.

Chapter 4: RadCalc Commissioning and Testing

4.1 Aims

The purpose of this chapter was to set-up and commission RadCalc for use in the IMRT quality assurance program at ICCC. This was broken down into the following steps:

1. Installation and functionality testing of RadCalc at ICCC
2. Commissioning of RadCalc for MU determination of conventional treatment field arrangements
3. Commissioning of RadCalc for MU determination of IMRT fields

4.2 RadCalc Installation and Setup

Initial testing of the RadCalc software was performed on a stand-alone system prior to its release on a user authenticated network. Data transfer between the Pinnacle[3] planning system and RadCalc was performed using an automated File Transfer Protocol (FTP) process that copied files from Pinnacle[3] onto the RadCalc system. These files were then manually imported into the RadCalc patient database. To test the integrity of the data transfer, several patient plans were exported from Pinnacle and the consistency of all the data imported into RadCalc confirmed. There were no errors detected, however several peculiarities were observed. These were that RadCalc could only import a plan that had dose calculated and also could only import one plan for a patient at a time, which presented workflow problems for multiple phase treatments.

Another observation was that occasionally the percentage blocked value for a given field differed between the plan summary printed by Pinnacle[3] and the value displayed in RadCalc. Upon further investigation it was found that this would occur for treatment fields that did not entirely intersect with the patient, such as breast tangents. The discrepancy was due to the fact that the value given by Pinnacle[3] was the percentage blocked, while the value displayed in RadCalc was the sum of the percentage blocked and the percentage of the unblocked field not intersecting the patient. While this value was not present on the plan summary printed by Pinnacle[3], it could be viewed and was verified on the Pinnacle[3] workstation.

Once the RadCalc software was installed, data was imported that was required for dose calculation, such as PDDs, beam profiles and output factors. RadCalc also requires a range of machine specific information including: source to axis distance, reference conditions, dose per MU calibration, the distance from the source to the top of the jaws, jaw transmission, minimum and maximum jaw positions and the direction of rotation of the couch, collimator and gantry. The standard used at the Illawarra Cancer Care Centre is IEC 1217[54]. Care had to be taken to ensure that the labels of things such as the jaws matched the labels used in Pinnacle[3]. Information regarding the MLCs was also required, including: the distance from the source to the top of the MLCs, MLC transmission, the minimum gap between leaves and the position and width of each leaf. Initially, the value entered into RadCalc for MLC transmission was 1.5%, the measured

intra-leaf transmission, where intra-leaf leakage is the amount of radiation transmitted through an individual MLC leaf, as opposed to the inter-leaf transmission, which is the amount of radiation transmitted between MLC leaves. However, a value of 2.4% was found to give better agreement to measured data for IMRT plans (refer to Chapter 5). The RadCalc doses presented in this chapter were recalculated subsequent to the changes made in section 5.4 using the new MLC transmission value.

A parameter can also be entered to account for transmission through the Varian round leaf ends, called the Radiation/Light Field Offset (RFO). The RFO is the difference between the 50% dose level of the radiation field and the projected light field at the source to axis distance. The RFO entered into RadCalc was 0.07cm, which is the value given in the RadCalc user manual and is supported by the literature for step and shoot IMRT[55,56].

Once all the required data had been imported into RadCalc, test plans were created to verify that RadCalc correctly looked up its factors. Plans were created within RadCalc with a range of depths and field sizes, for calculation points on central axis as well as off axis. For each plan, the S_c, S_p, TPR and OAR were checked against tables of measured data. RadCalc was confirmed to look up these factors correctly.

RadCalc was successfully installed, measured beam data was imported into RadCalc, and the RadCalc-Pinnacle^3 interface was setup so that plans could be exported from Pinnacle^3 and imported into RadCalc. Test plans confirmed the data integrity of plans imported from Pinnacle^3, as well as confirming that the correct data was being accessed by RadCalc for MU calculations.

4.3 Open field Verification Measurements

A test plan with open fields was created on RadCalc. Fields were created with a range of field sizes and depths, with central axis calculation points and off-axis calculation points, and with symmetric and asymmetric jaw positions. These fields were then delivered on the linac, using a Solid Water phantom, to determine whether RadCalc was calculating dose correctly. The NE 2571 Farmer chamber and 2570/1 Farmer electrometer were used for dose measurements. All measurements were performed at 100cm SSD. For each field, measurements were performed two or three times and the average taken. All chamber readings were normalised against the chamber reading when exposed to a known dose. The measured dose for each field was then compared to the dose predicted by RadCalc as shown in Table 4-1. The terms in brackets in column 3 refer to asymmetric fields (x_1, x_2) and (y_1, y_2) respectively.

Table 4-1. Measured and calculated doses (given in cGy), as well as percentage differences, for a series of open fields used to test RadCalc without effects from blocking. All fields were delivered to a Solid Water phantom, with SSD 100cm.

Beam	Depth (cm)	Field Size (cm)	OAD (x,y)	MU	Measured Dose (cGy)	RadCalc Dose (cGy)	Rad – Meas % Diff
1	1.5	5x5	0	100	94.3	94.8	0.5
2	1.5	10x10	0	100	100	100	0.0
3	1.5	20x20	0	100	105.5	105.7	0.2
4	1.5	(3,6)x(3,15)	0	100	99.9	101.5	1.6
5	1.5	10x10	3, 0	100	100.3	101.7	1.4
6	1.5	20x20	5, 5	100	107.7	109.3	1.5
7	5	5x5	0	100	80.1	80	-0.1
8	5	10x10	0	100	86.8	86.3	-0.6
9	5	20x20	0	100	92.4	92.3	-0.1
10	5	(3,6)x(3,15)	0	100	86.3	88.1	2.1
11	5	10x10	3, 0	100	85.8	87.1	1.5
12	5	20x20	5, 5	100	93.4	94.4	1.1
13	10	5x5	0	200	119.3	118	-1.1
14	10	10x10	0	200	134.2	132	-1.6
15	10	20x20	0	200	147.3	146	-0.9
16	10	(3,6)x(3,15)	0	200	132.8	136.1	2.5
17	10	10x10	3, 0	200	131.3	133	1.3
18	10	20x20	3,3	200	147.5	147.8	0.2

As shown in Table 4-1, for symmetric open fields, RadCalc calculates dose to within ±1.6% of measured dose. Differences of up to 2.5% were observed for the asymmetric fields.

A further test was performed to test RadCalc's ability to account for asymmetric fields and off-axis calculation points. A 10x10cm jaw opening was used for each field, with the calculation point at the centre of the field. However, the field was shifted off central axis, in 2cm steps as shown in Figure 4-1. These fields were treated isocentrically (91cm SSD, 9cm depth) on the I'mRT phantom, using the CC13 ionisation chamber and NE 2570/1 electrometer. The chamber was placed at the centre of field by shifting the phantom 2cm for each field. Table 4-2 contains the measured and calculated doses.

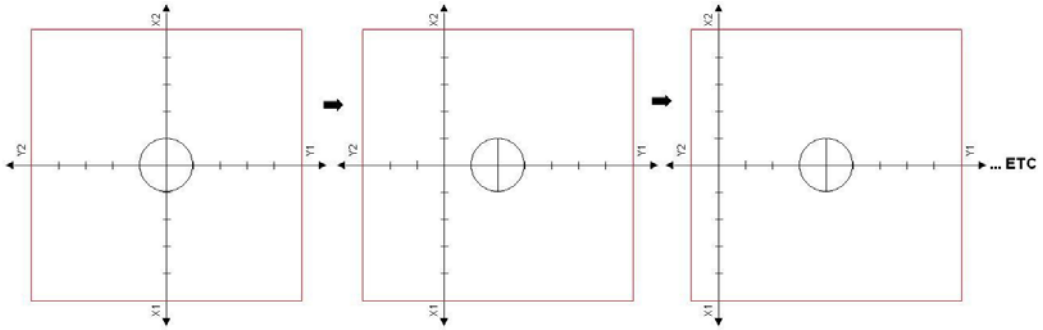

Figure 4-1. Diagram of 10x10cm off-axis fields, with calculation point placement, used to test RadCalc's off-axis calculation. Fields were shifted off axis in 2cm increments, while the measurement/calc point was kept in the centre of field for each beam.

Table 4-2. Measured and calculated doses, as well as percentage differences, for 10x10cm off-axis fields used to test RadCalc's off-axis calculation. All fields were delivered to the I'mRT phantom, with the chamber placed at 9cm depth, 91cm SSD.

Beam	Field Size (cm)	OAD (x,y)	MU	Measured Dose (cGy)	RadCalc Dose (cGy)	Rad – Meas % Diff
1	10x(3,7)	0, 2	100	82.7	81.7	-1.2
2	10x(1,9)	0, 4	100	83.3	81.6	-2.0
3	10x(-1,11)	0, 6	100	84.2	82	-2.6
4	10x(-3,13)	0, 8	100	84.5	82	-3.0
5	10x(-5,15)	0, 10	100	84.6	81.8	-3.3
6	10x(-7,17)	0, 12	100	84.8	82.3	-2.9
7	10x(-9,19)	0, 14	100	84.9	81.2	-4.4

As seen in Table 4-2 there was a systematic difference between the measured doses and the doses calculated by RadCalc for fields where the centre of field is off central axis. The difference increased as the distance between the centre of field and central axis increased, up to a difference of -4.4%. This is due to RadCalc's off axis ratio calculation method. As described in Chapter 2.4, RadCalc calculates OARs by taking the product of the POCR and the BF. From investigation, it appears that in this case RadCalc incorrectly determined the BF. For example, for the 10cm off-axis field, the expected

OAR would be approximately 1.019 (taken from a 40x40 beam profile @ d_{10}), while RadCalc uses an OAR of 1.005. If the field size is increased such that the calculation point is greater than 5cm from the field edge, this value increases to 1.022. Unfortunately, since RadCalc provides little information on how the BF is calculated, or how it can be corrected, there is no way to compensate for this. In addition to this, the S_c and S_p values used by RadCalc for the asymmetric fields were the same as for a symmetric 10x10cm field (1.000). Although the effect should be relatively minor, both the head scatter and phantom scatter conditions would be expected to be slightly different for an asymmetric field, contributing to the differences seen in Table 4-2.

Finally, a test was performed to determine RadCalc's agreement with measured doses for fields with oblique angle of incidence. 5x5cm, 10x10cm and 20x20cm fields with gantry angles 0, 10, 30 and 45 degrees were used to irradiate a Solid Water phantom. Doses were measured using the NE 2571 Farmer chamber, placed at a depth of 5cm, and 2570/1 Farmer electrometer, with the fields treated isocentrically.

Table 4-3. Measured and calculated doses, as well as percentage differences, for a series of oblique incidence fields. All fields were delivered to a Solid Water phantom, with the chamber placed at isocentre, at a depth of 5cm.

Beam	Field Size (cm)	Gantry Angle	MU	Measured Dose (cGy)	RadCalc Dose (cGy)	Rad – Meas % Diff
1	5x5	0	100	88.1	87.7	-0.5
2	5x5	10	100	87.9	87.4	-0.6
3	5x5	30	100	85.5	84.9	-0.7
4	5x5	45	100	81.1	80.4	-0.9
5	10x10	0	100	95.2	94.6	-0.6
6	10x10	10	100	95.2	94.4	-0.8
7	10x10	30	100	92.8	92.3	-0.5
8	10x10	45	100	88.6	88.2	-0.5
9	20x20	0	100	101.2	101.1	-0.1
10	20x20	10	100	101.1	100.9	-0.2
11	20x20	30	100	99.2	99	-0.2
12	20x20	45	100	95.4	95.6	0.2

It is expected that some difference would be observed between measured dose and the doses calculated by RadCalc for oblique fields, as RadCalc has no way of accounting for oblique incidence or surface curvature. Although RadCalc can account for the depth of measurement, it cannot account for the change in phantom scatter due to the angle of incidence of a radiation field. As seen in Table 4-3, for field sizes and gantry angles tested, the magnitude of this difference was less than %1 for all field sizes. The largest

observed difference was %-0.9 for the 5x5cm field at a 45 degree angle of incidence. Therefore, it is expected that oblique incidence will have some impact on RadCalc's accuracy for IMRT calculations, particularly in the head and neck region, because of the large curvature and surface irregularities. However, this impact will be minimal.

In summary, the agreement between RadCalc and measurement is such that RadCalc calculates dose to within ±1.6% of measurement for symmetric open fields, underestimates dose by a maximum of approximately 1% for oblique incidence less than 45 degrees and underestimates dose for asymmetric fields by up to 4.4%.

4.4 Blocked Field Verification Measurements

Similarly, the accuracy of RadCalc for blocked fields was tested by creating a test plan, treating the planned fields on the linac, and comparing the calculated and measured doses. The agreement between Pinnacle^3 planned dose and measured dose is also shown for comparison. Each field was created on Pinnacle^3 using a CT dataset of the I'mRT phantom and exported to RadCalc. The non-water density of the I'mRT phantom was taken into account as the effective path length to the calculation point for each field based on the CT dataset was exported from Pinnacle^3. Single segment MLC blocked fields were created as shown in Figure 4-2, including a series of square shapes decreasing in size down to 3cmx3cm (field (a)), a zigzag shape (field (b)), a diamond shape (field (c)), a series of rectangular shapes becoming increasingly elongated but with the same area (fields (d), (e) and (f)), a series with a 4x4cm square at the bottom of the field, which would surround the measurement point, and a rectangular opening of varying width at the top of the field (field (g)), and a field in which the MLCs blocked the calculation point (field (h)). These fields were then used to irradiate the I'mRT phantom on the linac. The phantom was placed at an SSD of 100cm and dose was measured using the CC13 chamber placed at a depth of 9cm, connected to a NE 2570/1 electrometer. Chamber readings were normalised against the chamber reading when exposed to a known dose.

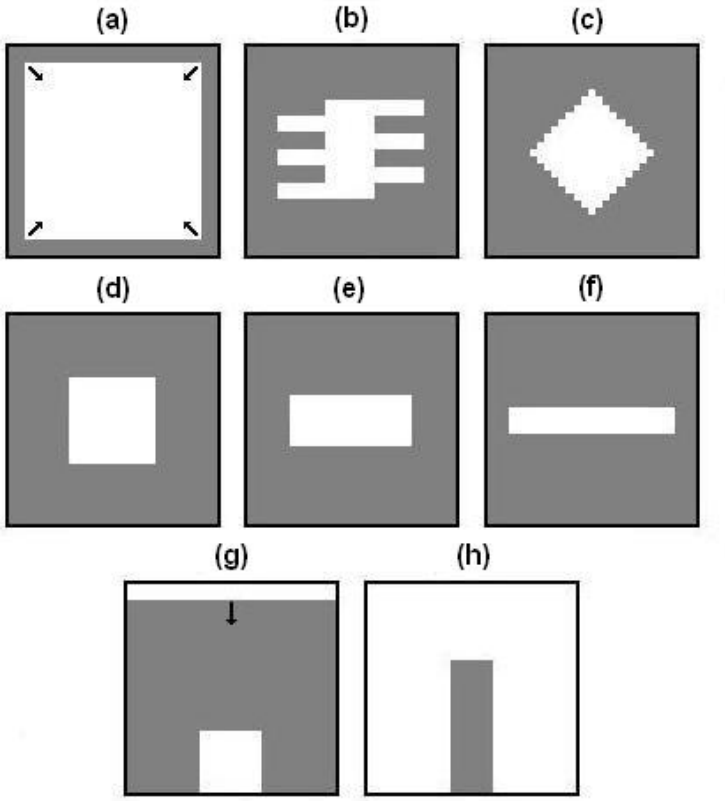

Figure 4-2. Diagram showing single segment MLC shapes used in blocked field verification experiment: a) a series of square fields with decreasing area; b) a zigzag shaped field with 36cm^2 area; c) a diamond shaped field with36cm^2 area; d) a square with 36cm^2 area; e) a rectangle with 36cm^2 area; f) a thinner rectangle with 36cm^2 area; g) a series of shapes with a 4x4 cm opening surrounding the measurement/calculation point at the bottom and a rectangular opening of increasing thickness at the top; and h) a field with a block covering the measurement/calculation point

Table 4-4. Measured and calculated doses, as well as percentage differences, for a series of blocked fields used to test RadCalc's modified Clarkson integral block correction. All fields were delivered to the I'mRT phantom with the chamber placed on central axis, at 9cm depth, 100cm SSD. Pinnacle calculated data is also presented for comparison.

Beam	Field Size (cm)	Blocking	MU	Measured Dose (cGy)	RadCalc Dose (cGy)	Rad - Meas % Diff	Pinnacle Dose (cGy)	Pinn - Meas % Diff
1	10x10	Shape (a) - 8x8	150	102.2	101.1	-1.1	101.1	-1.1
2	10x10	Shape (a) - 6x6	150	99.1	98.4	-0.7	98.1	-1.0
3	10x10	Shape (a) - 5x5	150	96.9	96.5	-0.4	96.0	-0.9
4	10x10	Shape (a) - 4x4	150	94.2	94.1	-0.1	93.4	-0.8
5	10x10	Shape (a) - 3x3	150	90.5	91.1	0.7	89.9	-0.7
6	10x10	Shape (a) - 2x2	150	85.3	87	2.0	85.4	0.1
7	15x15	Shape (d) - 6x6	150	100	99.9	-0.1	99.7	-0.3
8	15x15	Shape (e) - 4x9	150	98.2	98.7	0.5	98.8	0.6
9	15x15	Shape (f) - 3x12	150	95.9	96.9	1.0	95.7	-0.2
10	15x15	Shape (b) – 6x6(zigzag)	150	98.1	98.7	0.6	98.4	0.3
11	15x15	Shape (c) – 6x6(diamond)	150	100	100	0.0	99.9	-0.1
12	15x(2,13)	Shape (g) – 4x4 + 0x15	150	93.4	95.7	2.5	93.3	-0.1
13	15x(2,13)	Shape (g) – 4x4 + 2x15	150	93.7	96	2.5	93.5	-0.2
14	15x(2,13)	Shape (g) – 4x4 + 4x15	150	93.9	96.4	2.7	93.9	0.0
15	15x(2,13)	Shape (g) – 4x4 + 6x15	150	94.6	97.1	2.6	94.4	-0.2
16	15x(2,13)	Shape (g) – 4x4 + 8x15	150	95.6	98.1	2.6	95.0	-0.6
17	15x(2,13)	Shape (g) – 4x4 + 10x15	150	97.6	100	2.5	96.9	-0.7
18	10x10	Shape (h) – Chamb. Block	600	66.1	64	-3.2	64	-3.2

As shown in Table 4-4, RadCalc shows good agreement with measured doses. For the fields with square openings, the calculated doses agree with measured doses to within ±1%, down to a block field size of 3x3cm. For a field size of 2x2cm the difference was 2%. Part of this larger difference can be attributed to the volume averaging effect of the chamber[57]. While the dose calculated by RadCalc is for a point, the ion chamber dose is measured over a volume. For such a small field, the dose will not be homogenous over the entire chamber volume, with the dose averaged over the chamber volume. For the rectangular, diamond and zigzag fields, RadCalc doses agreed with measured doses to within ±1%. For the fields with the varying scatter contribution, there was a difference of approximately 2.5%, which remained relatively constant regardless of the size of the scatter volume. This difference is probably due to inaccuracy in RadCalc's asymmetric field calculation as noted in section 4.3, rather than its ability to account for the shape of the blocking. For the field with the calculation point blocked by the MLCs, the difference was -3.2%. Similar to the 2x2cm blocked field, this difference is mostly due

to volume averaging effects. The MLC block was 2cm wide, leading to a dose gradient across the chamber volume. The dose at the outer edges of the chamber would have been higher due to scatter from the adjacent high dose regions, while the dose at the centre of the chamber, where dose was calculated by RadCalc and Pinnacle^3 would have been lower, resulting in a higher measured dose than calculated dose. Interleaf leakage, which is not accounted for by RadCalc, may also have contributed to this difference. Overall, agreement between RadCalc and measured doses was similar to that between Pinnacle^3 and measured doses.

4.5 Segmented Field Verification Measurements

A series of segmented fields were used to test the accuracy of RadCalc's calculation algorithm in step and shoot IMRT fields. As with the blocked fields, each field was created on Pinnacle^3 using a CT dataset of the I'mRT phantom and exported to RadCalc. The non-water density of the I'mRT phantom was taken into account as the effective path length to the calculation point for each field based on the CT dataset was exported from Pinnacle^3. The fields were delivered to a flat, homogeneous phantom, such that the results would be independent of patient surface curvature and tissue heterogeneities. Fluence maps, taken from RadCalc, of the multi-segment fields created are shown in Figure 4-3. As opposed to intensity maps, which show a 2D map of the ideal beam intensity distribution, the fluence maps taken from Pinnacle^3 show an approximation of the delivered intensity distribution, including partial MLC transmission effects as seen in Figure 4-3. Field (a) was a step wedge pattern created by stepping the full MLC bank across the field in 1.5cm increments. Field (b) was created by stepping a 2cm wide opening along the field. Field (c) was a one dimensional pyramid profile with the maximum dose in the centre of the field. Field (d) was a one dimensional inverse pyramid profile, with the minimum dose at the centre of the field. Field (e) was a two dimensional pyramid profile, with the maximum dose at the centre of the field. Field (f) was a two dimensional inverse pyramid with the minimum dose at the centre of the field. For each field, all segment weights were equal. The segmented shapes used to create these fluence maps are shown in detail in Appendix A.

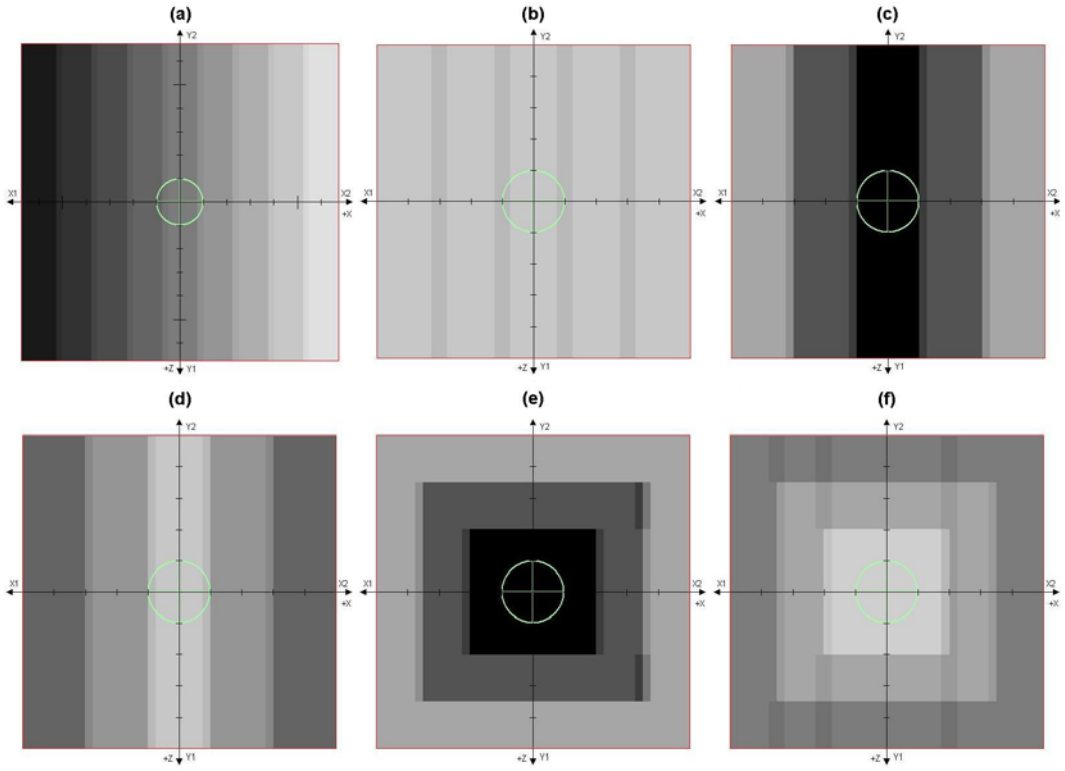

Figure 4-3. Diagram showing fluence maps of segmented fields used to further test RadCalc's block correction method: a) step-wedge pattern; b) a series of 2cm wide openings stepped across the field; c) a one dimensional pyramid pattern; d) a one dimensional inverse pyramid patter; e) a two dimensional pyramid patter; and f) a two dimensional inverse pyramid pattern.

These fields were then used to irradiate the I'mRT phantom on the linac. The fields were delivered perpendicular to the flat upper surface of the phantom. The phantom was placed at an SSD of 100cm and dose was measured using the CC13 chamber placed at a depth of 9cm, connected to a NE 2570/1 electrometer. Chamber readings were normalised against the chamber reading when exposed to a known dose. The monitor units for the standard reading were scaled to account for the depth dose in the I'mRT phantom. The measured and calculated doses are summarised in Table 4-5.

Table 4-5. Measured and calculated doses, as well as percentage differences, for a series of segmented fields used to test RadCalc's block correction method. All fields were delivered to the Im'RT phantom, with the chamber placed on central axis, at 9cm depth, 100cm SSD. Pinnacle calculated data is also presented for comparison.

Beam	Field Size (cm)	Blocking	MU	Measured Dose (cGy)	RadCalc Dose (cGy)	Rad - Meas % Diff	Pinnacle Dose (cGy)	Pinn - Meas % Diff
1	13.5x13.5	step wedge	300	111.1	110.9	-0.2	110.3	-0.7
2	10x10	2cm gaps	600	90.6	92.1	1.7	91.4	0.9
3	10x10	1D Pyramid	150	99.2	98.6	-0.6	98	-1.2
4	10x10	1D Inv Pyram	500	86.1	86.2	0.1	85.9	-0.2
5	10x10	2D Pyramid	150	99.9	99.1	-0.8	98.8	-1.1
6	10x10	2D Inv Pyram	500	70.3	72.2	2.7	71.9	2.3

For segmented fields, RadCalc and measured doses agreed to within ±3%. The largest discrepancies occurred for fields where the calculation point was heavily blocked by the MLCs. For theses fields, any inaccuracy in the MLC transmission value used by RadCalc, or in RadCalc's block correction algorithm, will have an increased effect, because a large proportion of the dose is due to transmission. If differences between measured and calculated dose have been observed for these relatively simple segmented fields, increased differences would be expected for complex IMRT fields, with greater differences for more heavily blocked fields. In IMRT, these fields usually occur when there are a large number of segments and a low dose per monitor unit ratio.

4.6 Anterior IMRT Field Verification Measurements

A total of 22 IMRT fields from patient plans were selected and delivered to the I'mRT phantom incident perpendicular to the phantom surface. Each field was created on Pinnacle^3 using a CT dataset of the I'mRT phantom and exported to RadCalc. The non-water density of the I'mRT phantom was taken into account as the effective path length to the calculation point for each field based on the CT dataset was exported from Pinnacle^3. As with the segmented field tests, the flat, homogeneous phantom meant that the accuracy of RadCalc's block correction algorithm could be tested independent of surface curvature and tissue inhomogeneity effects. The fluence map of a sample field is shown in Figure 4-4. All fields were delivered with the gantry at an angle of 0 degrees, with the SSD at 91cm and the CC13 chamber placed at 9cm depth. All chamber readings were taken on the central axis of the field regardless of the fluence distribution. This meant that, as with the field shown in Figure 4-4, the chamber was not always in the most ideal position (i.e. a region of both maximum and uniform dose). Chamber readings were normalised against the chamber reading when exposed to a known dose.

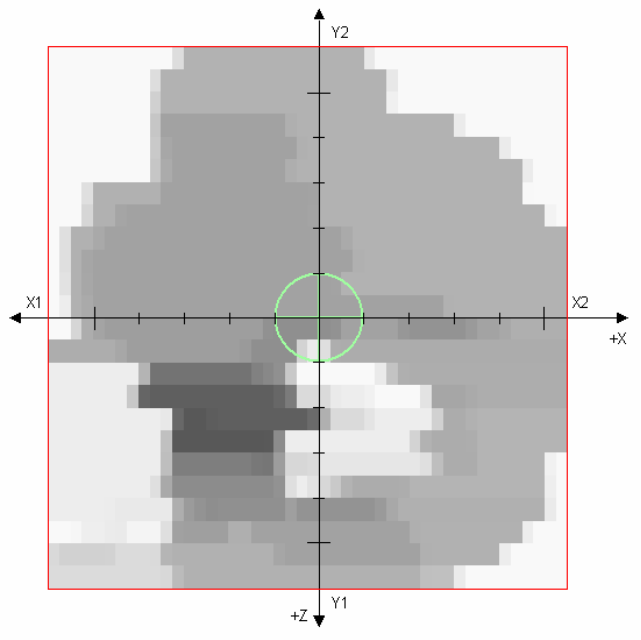

Figure 4-4. An example of a fluence map of an IMRT field.

Table 4-6. Measured and calculated doses, as well as percentage differences, for a series of IMRT fields delivered to the Im'RT phantom, with the chamber placed at 9cm depth, 91cm SSD with incidence perpendicular to the phantom surface. Pinnacle calculated data is presented for comparison.

Beam	MU	Measured Dose (cGy)	RadCalc Dose (cGy)	Pinnacle Dose (cGy)	Rad - Meas % Diff	Pinn - Meas % Diff
1	98	29.5	30.9	30.2	4.7	2.4
2	70	14.9	16.6	17.1	11.4	14.8
3	74	3.8	3.8	4.1	0.0	7.9
4	90	23.2	23.4	23.2	0.9	0.0
5	111	44.4	45.7	44	2.9	-0.9
6	75	23.1	23.4	23.1	1.3	0.0
7	64	25.0	25.8	25.5	3.1	1.9
8	61	27.7	27.6	27.5	-0.4	-0.7
9	74	17.1	18.0	17	5.3	-0.6
10	87	36.4	37.1	37.2	1.9	2.2
11	125	19.5	18.1	19.9	-7.2	2.1
12	98	48.4	48.2	48.6	-0.4	0.4
13	63	26.5	25.4	26.2	-4.2	-1.1
14	49	29.6	30.0	29.2	1.3	-1.4
15	86	36.2	36.1	36.5	-0.3	0.8
16	62	18.6	18.5	18.4	-0.3	-0.9
17	119	37.8	40.7	36.9	7.7	-2.4
18	290	27.1	24.6	27.7	-9.2	2.2
19	247	17.8	18.2	19.2	2.4	8.0
20	113	47.4	49.5	47.7	4.4	0.6
21	91	36.8	36.2	36.9	-1.5	0.3
22	93	38.6	41.2	39.6	6.7	2.6

As the data in Table 4-6 shows, significant differences between calculated and measured doses were observed. Analysis of each field showed no obvious correlation with the magnitude of the percentage difference. The mean difference was 1.4% with a standard deviation of 4.6%. For all but one field, RadCalc and measured doses agreed to within ±10%. This variation is substantially larger than the range observed for conventional fields and would make it difficult to identify subtle planning errors based on RadCalc calculations alone. However, gross errors (>10%) could still be identified. In comparison, the mean difference between Pinnacle[3] and measured doses was 1.7% with a standard deviation of 3.9%. However, it should be noted that with the exception of beams 2, 3 and 19, Pinnacle shows less deviation than RadCalc. Ignoring these beams, the mean difference would be 0.4% with a standard deviation of 1.5%. In practice, fields 2, 3 and 19 would be further investigated with the most likely course of action to be choosing a more suitable measurement point, and repeating the measurement. It should also be noted that while there were large percentage differences, the actual difference in dose was relatively small. As most IMRT treatments employ

multiple fields, the beam weights are often relatively small. The dose difference for these fields was never greater than 3cGy.

4.7 Conclusions

RadCalc was successfully installed, measured beam data was imported into RadCalc, and the RadCalc-Pinnacle^3 interface was set up so that plans could be exported from Pinnacle^3 and imported into RadCalc. Test plans verified the data integrity of plans imported from Pinnacle^3, as well as confirming the integrity of RadCalc's data look-up for MU calculations.

RadCalc was commissioned for conventional treatments by delivering test fields to a Solid Water phantom. For symmetric fields with a range of field sizes and for off-axis calculation points and oblique angles of incidence, the measured dose and the dose calculated by RadCalc were found to agree to within 1%. However, for asymmetric fields, there was found to be a systematic difference. A further test showed that if the calculation point is placed at the centre of field for asymmetric fields, there is a systematic difference in the opposite direction of up to -4.4%. This difference also tends to increase the further the centre of field is from the central axis of the machine. The effect was attributed to RadCalc overestimating boundary effects for asymmetric fields when the calculation point was within 5cm of the field edge. This has potential implications for head and neck IMRT plans that utilise asymmetric fields.

RadCalc was commissioned for MU determination of IMRT fields by performing phantom measurements of test fields for blocked, segmented and IMRT fields. For blocked fields, RadCalc and measured doses agreed to within ±2% for the symmetric fields, while for a series of asymmetric fields the difference increased to up to 2.7%. In comparison, Pinnacle^3 and measured doses agreed to within ±1.1% for these fields. For a field in which the MLCs blocked the measurement/calculation point, both RadCalc and Pinnacle underestimated dose by 3.2% compared to measured dose.

For segmented fields, RadCalc and measured doses agreed to within ±2.7%. In comparison Pinnacle^3 and measured doses agreed to within ±2.3%. A trend was noted that the greatest differences between calculated and measured dose occurred for beams where the calculation point was heavily blocked. For IMRT fields, the difference between RadCalc and measured doses varied over a wide range (-9.2% to 11.4%). The differences can be attributed to RadCalc's simplistic MLC modelling, approximations in

the RadCalc block correction algorithm, and volume averaging chamber effects. The difference was less than 10% for most fields, with an average difference of 1.4%. The difference between Pinnacle and measured dose varied from -2.4% to 14.8%, with an average difference of 1.7%. For routine use of RadCalc in IMRT QA to be practical, an action level greater than that for conventional fields would be required.

Chapter 5: IMRT Patient Cases

5.1 Aims

The purpose of this chapter was to determine RadCalc's suitability for use in IMRT plan QA. This was broken down into the following steps:

1. Compare RadCalc calculated dose to measured dose for IMRT phantom plans, and compare Pinnacle^3 dose to measured dose for comparison with the RadCalc data
2. Analyse these data and make adjustments in RadCalc to maximise agreement between RadCalc calculated dose and measured dose
3. Compare RadCalc dose with Pinnacle^3 dose for IMRT patient plans
4. Determine the strengths and weaknesses of RadCalc for IMRT plan verification

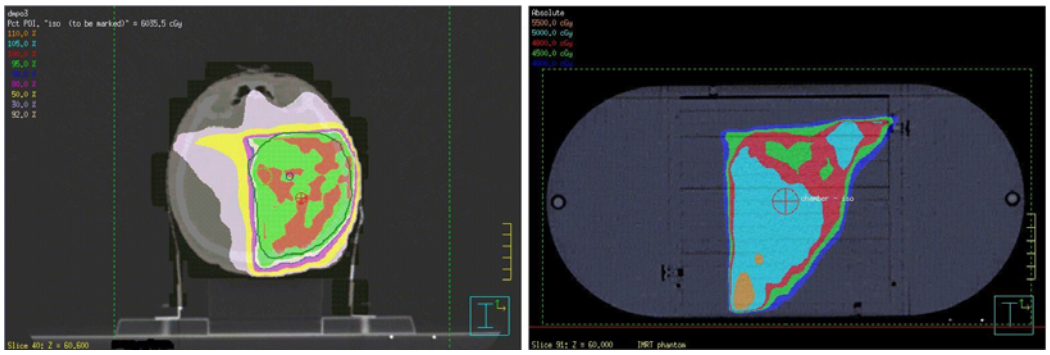

Figure 5-1. Transverse CT slice of a patient (left), showing isodose curves for a sample IMRT plan, as well as a transverse CT slice of the I'mRT phantom (right) showing isodose curves calculated from the sample patient plan, which has been copied onto the phantom dataset.

Thirty-two patient cases, since the ICCC's acquisition of the I'mRT phantom and Pinnacle^3 version 7.4, were included in this project. Each patient was treated in the head and/or neck region as that was the only clinical site currently treated using IMRT at ICCC. All plans were created on a Pinnacle^3 workstation by ICCC radiotherapists. Once a plan was completed, a phantom plan was created. The beams from the patient plan were transferred to a new plan with the patient CT dataset replaced with an I'mRT phantom CT dataset. A sample IMRT plan is shown in Figure 5-1, showing isodose curves for both the patient plan and the phantom plan. A phantom measurement was then performed by a medical physicist. The isocentre was positioned such that it aligned with the centre of the ionisation chamber. The monitor units for both plans were kept the same; hence the segment weights and MU were identical for patient and phantom delivery. However, the dose to the calculation point differed between the two plans due to the effective path length and surface contours being different. Generally, the dose at the calculation point for the phantom plan was lower than the dose for the patient plan as the effective path length was usually greater for the phantom plan.

The patient plan and the phantom plan were exported to RadCalc, and the total dose and dose per field recorded. The phantom plan was exported to the record-and-verify system, Varis. The plan was delivered to the I'mRT phantom on the linac. The CC13 chamber connected to the NE 2570/1 electrometer was used for dose measurements. As with previous measurements, chamber readings were normalised against the chamber

reading when exposed to a known dose. These data were then entered into a spreadsheet, where it was analysed and compared to the doses calculated by RadCalc and Pinnacle[3]. Table 5-1 and Table 5-2 contain the data collected for a sample patient. Appendix B contains the complete data collected for all patients.

Table 5-1. Calculated and measured dose data, as well as percentage differences, for a sample I'mRT phantom plan (Patient 31 in Appendix B). Measurements were performed on the I'mRT phantom, with the chamber placed at the calculation point of the plan. Pinnacle calculated data is presented for comparison.

Beam Name	MU	Measured Dose (cGy)	RadCalc Dose (cGy)	Pinnacle Dose (cGy)	RadCalc vs Measured % Difference	Pinnacle vs Measured % Difference
30	81	33.3	32.9	32.7	-1.2	-1.8
82	135	25.9	25.2	25	-2.7	-3.5
140	71	24.3	24.1	24.1	-0.8	-0.8
180	143	35.7	35.7	34.7	0.0	-2.8
210	83	32.8	35.1	35.3	7.0	7.6
275	65	7.3	6.9	7	-5.5	-4.1
310	31	12.9	13.0	12.7	0.8	-1.6
	Total	172.2	172.9	171.5	0.4	-0.4

Table 5-2. Pinnacle and RadCalc dose data for a sample patient (Patient 31in Appendix B) CT dataset plan.

Beam Name	MU	Pinnacle Dose (cGy)	RadCalc Dose (cGy)	% Difference
30	81	36.1	36.9	2.2
82	135	58.7	57.9	-1.4
140	71	27.0	28.0	3.7
180	143	42.6	41.9	-1.6
210	83	21.4	21.9	2.3
275	65	6.0	6.1	1.7
310	31	10.9	10.9	0.0
	Total	202.7	203.6	0.4

Measurements performed with repeated set-ups showed that the precision of the electrometer was the greatest limiting factor in the reproducibility and precision of these phantom measurements. The standard deviation of measurements for repeated set-ups was 0.0052 nC and the precision of the electrometer was 0.005 nC. The limitation of this precision is most evident for low charge readings, which are common for clinical IMRT fields. Of the seven clinical fields measured the lowest charge recorded was 0.250 nC and therefore a precision of 0.005 nC equates to 2%. The full results of this experiment are contained in Appendix C.

5.3 IMRT Phantom Plan Results

Once measurements and calculations had been performed for all patients, the data was analysed to determine the agreement between RadCalc and measured dose. A scatter plot of the percentage difference between RadCalc and measured dose versus the percentage difference between Pinnacle[3] and measured dose for the individual IMRT fields is shown in Figure 5-2.

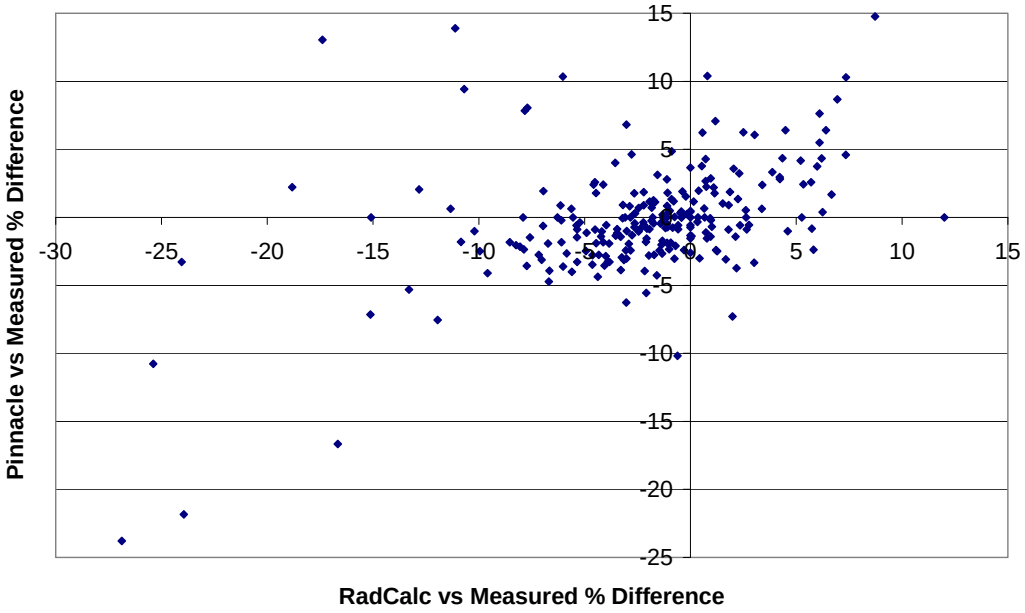

Figure 5-2. Scatter plot of percentage difference in dose per field between RadCalc and ion chamber measurement, versus Pinnacle and ion chamber measurement, for I'mRT phantom plans.

The data in Figure 5-2 shows a wide variation in the percentage difference between RadCalc and measured dose. As with the IMRT fields from section 4.6, for many of the fields, the percentage differences between RadCalc and measured dose are much greater than would normally be accepted for conventional treatments. These large differences are due to a combination of effects mentioned previously in Chapter 4: non-ideal calculation/measurement points, volume averaging effects of the measurement chamber, and inaccuracies in RadCalc's calculation algorithm. As noted in section 4.6, the dose delivered per field is frequently relatively small (less than 10-20 cGy). While the percentage difference may be quite large, the actual difference in cGy may be small, and of little clinical significance. The average percentage difference between RadCalc and

measured dose was -2.3%, with a standard deviation of 5.5%. The systematic under-prediction of dose by RadCalc is addressed in section 5.4. In comparison, the average percentage difference per field between Pinnacle and measured dose was -0.2%, with a standard deviation of 4.3%.

Since the percentage difference in total dose is commonly used to express treatment QA results, a scatter plot was created showing the percentage difference per plan between RadCalc and the measured dose versus the percentage difference per plan between Pinnacle[3] and the measured dose for the I'mRT phantom plans. .

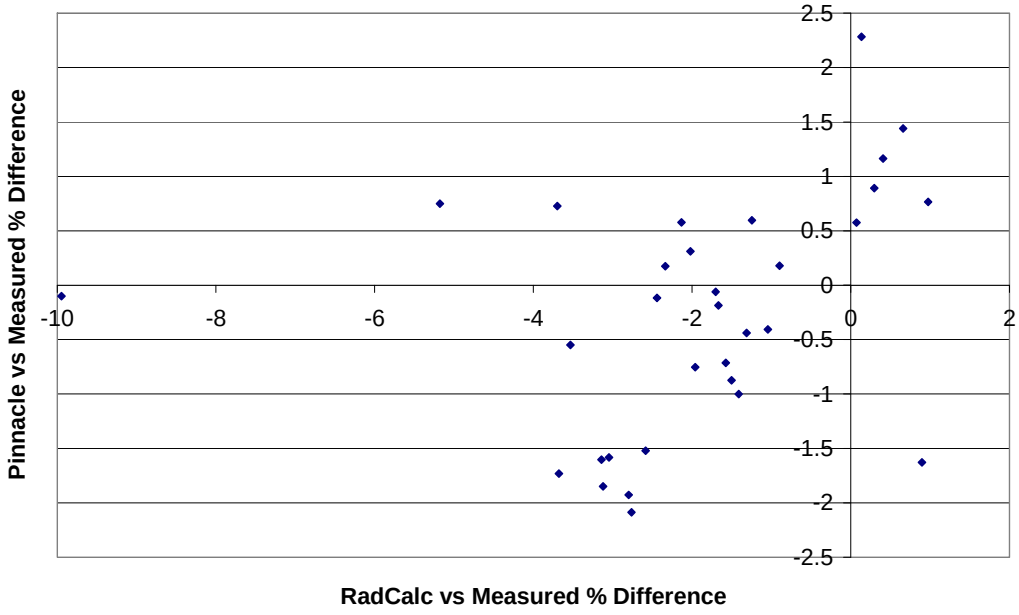

Figure 5-3. Scatter plot of percentage difference in total treatment dose between RadCalc and ion chamber measurement versus Pinnacle and ion chamber measurement, for I'mRT phantom plans.

As Figure 5-3 shows, there is much less variation in percentage difference per plan between RadCalc and measured dose, than for the dose per field. Although the percentage differences per field were often large, the actual dose differences are small. If these are positive and negative differences, they tend to compensate for one another, resulting in closer agreement for the total plan dose. The average percentage difference between RadCalc and measured dose was -1.9%, with a standard deviation of 1.8%. In comparison, the average percentage difference between Pinnacle[3] and the measured dose was -0.3%, with a standard deviation of 1.1%. There appears to be no correlation

between the RadCalc vs Measured and Pinnacle vs Measured datasets, although this may be due to the small number of data points.

5.4 MLC Transmission Effect

It is apparent from Figure 5-2 and Figure 5-3 and the mean dose differences that RadCalc systematically under-predicted dose by an average of 2.3% compared to measured doses. It was found that the dose calculated by RadCalc could be adjusted by changing the MLC transmission parameter. The results in section 5.3 were calculated with the MLC transmission parameter set to 1.5%, which was the measured intra-leaf transmission. This value is consistent with values of MLC transmission published in the literature[58,59]. The new MLC transmission value was determined by recalculating the RadCalc doses for each I'mRT phantom plan, and determining the average percentage difference between the RadCalc dose and the measured dose. An MLC transmission of 2.4% was found to give optimal agreement between RadCalc and the measured data. This increased transmission may compensate for inter-leaf transmission or other MLC effects, which are not accounted for by RadCalc's calculation algorithm. To illustrate this improvement, the scatter plots shown in Figure 5-2 and Figure 5-3 were recreated with the new data, as shown in Figure 5-4 and Figure 5-5.

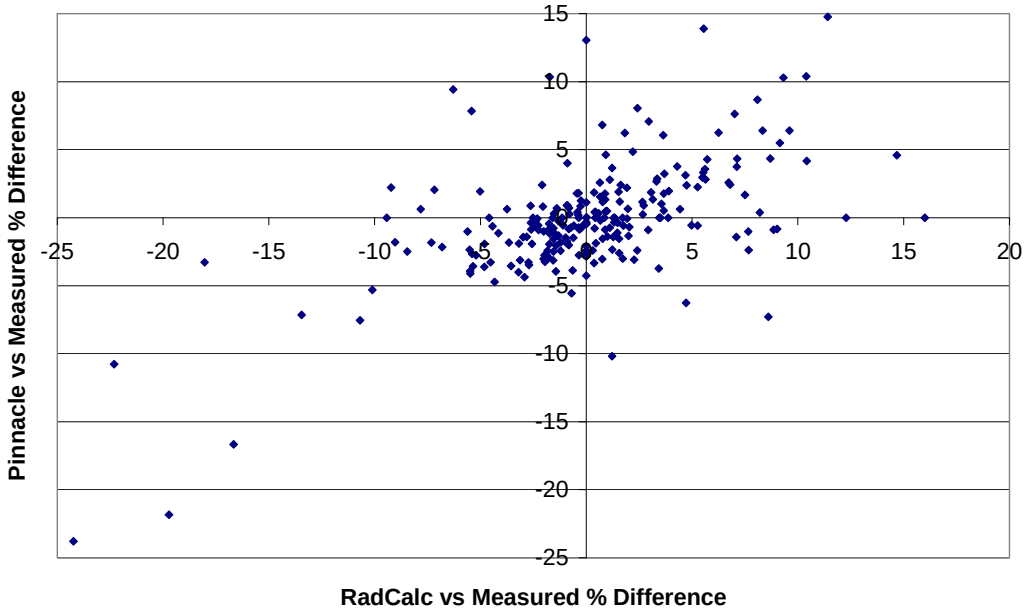

Figure 5-4. Scatter plot of percentage difference in dose per field between RadCalc and ion chamber measurement, versus Pinnacle and ion chamber measurement, for I'mRT phantom plans with MLC transmission increased to %2.4.

The new average percentage difference per field between RadCalc and measured dose the I'mRT phantom plans was 0.1% with a standard deviation 5.3%. This is comparable to the agreement between Pinnacle[3] and measure dose. Although greater than the physically measured value, the increased MLC transmission compensates for RadCalc's under-prediction of dose for IMRT fields, resulting in better agreement with the measured data.

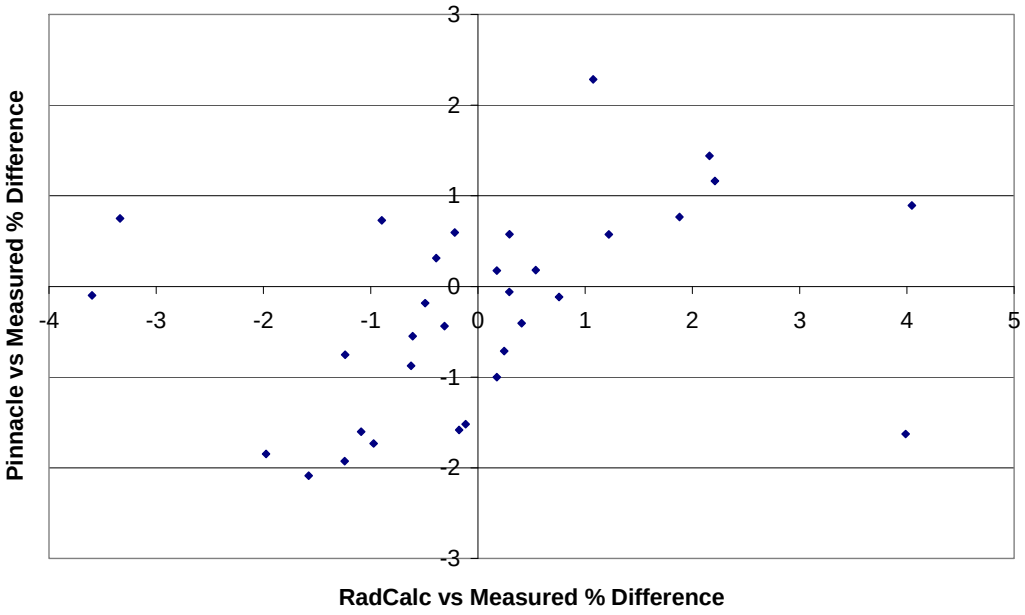

Figure 5-5. Scatter plot of percentage difference in total treatment dose between RadCalc and ion chamber measurement versus Pinnacle and ion chamber measurement, for I'mRT phantom plans with MLC transmission increased to %2.4.

The new average percentage difference per plan for the I'mRT phantom plans between RadCalc and measured dose was 0.0% with a standard deviation 1.7%. All RadCalc doses were within ±4% of the measured dose.

While the adjustment in MLC transmission has resulted in an improvement in the agreement between RadCalc and measured dose, as with the previous graphs, the new scatter plots show no obvious correlation between the RadCalc vs Measured and Pinnacle vs Measured datasets. While for 22 out of the 32 plans, the RadCalc and Pinnacle[3] results agree to within ±1%, larger differences occurred for the remaining 10 plans. Plans 4, 7, 8 and 24 in particular show large differences.

5.5 Effect of MLC Blocking

The relationship between the level of blocking per beam and the agreement between RadCalc dose and measured dose was investigated. As step and shoot IMRT fields use multiple segments of non-uniform shapes, each of which may or may not cover the calculation point, it is difficult to determine a direct measure of the level of blocking for a given field. Instead, an indirect indication may be determined by calculating the delivered dose divided by the monitor units for a given field. If a beam requires a large number of monitor units to deliver a relatively low dose, then it can be assumed that the field is heavily blocked, and therefore, the accuracy of the MU calculation will be heavily dependent on the algorithm's ability to account for MLC blocking effects. The fields from each of the phantom plans were sorted by dose per monitor unit (divided by the TMR for each beam to remove any dependence on calculation point depth). These fields were then placed in bins, and the standard deviation of the percentage difference per field between RadCalc dose and measured dose was calculated. The data is plotted in Figure 5-6.

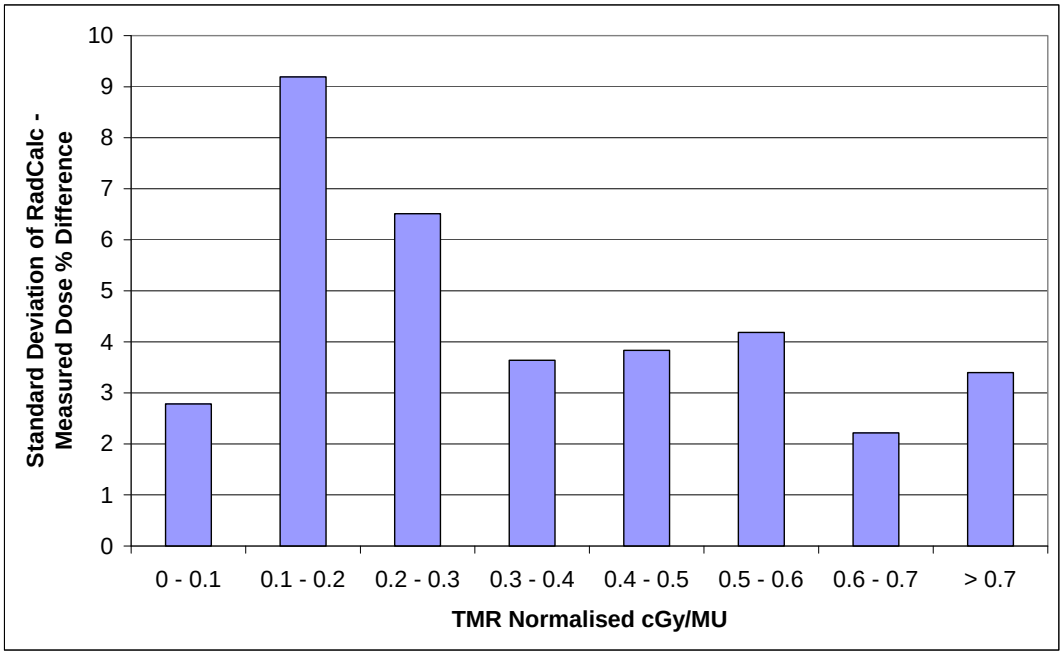

Figure 5-6. Graph of the standard deviation of the percentage difference per field between RadCalc and measured dose against dose delivered per monitor unit (normalised by TMR) for IMRT phantom plans.

Figure 5-6 shows a noticeable trend that, with the exception of the 0-0.1 cGy/MU bin, for fields with low dose per MU, indicating a high level of blocking, the standard deviation of the percentage difference between RadCalc and measured dose is greater than for fields with higher dose per monitor unit. This is consistent with the results from the segmented test field measurements in Chapter 4. The low value for the 0-0.1cGy/MU bin is due to the fact that there were only three fields in this category, resulting in unreliable statistics.

5.6 IMRT Patient Plan Results

Up to this point, doses calculated by RadCalc have been compared to ion chamber measurements as benchmarking tests. In routine clinical use, RadCalc would be used to check IMRT plans created on Pinnacle[3] for patient CT datasets by comparing the dose or MUs from RadCalc to those from Pinnacle[3], the same as for routine conformal radiotherapy plans. For the same group of 32 patients used in the previous sections, the patient CT dataset plans were exported to RadCalc. Doses for these plans were calculated and compared to the planned dose. Appendix B contains the full data for all 32 patients. A scatter plot of the percentage difference per field between the RadCalc calculated dose and the Pinnacle[3] calculated dose is shown in Figure 5-7, demonstrating the agreement between RadCalc and Pinnacle[3] for the IMRT patient plans.

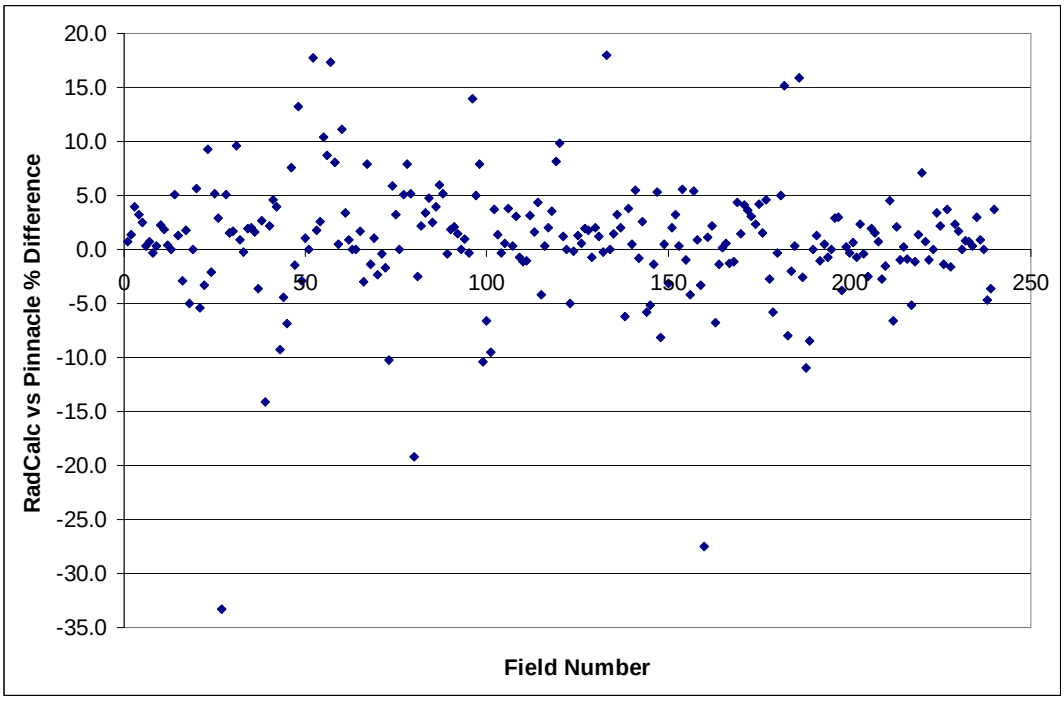

Figure 5-7. Scatter plot of percentage difference in dose per field between RadCalc and Pinnacle for plans created on patient CT datasets, with MLC transmission increased to %2.4.

As shown in Figure 5-7, the agreement between RadCalc and Pinnacle[3] dose for the patient plans is similar to the agreement between RadCalc and measured dose as seen in Figure 5-4. The average percentage difference per field between RadCalc and Pinnacle was 0.8% with a standard deviation of 5.6%. For most of the fields, the percentage

difference is within ±10%. However, there are several outlying points. A contributing factor to these differences may be the significant difference in the two dose calculation algorithms. RadCalc is not a 3D dose calculation algorithm and cannot adequately correct for changes in scatter conditions due to surface curvatures and tissue inhomogeneities. Also, as discussed previously, RadCalc has difficulty in accurately calculating dose for heavily blocked fields, which would contribute to the large differences seen in Figure 5-7.

The main criteria used to judge whether a plan is suitable is the agreement between RadCalc and Pinnacle[3] for the total treatment dose. A scatter plot of the percentage difference per plan between the RadCalc calculated dose and the Pinnacle[3] calculated dose is shown in Figure 5-8.

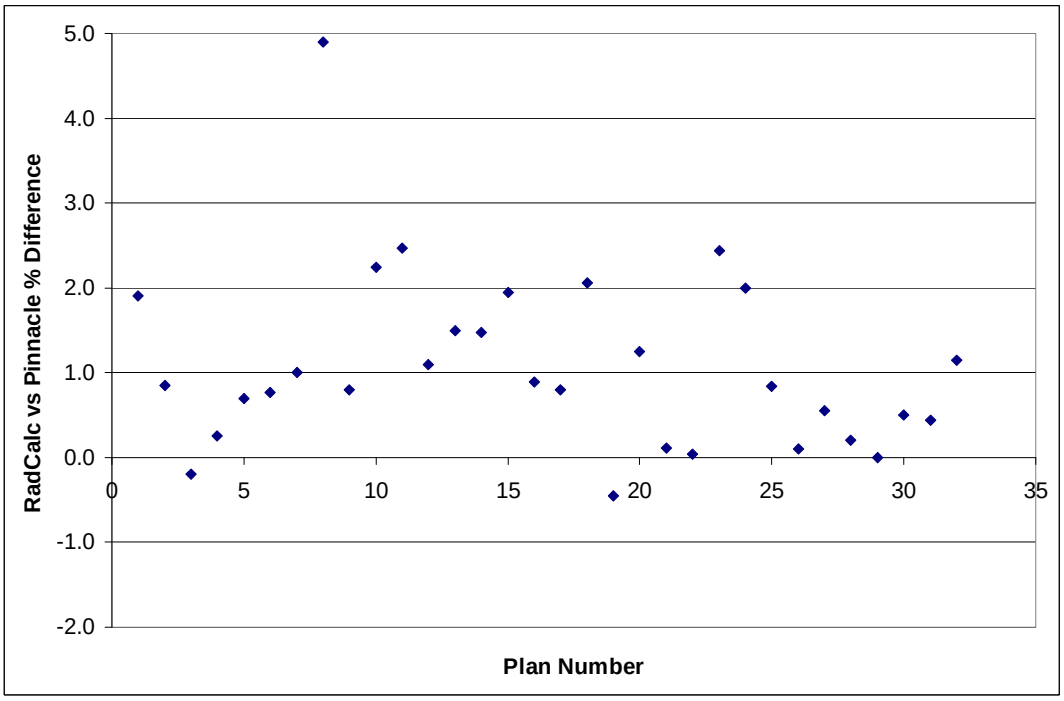

Figure 5-8. Scatter plot of percentage difference in total treatment dose between RadCalc and Pinnacle for plans created on patient CT datasets, with MLC transmission increased to %2.4.

For all but one plan, RadCalc shows good agreement with Pinnacle[3] for total treatment dose. The one outlying point was further investigated, and the large difference was due to a low density tissue inhomogeneity in close proximity to the calculation point. In practice, this plan would be investigated and the dose recalculated at a more suitable

calculation point. The average percentage difference per plan was 1.1% with a standard deviation of 1.1%. As with the percentage differences per field, RadCalc systematically overestimates dose compared to Pinnacle[3] for total treatment dose. This is most likely due to a combination of effects. Many head and neck IMRT plans involve steep surface curvatures. As shown in section 4.2, RadCalc calculates dose to within ±1% of measured dose for fields with oblique incidence less than 45 degrees. However, steeper angles of incidence can occur in clinical situations, and may not be accounted for by RadCalc. In addition to this, many head and neck plans involve tissue inhomogeneities. Calculation points are often placed close to low density structures such as cavities in the nose, mouth or throat. RadCalc only uses an equivalent path length correction in its IMRT calculation. As stated in section 2.1, the equivalent path length method only takes into account changes in the attenuation of the primary beam, without accounting for changes in scatter conditions or the position of the calculation point relative to the inhomogeneity. Therefore it will tend to overestimate dose to the calculation point in these cases, as the reduction in dose due to a lack of scatter from low density inhomogeneities as well as lateral electron disequilibrium will not be accounted for. Convolution models, on the other hand, account for both of these effects in their dose calculations[60].

5.7 Conclusions

The doses for 32 IMRT plans created on Pinnacle[3] were calculated using the RadCalc software, and measured on the I'mRT phantom. The data showed a systematic difference between RadCalc and measured dose, which was rectified by adjusting the MLC transmission parameter in RadCalc. While the percentage difference between RadCalc and measured dose, and RadCalc and Pinnacle[3] calculated dose, showed a wide variation for individual fields, the variation for total treatment dose was much less. For the plans created using the I'mRT phantom dataset, the average percentage difference per plan was 0.0% between RadCalc and measured dose with a standard deviation of 1.7%, compared to the average percentage difference between Pinnacle[3] and measured dose of -0.3% with a standard deviation of 1.1%. For the plans created using patient CT data sets, the average percentage difference per plan between RadCalc and Pinnacle[3] calculated dose was 1.1% with a standard deviation of 1.1%.

In section 2.3, a difference of less than 4% between planned dose and dose calculated by independent calculation was proposed as being acceptable in light of the recommendations of Ezzell et al[41]. If a 4% action level was set for RadCalc IMRT calculations, then from the data comparing RadCalc and Pinnacle[3] doses for patient plans, only 1 of the 32 patient plans would have failed and required further investigation. With a mean percentage difference of 1.1% and a standard deviation of 1.1% for total plan dose, the expected percentage of plans outside the action level would be less than 5%. Therefore, RadCalc could be used routinely for IMRT plan verification.

A relationship exists between the level of blocking and the distribution of the percentage difference between RadCalc and measured dose. Since RadCalc showed better agreement with measured dose for fields with low blocking, it would perform best for treatments requiring a low number of segments per beam. A small systematic difference between RadCalc and Pinnacle was also observed due to surface curvature and tissue inhomogeneity effects, which are not fully accounted for by RadCalc's equivalent path length correction. It should be noted that head and neck cases often present the greatest challenges in IMRT planning. The PTVs are often complicated, requiring asymmetric fields, off-axis calculation points and a large number of beam

angles and segments per beam. Therefore, it is probable that RadCalc would perform better in situations such as IMRT for the pelvis where the beam arrangements would generally be simpler, with central axis calculation points and fewer segments per beam.

If RadCalc is to be used routinely as a quality assurance tool for independent verification of IMRT plans, care must be taken to provide it with the required data, perform the setup correctly and carry out testing to ensure it is working properly. If this is not done, the agreement between RadCalc and measured dose would be different to that given in this thesis.

While RadCalc is capable of performing an independent check of IMRT treatment plans, it is not capable of verifying IMRT treatment delivery. As stated by Ezzell et al[41], there are 3 elements that need to be verified for each IMRT plan: dose and MU calculation, information transfer from planning system to record and verify system to delivery system, and treatment delivery. RadCalc can ensure that the treatment planning system has calculated dose correctly, but it cannot verify the information transfer to the record and verify system and delivery system or that the treatment will be delivered correctly on the linac. Correct delivery of an IMRT plan requires precise MLC positional accuracy and control of the dose rate. Therefore, at present a separate treatment delivery check is required. As stated in Ezzell et al[41] "In principle, independent dose calculations could include information derived from the delivery itself, such as from electronic portal imaging device measurements or MLC log files, but such methods are still under development.".

The final recommendation is that RadCalc is accurate enough to routinely check IMRT plan calculations. For plans outside the ±4% action level, the plan should be further investigated. If appropriate, the calculation point can be repositioned and the calculation repeated. If unacceptable differences still occur, an ion chamber phantom measurement may be performed. It is also recommended that the RadCalc check should be used in conjunction with a further test to verify data transfer and treatment delivery. At ICCC, this is currently performed by ion chamber, film, and occasionally EPID measurements.

References

[1] Tracey EA, Chen S, Baker D, Bishop J, Jelfs, P. "Cancer in NSW. Incidence and Mortality 2004." Cancer Institute NSW, 2006.

[2] Australian Institute of Health and Welfare 2006, "Australia's Health 2006".

[3] Cancer Institute NSW, "NSW Cancer Plan 2007-2010", 2006.

[4] Cancer Institute NSW, "NSW Cancer Services Review: A Discussion Paper", 2005.

[5] AAPM Report No. 46 "Comprehensive QA for Radiation Oncology".

[6] IAEA-TECDOC-896 "Radiation dose in radiotherapy from prescription to delivery".

[7] IAEA, "Investigation of an accidental exposure of radiotherapy patients in Panama", Report of a Team of Experts, 26 May–1 June 2001.

[8] A Boyer, L Xing, C M Ma, "Theoretical considerations of monitor unit calculations for intensity modulated beam treatment planning", Med. Phys., 26 (2), 187-195, 1999.

[9] F M Khan, "The physics of Radiation Therapy", Lippincott Williams & Wilkins, 1984.

[10] A Ahnesjö, "Analytical modelling of photon scatter from flattening filters in photon therapy beams", Med. Phys., 21 (8), (1994).

[11] F M Khan, W Sewchand, J Lee, and J F Williamson, "Revision of tissue-maximum ratio and scatter-maximum ratio concepts for cobalt-60 and higher energy x-ray beams", Med. Phys., 7, 1980.

[12] J J M. van Gasteren, S Heukelom, H J van Kleffens, R van der Laarse, J L M Venselaar and C F Westermann, "The determination of phantom and collimator scatter components of the output of megavoltage photon beams: measurement of the collimator scatter part with a beam-coaxial narrow cylindrical phantom", Radiother. and Onc., 20, 1991.

[13] J Milan, R E Bentley, "The storage and manipulation of radiation dose data in a small digital computer" Br. J. Radiol., 45, 1974.

[14] H F Batho, "Lung corrections in cobalt 60 beam therapy", J. Can. Assn. Radiol., 1964.

[15] M R Sontag, J R Cunningham, "Corrections to absorbed dose calculations for tissue inhomogeneities", Med. Phys., 1977.

[16] W Tang, F M Khan and B J Gerbi, "Validity of lung correction algorithms", Med. Phys., 13 (5), 683-686, 1986.

[17] IAEA Educational Reports Series, "Review of Radiation Oncology Physics: A Handbook for Teachers and Students", E. Podgorsak, May 2003.

[18] J Clarkson, "A note on depth doses in fields of irregular shape", Brit. J. Radiol. **14**, 265 (1941).

[19] H E Johns, J R Cunningham , "The Physics of Radiology", Springfield, IL:Charles C Thomas, 1969.

[20] J R Cunningham, "Scatter-air ratios", Phys. Med. Biol., 1972.

[21] P Metcalfe, T Kron, P Hoban, "The Physics of Radiotherapy X-rays", Medical Physics Publishing, 1997.

[22] T R Mackie, J W Scrimger and J J Battista, "A convolution method of calculating dose for 15-MVx rays", Med. Phys., 12, 1985.

[23] A L Boyer and E C Mok,. "Calculation of photon beam dose distributions in an inhomogeneous medium using convolutions" Med. Phys., 13, 1986.

[24] R Mohan, C Chui, L Lidofsky, "Differential pencil beam dose computation model for photons", Med. Phys., 13, 1986.

[25] A Ahnesjö, "Collapsed Cone Convolution of Radiant Energy for Photon Dose Calculation in Heterogeneous Media", Med. Phys., 16 (4), 577-592, 1989.

[26] G Hounsfield, "Computerised transverse axial scanning (tomography): Part 1 description of the system." Br. J. Radiol., 46, 1016-1022, 1973.

[27] J J Battista and M J Bronskill, "Compton scatter imaging of transverse sections: an overall appraisal and evaluation for radiotherapy planning", Phys. Med. Biol., 26 (1), 81-99, 1981.

[28] E C McCullough and T W Holmes, "Acceptance testing computerized radiation therapy treatment planning systems: Direct utilization of CT scan data", Med. Phys., 12 (2), 237-242, 1985.

[29] Seco J, Evans P M, "Assessing the effect of electron density in photon dose calculations", Med Phys, 33 (2), 540-552, 2006.

[30] Pinnacle^3, "Pinnacle^3 Physics – Instructions for use", release 7.4, 2004

[31] http://www.cirsinc.com

[32] P Metcalfe, T Kron, P Hoban, "The Physics of Radiotherapy X-Rays From Linear Accelerators", Medical Physics Publishing, 1997.

[33] T McNutt, "The ADAC Pinnacle^3 Collapsed Cone Convolution Superposition Dose Model", http://www.medical.philips.com.

[34] A Ahnesjö, A Trepp, S Richter, "Photon Beam Characterization for 3D Treatment Planning Dose Calculations", Poster presented at American Association of Physicists in Medicine 31st annual meeting, Memphis, Tennessee, 1989.

[35] P E Metcalfe, P W Hoban, D C Murray, W H Round, "Beam hardening of 10MV radiotherapy x-rays: analysis using a convolution/superposition method", Phys. Med. Biol., 35, 1990.

[36] T R Mackie, A F Bielajew, D W O Rogers, J J Battista, "Generation of Photon Energy Deposition Kernels Using the EGS Monte Carlo Code", Phys. Med. Biol., 33, 1-20, 1988.

[37] A Ahnesjö and M M Aspradakis, "Dose Calculations for External Photon Beams in Radiotherapy", Phys. Med. Biol., 44, 1999.

[38] R L Siddon, "Fast calculation of the exact radiological path for a three-dimensional CT array", Med. Phys., 12, 1985.

[39] P Keall and P Hoban, "Accounting for primary electron scatter in x-ray beam convolution calculations", Med. Phys., 22 (9), 1413-1418, 1995.

[40] P Keall and P Hoban, "Superposition dose calculation incorporating Monte Carlo generated track kernels", Med. Phys., 23 (4), 479-485, 1996.

[41] G Ezzell, J Galvin, D Low, J Palta, I Rosen, M Sharpe, P Xia, Y Xiao, L Xing and C Yu, "AAPM Report No. 82: Guidance document on delivery, treatment planning, and clinical implementation of IMRT: Report of the IMRT subcommittee of the AAPM radiation therapy committee", Med. Phys., 30 (8), 2089-2115, 2003.

[42] J Löf, H Rehbinder, T McNutt and S Johnson, "P3IMRT - Inverse planning optimization", Pinnacle^3 White Paper, www.medical.philips.com.

[43] P3IMRT - Instructions for use, Release 2.0.

[44] Y Wu, D. Yan, M B Sharpe, B Miller and J W Wong, "Implementing multiple static field delivery for intensity modulated beams." Med. Phys., 28 (11), 2188-97, 2001.

[45] D M Shepard, M. A. Earl, X A Li, S Nagvi and C Yu, "Direct aperture optimization: a turnkey solution for step-and-shoot IMRT." Med. Phys., 29 (6), 1007-18, 2002.

[46] Department of Health "Radiotherapy - Prescription and treatment sheets for NSW Health radiation therapy facilities", document number PD2006_039, 2006.

[47] K. M. Ayyangar, P. S. Nizin, C. B. Saw, D. Gearheart, B. Shen, and C. A. Enke, ''Independent dose calculations for the CORVUS MLC IMRT,'' Med. Dosim., 26 (2), 2001.

[48] J Fan, J Li, L Chen, S Stathakis, W Luo, F Du Plessis, W Xiong, J Yang and C-M Ma, " A practical Monte Carlo MU verification tool for IMRT quality assurance", Phys. Med. Biol., 51, 2503-2525, 2006.

[49] J H Kung, G T Y Chen and F K Kuchnir, "A monitor unit verification calculation in intensity modulated radiotherapy as a dosimetry quality assurance", Med. Phys., 27 (10), 2226-2230, 2000.

[50] C Chui and R Mohan, "Off centre ratios for three-dimensional dose calculations", Med. Phys., 13 (3), 409-412, 1986.

[51] C Chui, R Mohan, D Fontenla, "Dose computations for asymmetric fields defined by independent jaws", Med. Phys., 15 (1), 92-95, 1988.

[52] P Nizin, G Qian and H Rashid, ""Zero-field" dose data for ^{60}Co and other higher-energy photon beams in water", Med. Phys., 20 (5), 1353-1360, 1993.

[53] S Kim, J Palta and T Zhu, "A generalized solution for the calculation of in-air output factors in irregular fields", Med. Phys., 25 (9), 1692-1701, 1998.

[54] IEC 1217, "Radiotherapy Equipment. Coordinates, movements and scales", 1996.

[55] P Cadman, R Bassalow, N Sidhu, G Ibbott and A Nelson, "Dosimetric considerations for validation of a sequential IMRT process with a commercial treatment planning system", Phys. Med. Biol., 47, 3001-3010, 2002.

[56] P Vial, L Oliver, P Greer and C Baldock, "An experimental investigation into the radiation field offset of a dynamic multileaf collimator", Phys. Med. Biol., 51, 5517-5538, 2006.

[57] C Martins, C De Wagter and W De Neve, "The value of the Pinpoint ion chamber for characterization of small field segments used in intensity-modulated radiotherapy", Phys. Med. Biol., 45, 2519-2530, 2000.

[58] E E Klein, W B Harms, D A Low, V Willcut and J A Purdy, "Clinical implementation of a commercial multileaf collimator: dosimetry, networking, simulation and quality assurance", Int. J. Rad. Onc. Biol. Phys., 33 (5), 1195-1208, 1995.

[59] M R Arnfield, J V Siebers, J O Kim, Q Wu, P J Keall, R Mohan, "A method for determining multileaf collimator transmission and scatter for dynamic intensity modulated radiotherapy", Med. Phys., 27 (10), 2231-2241, 2000.

[60] AAPM Report No. 85 "Tissue inhomogeneity corrections for megavoltage photon beams", 2004.

Appendix A: Segment shapes

1. 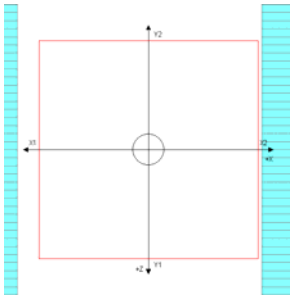

2. 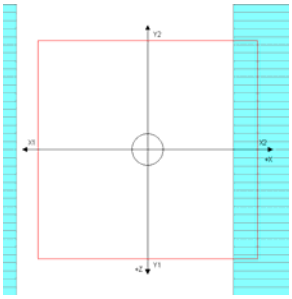

3. 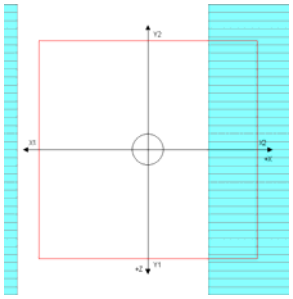

4. 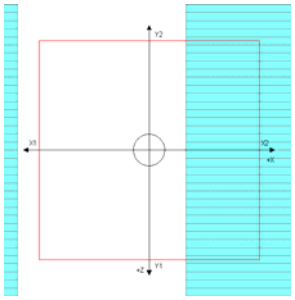

5. 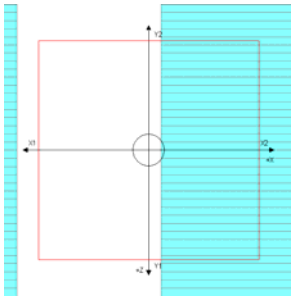

6. 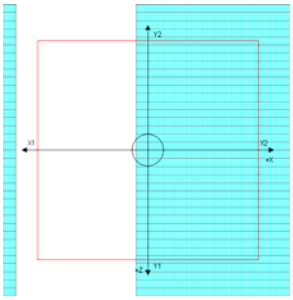

7. 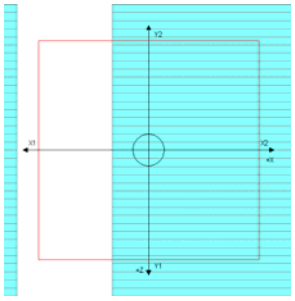

8. 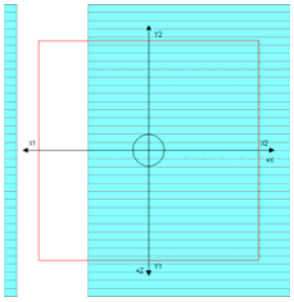

9. 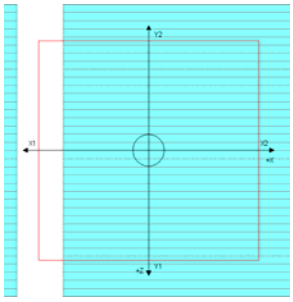

10. 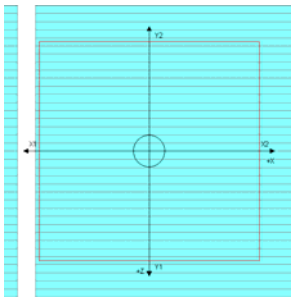

Figure A-1. Field (a): Step wedge

1. 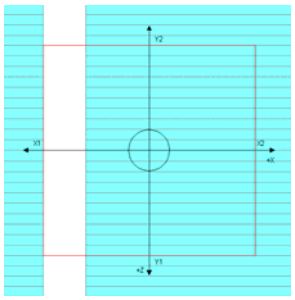 2. 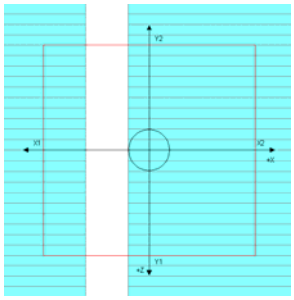 3. 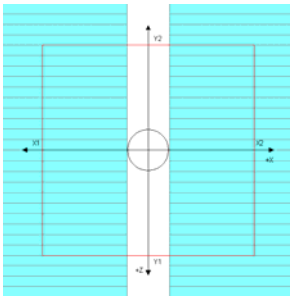

4. 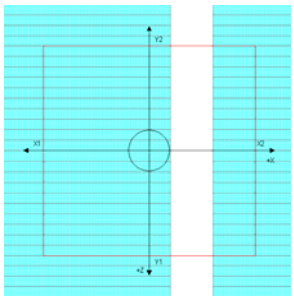 5. 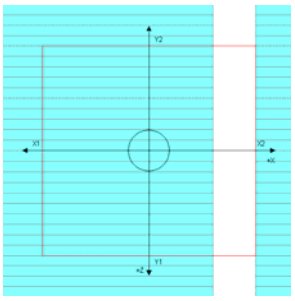

Figure A-2. Field (b): 2cm gaps

1. 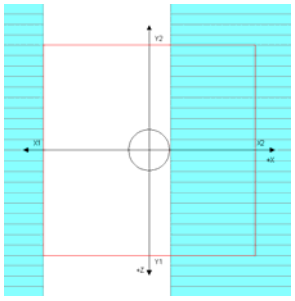 2. 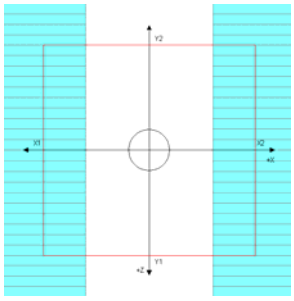 3. 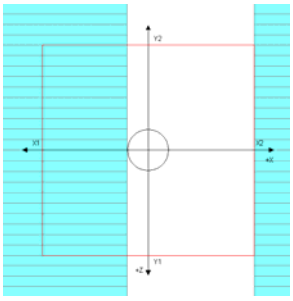

Figure A-3. Field (c): 1D pyramid

1. 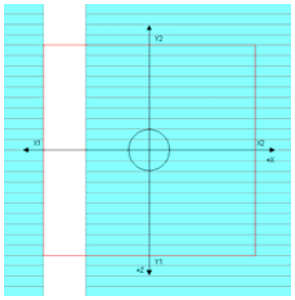 2. 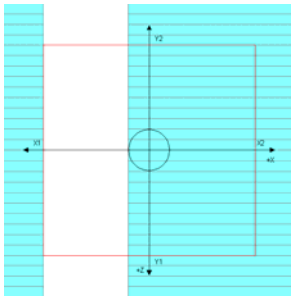 3. 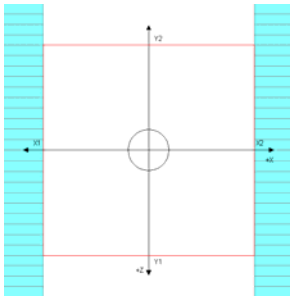

4. 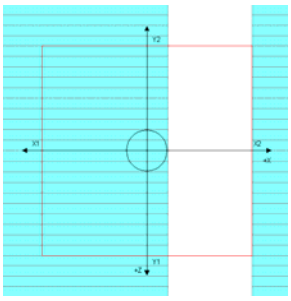 5. 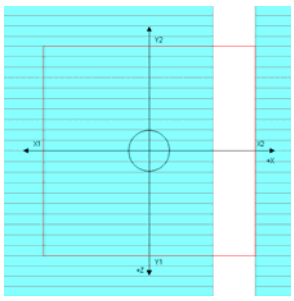

Figure A-4. Field (d): 1D inverse pyramid

1. 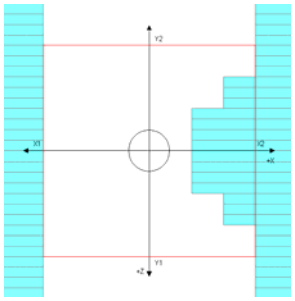 2. 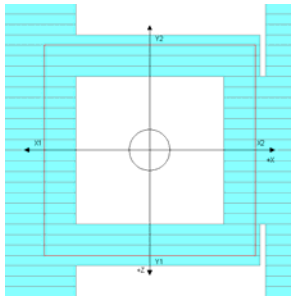 3. 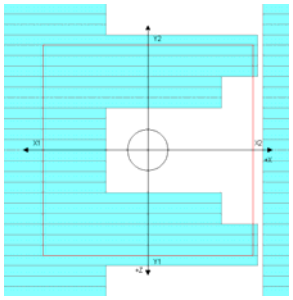

Figure A-5. Field (e): 2D pyramid

1. 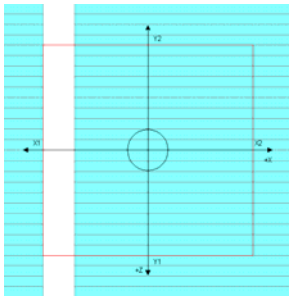
2. 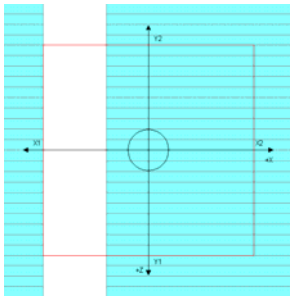
3. 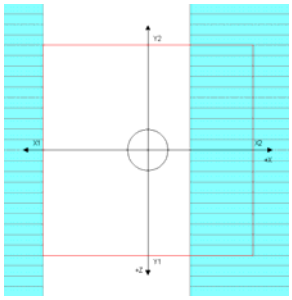
4. 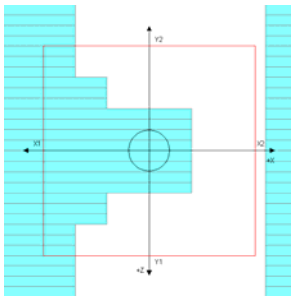
5. 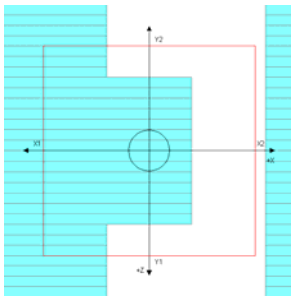
6. 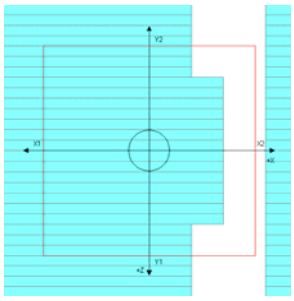

Figure A-6. Field (f): 2D inverse pyramid

Appendix B: IMRT Patient Data

Plan 1

Table B-1. Phantom plan

Beam Name	MU	Measured Dose (cGy)	RadCalc Dose (cGy)	Pinnacle Dose (cGy)	RadCalc vs Measured % Difference	Pinnacle vs Measured % Difference
0	98	29.5	30.9	30.2	4.7	2.4
120	74	19.9	19.5	19.7	-2.0	-1.0
250	96	20.4	22.3	22.5	9.3	10.3
310	110	22.5	22.7	22.8	0.9	1.3
35	153	25.6	26.6	26.1	3.9	2.0
75	85	15.4	15.1	14.9	-1.9	-3.2
90	142	22.7	17.2	17.3	-24.2	-23.8
	Total	156	154.3	153.5	-1.1	-1.6

Table B-2. Patient Plan

Beam Name	MU	Pinnacle Dose (cGy)	RadCalc Dose (cGy)	% Difference
250	96	28.3	28.5	0.7
310	110	28.4	28.8	1.4
0	98	32.9	34.2	4.0
35	153	31.3	32.3	3.2
75	85	24.0	24.6	2.5
90	142	27.9	28.0	0.4
120	74	26.9	27.1	0.7
	Total	199.7	203.5	1.9

Plan 2

Table B-3. Phantom plan

Beam Name	MU	Measured Dose (cGy)	RadCalc Dose (cGy)	Pinnacle Dose (cGy)	RadCalc vs Measured % Difference	Pinnacle vs Measured % Difference
50	122	22.5	22.3	23.4	-0.9	4.0
25	74	28.7	28.3	28.9	-1.4	0.7
345	53	34.1	33.9	33.9	-0.6	-0.6
330	67	29.8	30.2	29.8	1.3	0.0
110	48	16.5	17.1	17.5	3.6	6.1
250	59	17.3	18.7	18.8	8.1	8.7
	Total	148.9	150.5	152.3	1.1	2.3

Table B-4. Patient Plan

Beam Name	MU	Pinnacle Dose (cGy)	RadCalc Dose (cGy)	% Difference
50	122	33.5	33.4	-0.3
25	74	34.7	34.8	0.3
345	53	39.8	40.7	2.3
330	67	37.1	37.8	1.9
110	48	26.6	26.7	0.4
250	59	28.4	28.4	0.0
	Total	200.1	201.8	0.8

Plan 3

Table B-5. Phantom plan

Beam Name	MU	Measured Dose (cGy)	RadCalc Dose (cGy)	Pinnacle Dose (cGy)	RadCalc vs Measured % Difference	Pinnacle vs Measured % Difference
195	130	15.1	16.4	14	8.6	-7.3
255	102	16.4	15.8	16.1	-3.7	-1.8
290	138	17.5	17.5	17	0.0	-2.9
330	78	25.5	25.6	25.3	0.4	-0.8
0	70	14.9	16.6	17.1	11.4	14.8
30	90	22.2	21.7	22	-2.3	-0.9
70	132	18.8	16.9	17.8	-10.1	-5.3
110	109	13.2	13.3	14.1	0.8	6.8
165	163	28.4	29.5	28.4	3.9	0.0
	Total	172	173.3	171.8	0.8	-0.1

Table B-6. Patient Plan

Beam Name	MU	Pinnacle Dose (cGy)	RadCalc Dose (cGy)	% Difference
195	130	17.8	18.7	5.1
255	102	23.5	23.8	1.3
290	138	20.7	20.1	-2.9
330	78	22.9	23.3	1.7
0	69	18.0	17.1	-5.0
30	90	26.8	26.8	0.0
70	132	24.9	26.3	5.6
110	108	18.4	17.4	-5.4
165	161	27.3	26.4	-3.3
	Total	200.3	199.9	-0.2

Plan 4

Table B-7. Phantom plan

Beam Name	MU	Measured Dose (cGy)	RadCalc Dose (cGy)	Pinnacle Dose (cGy)	RadCalc vs Measured % Difference	Pinnacle vs Measured % Difference
bst 220	146	20.8	20.3	20.2	-2.4	-2.9
bst 260	85	16.2	15.4	16.1	-4.9	-0.6
bst 290	76	18.1	17.2	17.5	-5.0	-3.3
bst 330	103	17.1	15.5	15.9	-9.4	-7.0
bst 0	74	3.8	3.8	4.1	0.0	7.9
bst 30	129	16	15.6	15.9	-2.5	-0.6
bst 70	77	23.2	22.5	22.9	-3.0	-1.3
bst 100	96	16.9	17.4	17.6	3.0	4.1
bst140	169	20.7	15.0	17.7	-27.5	-14.5
	Total	152.8	142.7	147.9	-6.6	-3.2

Table B-8. Patient Plan

Beam Name	MU	Pinnacle Dose (cGy)	RadCalc Dose (cGy)	% Difference
bst 220	146	17.3	18.9	9.2
bst 260	85	24.2	23.7	-2.1
bst 290	76	25.3	26.6	5.1
bst 330	103	20.7	21.3	2.9
bst 0	33	17.4	11.6	-33.3
bst 30	129	5.9	6.2	5.1
bst 70	77	39.6	40.2	1.5
bst 100	96	29.4	29.9	1.7
bst140	168	19.8	21.7	9.6
	Total	199.6	200.1	0.3

Plan 5

Table B-9. Phantom plan

Beam Name	MU	Measured Dose (cGy)	RadCalc Dose (cGy)	Pinnacle Dose (cGy)	RadCalc vs Measured % Difference	Pinnacle vs Measured % Difference
160	111	21.8	21.6	21.4	-0.9	-1.8
60	136	25.4	24.9	24.7	-2.0	-2.8
30	85	21.9	21.7	22.1	-0.9	0.9
0	90	23.2	23.4	23.2	0.9	0.0
325	114	25.3	25.7	25.6	1.6	1.2
300	168	19.6	18.5	19.4	-5.6	-1.0
200	165	26.9	27.3	26.8	1.5	-0.4
	Total	164.1	163.1	163.2	-0.6	-0.5

Table B-10. Patient Plan

Beam Name	MU	Pinnacle Dose (cGy)	RadCalc Dose (cGy)	% Difference
160	111	23.5	23.7	0.9
60	136	37.7	37.6	-0.3
30	85	25.6	26.1	2.0
0	90	25.3	25.8	2.0
325	114	30.6	31.1	1.6
300	167	27.8	26.8	-3.6
200	165	29.9	30.7	2.7
	Total	200.4	201.8	0.7

Plan 6

Table B-11. Phantom plan

Beam Name	MU	Measured Dose (cGy)	RadCalc Dose (cGy)	Pinnacle Dose (cGy)	RadCalc vs Measured % Difference	Pinnacle vs Measured % Difference
230	128	15.9	14.9	17.4	-6.3	9.4
270	65	24.6	24.7	24.7	0.4	0.4
300	89	33.2	33.3	32.4	0.3	-2..4
0	111	44.4	45.7	44	2.9	-0.9
20	86	10.6	9.6	10.6	-9.4	0.0
	Total	128.7	128.2	129.1	-0.4	0.3

Table B-12. Patient Plan

Beam Name	MU	Pinnacle Dose (cGy)	RadCalc Dose (cGy)	% Difference
230	96	22.0	18.9	-14.1
270	65	45.4	46.4	2.2
300	89	54.1	56.6	4.6
0	111	50.7	52.7	3.9
20	85	10.8	9.8	-9.3
	Total	183.0	184.4	0.8

Plan 7

Table B-13. Phantom plan

Beam Name	MU	Measured Dose (cGy)	RadCalc Dose (cGy)	Pinnacle Dose (cGy)	RadCalc vs Measured % Difference	Pinnacle vs Measured % Difference
200	88	23.8	20.6	22.1	-13.4	-7.1
330	79	16.6	15.7	17.9	-5.4	7.8
170	84	19.1	18.8	18.9	-1.6	-1.0
110	62	16.4	15.2	16.1	-7.3	-1.8
85	83	17.9	17.9	18.1	0.0	1.1
40	120	33.9	34.9	36.3	2.9	7.1
280	77	19.1	18.8	18.5	-1.6	-3.1
	Total	146.8	141.9	147.9	-3.3	0.7

Table B-14. Patient Plan

Beam Name	MU	Pinnacle Dose (cGy)	RadCalc Dose (cGy)	% Difference
200	88	20.4	19.5	-4.4
280	76	29.2	27.2	-6.8
330	79	21.0	22.6	7.6
40	120	48.0	47.3	-1.5
85	82	34.8	39.4	13.2
110	62	27.5	26.7	-2.9
170	84	19.2	19.4	1.0
	Total	200.1	202.1	1.0

Plan 8

Table B-15. Phantom plan

Beam Name	MU	Measured Dose (cGy)	RadCalc Dose (cGy)	Pinnacle Dose (cGy)	RadCalc vs Measured % Difference	Pinnacle vs Measured % Difference
a200	67	5.7	6.4	5.7	12.3	0.0
b200	91	9.6	10.6	10	10.4	4.2
a290	84	11.2	11.0	11.1	-1.8	-0.9
b290	102	11.6	11.4	12.8	-1.7	10.3
a320	66	5	5.8	5	16.0	0.0
b320	75	19.2	19.5	18.7	1.6	-2.6
a0	115	10.9	12.5	11.4	14.7	4.6
b0	96	11.3	12.3	11.2	8.8	-0.9
a40	80	18.1	19.0	18	5.0	-0.6
b40	81	12.5	13.7	13.3	9.6	6.4
a70	87	11.4	11.1	11.5	-2.6	0.9
b70	100	12.2	13.3	12.1	9.0	-0.8
a160	69	16.8	15.9	16.2	-5.4	-3.6
b160	84	12.6	12.4	12.6	-1.6	0.0
	Total	168.1	174.9	169.6	4.0	0.9

Table B-16. Patient Plan

Beam Name	MU	Pinnacle Dose (cGy)	RadCalc Dose (cGy)	% Difference
a200	66	2.4	2.7	12.5
b200	91	4.2	4.2	0.0
a290	84	19.2	20.2	5.2
b290	102	19.7	20.9	6.1
a320	65	8.7	9.9	13.8
b320	75	21.6	22.4	3.7
a0	113	8.6	9.7	12.8
b0	95	9.5	10.4	9.5
a40	80	21.5	23.2	7.9
b40	79	13.1	15.3	16.8
a70	87	20.5	20.2	-1.5
b70	99	15.8	15.4	-2.5
a160	68	23.0	27.1	17.8
b160	83	11.5	13.7	19.1
	Total	199.3	215.3	8.0

Plan 9

Table B-17. Phantom plan

Beam Name	MU	Measured Dose (cGy)	RadCalc Dose (cGy)	Pinnacle Dose (cGy)	RadCalc vs Measured % Difference	Pinnacle vs Measured % Difference
180	68	29.1	29.0	28.3	-0.3	-2.7
135	54	18.1	19.1	18.7	5.5	3.3
90	94	23.2	23.6	22.5	1.7	-3.0
50	150	22.7	23.2	23.8	2.2	4.8
20	57	22.8	22.4	22.7	-1.8	-0.4
220	63	26.7	26.7	26.7	0.0	0.0
200	56	24.4	23.9	24.6	-2.0	0.8
	Total	167	167.9	167.3	0.5	0.2

Table B-18. Patient Plan

Beam Name	MU	Pinnacle Dose (cGy)	RadCalc Dose (cGy)	% Difference
180	68	29.4	29.9	1.7
135	54	16.8	16.3	-3.0
90	93	32.9	35.5	7.9
50	150	42.7	42.1	-1.4
20	57	28.6	28.9	1.0
220	63	25.3	24.7	-2.4
200	56	24.2	24.1	-0.4
	Total	199.9	201.5	0.8

Plan 10

Table B-19. Phantom plan

Beam Name	MU	Measured Dose (cGy)	RadCalc Dose (cGy)	Pinnacle Dose (cGy)	RadCalc vs Measured % Difference	Pinnacle vs Measured % Difference
a160	69	10.8	10.9	11.3	0.9	4.6
b160	56	13	10.1	11.6	-22.3	-10.8
a85	51	11.4	11.8	11.4	3.5	0.0
b85	48	8.2	8.3	8.5	1.2	3.7
a45	52	16.6	15.8	16	-4.8	-3.6
b45	77	11.3	11.4	11.5	0.9	1.8
a0	60	17.1	17.4	17	1.8	-0.6
b0	56	19.1	19.8	19.2	3.7	0.5
a330	52	2.3	2.3	2.6	0.0	13.0
b330	69	6.4	6.7	6.6	4.7	3.1
a285	79	8.1	8.1	7.9	0.0	-2.5
b285	63	8.7	9.0	8.7	3.4	0.0
a200	93	16.4	17.9	17.3	9.1	5.5
b200	56	21.8	22.0	21.9	0.9	0.5
	Total	171.2	171.5	171.5	0.2	0.2

Table B-20. Patient Plan

Beam Name	MU	Pinnacle Dose (cGy)	RadCalc Dose (cGy)	% Difference
a160	69	11.6	11.4	-1.7
b160	55	11.7	10.5	-10.3
a85	51	17.0	18.0	5.9
b85	48	12.5	12.9	3.2
a45	52	17.4	17.4	0.0
b45	77	11.9	12.5	5.0
a0	60	16.5	17.8	7.9
b0	56	19.3	20.3	5.2
a330	52	2.6	2.1	-19.2
b330	69	7.9	7.7	-2.5
a285	79	14.0	14.3	2.1
b285	63	14.8	15.3	3.4
a200	93	19.0	19.9	4.7
b200	56	24.0	24.6	2.5
	Total	200.2	204.7	2.2

Plan 11

Table B-21. Phantom plan

Beam Name	MU	Measured Dose (cGy)	RadCalc Dose (cGy)	Pinnacle Dose (cGy)	RadCalc vs Measured % Difference	Pinnacle vs Measured % Difference
200	53	21.3	22.5	21.9	5.6	2.8
280	45	12	12.9	12.2	7.5	1.7
310	76	20.5	20.5	20	0.0	-2.4
335	100	18.6	19.4	19.3	4.3	3.8
0	75	23.1	23.4	23.1	1.3	0.0
20	55	23.5	23.6	23.6	0.4	0.4
50	79	17.9	18.1	18.4	1.1	2.8
80	62	14.2	13.8	14	-2.8	-1.4
160	80	20.9	21.6	21.5	3.3	2.9
	Total	172	175.8	174	2.2	1.2

Table B-22. Patient plan

Beam Name	MU	Pinnacle Dose (cGy)	RadCalc Dose (cGy)	% Difference
200	53	22.8	23.7	3.9
280	45	23.5	24.9	6.0
310	76	29.1	30.6	5.2
335	99	24.0	23.9	-0.4
0	75	26.6	27.1	1.9
20	55	24.0	24.5	2.1
50	79	20.2	20.5	1.5
80	62	20.6	20.6	0.0
160	80	20.2	20.4	1.0
	Total	211.0	216.2	2.5

Plan 12

Table B-23. Phantom plan

Beam Name	MU	Measured Dose (cGy)	RadCalc Dose (cGy)	Pinnacle Dose (cGy)	RadCalc vs Measured % Difference	Pinnacle vs Measured % Difference
190	88	25.7	25.8	25.2	0.5	-1.9
290	112	33.9	34.2	33.6	0.9	-0.9
320	102	24.6	25.3	24.7	2.7	0.2
0	64	25.0	25.8	25.5	3.1	1.9
40	101	24.5	24.0	25.1	-2.1	2.4
70	144	22.4	22.7	21.9	1.2	-2.3
170	87	14.2	13.1	14.3	-7.8	0.6
	Total	170.4	170.9	170.3	0.3	-0.1

Table B-24. Patient plan

Beam Name	MU	Pinnacle Dose (cGy)	RadCalc Dose (cGy)	% Difference
190	88	29.7	29.6	-0.3
290	111	50.9	58.0	13.9
320	102	15.9	16.7	5.0
0	64	25.3	27.3	7.9
40	100	30.8	27.6	-10.4
70	144	40.8	38.1	-6.6
170	86	16.8	15.2	-9.5
	Total	210.2	212.5	1.1

Plan 13

Table B-25. Phantom plan

Beam Name	MU	Measured Dose (cGy)	RadCalc Dose (cGy)	Pinnacle Dose (cGy)	RadCalc vs Measured % Difference	Pinnacle vs Measured % Difference
220	107	29.8	29.8	29.7	0.0	-0.3
275	119	20.8	19.8	20.4	-4.8	-1.9
300	135	25	24.2	24	-3.2	-4.0
7	66	26.7	28.6	27.7	7.1	3.7
85	130	28	27.9	28	-0.4	0.0
160	130	39.5	39.8	38.3	0.8	-3.0
	Total	169.8	170.1	0.2	168.1	-1.0

Table B-26. Patient Plan

Beam Name	MU	Pinnacle Dose (cGy)	RadCalc Dose (cGy)	% Difference
7	66	27.0	28.0	3.7
300	135	36.2	36.7	1.4
275	119	34.3	34.2	-0.3
90	130	34.9	35.1	0.6
160	130	34.0	35.3	3.8
210	107	33.8	33.9	0.3
	Total	200.2	203.2	1.5

Plan 14

Table B-27. Phantom plan

Beam Name	MU	Measured Dose (cGy)	RadCalc Dose (cGy)	Pinnacle Dose (cGy)	RadCalc vs Measured % Difference	Pinnacle vs Measured % Difference
150	75	27.7	27.6	28.2	-0.4	1.8
118	65	19.3	19.0	19	-1.6	-1.6
90	71	15.7	15.2	15.4	-3.2	-1.9
68	77	17.3	17.0	17.1	-1.7	-1.2
30	142	27.1	27.2	27.6	0.4	1.8
0	61	27.7	27.6	27.5	-0.4	-0.7
345	58	27.2	27.6	26.9	1.5	-1.1
	Total	162.0	161.2	161.7	-0.5	-0.2

Table B-28. Patient Plan

Beam Name	MU	Pinnacle Dose (cGy)	RadCalc Dose (cGy)	% Difference
150	75	29.6	30.5	3.0
118	65	27.0	26.8	-0.7
90	71	26.8	26.5	-1.1
68	77	28.0	27.7	-1.1
30	142	34.8	35.9	3.2
0	61	31.7	32.2	1.6
345	58	32.4	33.8	4.3
	Total	210.3	213.4	1.5

Plan 15

Table B-29. Phantom plan

Beam Name	MU	Measured Dose (cGy)	RadCalc Dose (cGy)	Pinnacle Dose (cGy)	RadCalc vs Measured % Difference	Pinnacle vs Measured % Difference
200	66	20.1	18.4	19.6	-8.5	-2.5
260	48	19.7	19.0	19	-3.6	-3.6
295	61	16.4	16.1	16	-1.8	-2.4
355	47	14.4	14.3	13.6	-0.7	-5.6
0	74	17.1	18.0	17	5.3	-0.6
25	110	19.6	21.1	19.4	7.7	-1.0
65	70	24.0	24.1	24	0.4	0.0
100	34	12.9	12.7	12.8	-1.6	-0.8
160	55	16.6	15.1	16.3	-9.0	-1.8
	Total	160.8	158.8	157.7	-1.2	-1.9

Table B-30. Patient Plan

Beam Name	MU	Pinnacle Dose (cGy)	RadCalc Dose (cGy)	% Difference
200	66	19.2	18.4	-4.2
260	48	28.5	28.6	0.4
295	61	24.4	24.9	2.0
355	47	16.8	17.4	3.6
0	74	19.7	21.3	8.1
25	110	24.3	26.7	9.9
65	70	40.3	40.8	1.2
100	34	21.2	21.2	0.0
160	55	16.0	15.2	-5.0
	Total	210.4	214.5	1.9

Plan 16

Table B-31. Phantom plan

Beam Name	MU	Measured Dose (cGy)	RadCalc Dose (cGy)	Pinnacle Dose (cGy)	RadCalc vs Measured % Difference	Pinnacle vs Measured % Difference
0	98	48.4	48.2	48.6	-0.4	0.4
340	114	45.7	46.0	46.4	0.7	1.5
290	154	37.7	37.4	37.8	-0.8	0.3
200	121	53	52.8	53.1	-0.4	0.2
	Total	184.8	184.4	185.9	-0.2	0.6

Table B-32. Patient Plan

Beam Name	MU	Pinnacle Dose (cGy)	RadCalc Dose (cGy)	% Difference
0	98	57.4	57.3	-0.2
340	114	55.1	55.8	1.3
290	154	54.9	55.2	0.5
200	121	57.7	58.8	1.9
	Total	225.1	227.1	0.9

Plan 17

Table B-33. Phantom plan

Beam Name	MU	Measured Dose (cGy)	RadCalc Dose (cGy)	Pinnacle Dose (cGy)	RadCalc vs Measured % Difference	Pinnacle vs Measured % Difference
280	92	22.6	22.4	22.8	-0.9	0.9
310	90	29.5	30.1	29.3	2.0	-0.7
0	87	36.4	37.1	37.2	1.9	2.2
50	80	30.3	30.7	30.2	1.3	-0.3
80	95	20.5	20.7	20.6	1.0	0.5
	Total	139.3	141	140.1	1.2	0.6

Table B-34. Patient Plan

Beam Name	MU	Pinnacle Dose (cGy)	RadCalc Dose (cGy)	% Difference
280	92	39.8	40.5	1.8
310	90	40.7	40.4	-0.7
0	87	40.1	40.9	2.0
50	80	42.2	42.7	1.2
80	95	37.7	37.6	-0.3
	Total	200.5	202.1	0.8

Plan 18

Table B-35. Phantom plan

Beam Name	MU	Measured Dose (cGy)	RadCalc Dose (cGy)	Pinnacle Dose (cGy)	RadCalc vs Measured % Difference	Pinnacle vs Measured % Difference
200	118	15.6	16.9	16.6	8.3	6.4
290	131	26.8	26.1	26.7	-2.6	-0.4
330	131	39.4	40.8	39.8	3.6	1.0
0	125	19.5	18.1	19.9	-7.2	2.1
30	105	25.9	26.1	26.2	0.8	1.2
60	95	25.9	24.6	26.4	-5.0	1.9
160	123	25.4	24.3	24.2	-4.3	-4.7
	Total	178.5	176.9	179.8	-0.9	0.7

Table B-36. Patient Plan

Beam Name	MU	Pinnacle Dose (cGy)	RadCalc Dose (cGy)	% Difference
200	118	8.9	10.5	18.0
290	131	46.1	46.1	0.0
330	131	34.2	34.7	1.5
0	125	27.7	28.6	3.2
30	105	24.6	25.1	2.0
60	95	16.1	15.1	-6.2
160	123	41.9	43.5	3.8
	Total	199.5	203.6	2.1

Plan 19

Table B-37. Phantom plan

Beam Name	MU	Measured Dose (cGy)	RadCalc Dose (cGy)	Pinnacle Dose (cGy)	RadCalc vs Measured % Difference	Pinnacle vs Measured % Difference
250	79	18.2	18.0	18.1	-1.1	-0.5
280	80	20.6	22.0	21.1	6.8	2.4
0	86	36.2	36.1	36.5	-0.3	-0.8
40	54	27.8	27.4	26.7	-1.4	-4.0
65	65	15.9	14.2	14.7	-10.7	-7.5
90	68	12.7	12.0	12.4	-5.5	-2.4
125	96	25.5	24.1	24.5	-5.5	-3.9
	Total	156.9	153.8	154	-2.0	-1.8

Table B-38. Patient Plan

Beam Name	MU	Pinnacle Dose (cGy)	RadCalc Dose (cGy)	% Difference
250	79	20.5	20.6	0.5
280	80	25.7	27.1	5.4
0	86	35.9	35.6	-0.8
40	54	34.4	35.3	2.6
65	65	24.0	22.6	-5.8
90	68	21.3	20.2	-5.2
125	96	37.2	36.7	-1.3
	Total	199.0	198.1	-0.5

Plan 20

Table B-39. Phantom plan

Beam Name	MU	Measured Dose (cGy)	RadCalc Dose (cGy)	Pinnacle Dose (cGy)	RadCalc vs Measured % Difference	Pinnacle vs Measured % Difference
200	76	38	37.5	37.9	-1.3	-0.3
240	55	15.6	15.2	15.3	-2.6	-1.9
270	55	13.7	13.3	13.1	-2.9	-4.4
310	52	15.3	15.6	15.4	2.0	0.7
340	55	23.7	25.0	24.4	5.5	3.0
0	63	26.5	25.4	26.2	-4.2	-1.1
10	64	27	27.3	26.8	1.1	-0.7
	Total	159.8	159.3	159.1	-0.3	-0.4

Table B-40. Patient Plan

Beam Name	MU	Pinnacle Dose (cGy)	RadCalc Dose (cGy)	% Difference
200	76	37.8	39.8	5.3
240	55	12.3	11.3	-8.1
270	55	19.7	19.8	0.5
310	52	22.5	21.8	-3.1
340	55	34.9	35.6	2.0
0	63	40.2	41.5	3.2
10	64	33.0	33.1	0.3
	Total	200.4	202.9	1.2

Plan 21

Table B-41. Phantom plan

Beam Name	MU	Measured Dose (cGy)	RadCalc Dose (cGy)	Pinnacle Dose (cGy)	RadCalc vs Measured % Difference	Pinnacle vs Measured % Difference
250	70	21.47	23.0	22.4	7.1	4.3
270	79	19.66	19.5	19.8	-0.8	0.7
320	52	16.82	17.2	16.3	2.3	-3.1
0	49	29.62	30.0	29.2	1.3	-1.4
80	77	15.91	16.2	16.9	1.8	6.2
120	96	15.39	15.9	15.8	3.3	2.7
145	51	24.83	24.6	24.4	-0.9	-1.7
	Total	143.7	146.4	144.8	1.9	0.8

Table B-42. Patient Plan

Beam Name	MU	Pinnacle Dose (cGy)	RadCalc Dose (cGy)	% Difference
250	70	30.7	32.4	5.5
270	79	32.0	31.7	-0.9
320	52	14.3	13.7	-4.2
0	49	35.4	37.3	5.4
80	77	46.9	47.3	0.9
120	96	12.1	11.7	-3.3
145	51	9.1	6.6	-27.5
	Total	180.5	180.7	0.1

Plan 22

Table B-43. Phantom plan

Beam Name	MU	Measured Dose (cGy)	RadCalc Dose (cGy)	Pinnacle Dose (cGy)	RadCalc vs Measured % Difference	Pinnacle vs Measured % Difference
200	117	41.24	40.7	40.7	-1.3	-1.3
290	81	19.97	20.5	20.2	2.7	1.2
320	105	12.89	13.1	13.2	1.6	2.4
0	62	18.56	18.5	18.4	-0.3	-0.9
40	120	52.19	52.2	52.2	0.0	0.0
70	115	30.02	30.6	30	1.9	-0.1
160	149	34.02	33.8	32.7	-0.6	-3.9
	Total	208.89	209.4	207.4	0.2	-0.7

Table B-44. Patient Plan

Beam Name	MU	Pinnacle Dose (cGy)	RadCalc Dose (cGy)	% Difference
200	117	43.8	44.3	1.1
290	81	41.5	42.4	2.2
320	105	13.3	12.4	-6.8
0	62	22.0	21.7	-1.4
40	120	64.5	64.6	0.2
70	115	34.2	34.4	0.6
160	149	30.3	29.9	-1.3
	Total	249.6	249.7	0.0

Plan 23

Table B-45. Phantom plan

Beam Name	MU	Measured Dose (cGy)	RadCalc Dose (cGy)	Pinnacle Dose (cGy)	RadCalc vs Measured % Difference	Pinnacle vs Measured % Difference
b200	108	19.6	20.7	20.3	5.6	3.6
a200b	77	13.3	14.0	13.6	5.3	2.3
270	47	14.3	14.3	14	0.0	-2.1
315	89	14.2	11.4	11.1	-19.7	-21.8
a0	94	16.7	16.3	16.6	-2.4	-0.6
b0	100	11.5	12.5	12	8.7	4.3
a40	99	23	23.0	22.9	0.0	-0.4
b40	55	18.3	17.8	17.7	-2.7	-3.3
80	56	12.9	13.1	12.7	1.6	-1.6
a160	107	14	14.8	14.6	5.7	4.3
b160	77	12.8	12.4	12.4	-3.1	-3.1
	Total	170.6	170.3	167.9	-0.2	-1.6

Table B-46. Patient Plan

Beam Name	MU	Pinnacle Dose (cGy)	RadCalc Dose (cGy)	% Difference
b200	108	18.0	17.8	-1.1
a200b	77	18.3	19.1	4.4
270	47	13.9	14.1	1.4
315	89	21.7	22.6	4.1
a0	94	22.2	23.0	3.6
b0	100	16.5	17.0	3.0
a40	99	21.3	21.8	2.3
b40	55	19.2	20.0	4.2
80	56	19.6	19.9	1.5
a160	107	15.2	15.9	4.6
b160	77	14.8	14.4	-2.7
	Total	200.7	205.6	2.4

Plan 24

Table B-47. Phantom plan

Beam Name	MU	Measured Dose (cGy)	RadCalc Dose (cGy)	Pinnacle Dose (cGy)	RadCalc vs Measured % Difference	Pinnacle vs Measured % Difference
200	94	26.2	26.6	26.7	1.5	1.9
290	165	49.1	49.7	44.1	1.2	-10.2
330	159	12.5	13.8	13.8	10.4	10.4
0	119	37.8	40.7	36.9	7.7	-2.4
30	138	22.4	22.3	22.8	-0.4	1.8
60	133	16	17.0	17	6.3	6.3
160	116	14.1	15.1	13.9	7.1	-1.4
	Total	178.1	185.2	175.2	4.0	-1.6

Table B-48. Patient Plan

Beam Name	MU	Pinnacle Dose (cGy)	RadCalc Dose (cGy)	% Difference
200	94	5.2	4.9	-5.8
290	165	28.9	28.8	-0.3
330	159	34.2	35.9	5.0
0	119	31.6	36.4	15.2
30	138	13.8	12.7	-8.0
60	133	55.1	54.0	-2.0
160	116	31.3	31.4	0.3
	Total	200.1	204.1	2.0

Plan 25

Table B-49. Phantom plan

Beam Name	MU	Measured Dose (cGy)	RadCalc Dose (cGy)	Pinnacle Dose (cGy)	RadCalc vs Measured % Difference	Pinnacle vs Measured % Difference
0	290	27.1	24.6	27.7	-9.2	2.2
280	76	18.8	18.8	18	0.0	-4.3
310	89	25.6	27.7	25.7	8.2	0.4
50	89	32.1	33.2	30.9	3.4	-3.7
80	73	15	15.3	14.8	2.0	-1.3
150	109	32.3	30.1	31.6	-6.8	-2.2
210	130	33.9	33.3	32.9	-1.8	-2.9
	Total	184.8	183	181.6	-1.0	-1.7

Table B-50. Patient Plan

Beam Name	MU	Pinnacle Dose (cGy)	RadCalc Dose (cGy)	% Difference
0	290	33.3	38.6	15.9
280	76	27.3	26.6	-2.6
310	89	16.4	14.6	-11.0
50	89	15.3	14.0	-8.5
80	73	23.3	23.3	0.0
150	109	37.6	38.1	1.3
210	130	36.8	36.4	-1.1
	Total	190.0	191.6	0.8

Plan 26

Table B-51. Phantom plan

Beam Name	MU	Measured Dose (cGy)	RadCalc Dose (cGy)	Pinnacle Dose (cGy)	RadCalc vs Measured % Difference	Pinnacle vs Measured % Difference
215	131	40	39.9	40.5	-0.3	1.3
290	95	24.9	25.5	24.3	2.4	-2.4
315	82	20.75	20.6	20.6	-0.7	-0.7
0	247	17.77	18.2	19.2	2.4	8.0
45	81	15.82	16.4	16.1	3.7	1.8
70	95	20.36	19.3	19.8	-5.2	-2.8
145	102	37.48	37.7	37.6	0.6	0.3
	Total	177.08	177.6	178.1	0.3	0.6

Table B-52. Patient Plan

Beam Name	MU	Pinnacle Dose (cGy)	RadCalc Dose (cGy)	% Difference
215	131	39.0	39.2	0.5
290	95	28.7	28.5	-0.7
315	82	26.4	26.4	0.0
0	247	20.4	21.0	2.9
45	81	20.3	20.9	3.0
70	95	29.0	27.9	-3.8
145	102	36.4	36.5	0.3
	Total	200.2	200.4	0.1

Plan 27

Table B-53. Phantom plan

Beam Name	MU	Measured Dose (cGy)	RadCalc Dose (cGy)	Pinnacle Dose (cGy)	RadCalc vs Measured % Difference	Pinnacle vs Measured % Difference
0	113	47.4	49.5	47.7	4.4	0.6
330	93	44.53	43.5	44.5	-2.3	-0.1
280	53	24.09	23.0	23.3	-4.5	-3.3
260	38	21.88	20.7	21.3	-5.4	-2.7
200	49	21.09	21.3	20.8	1.0	-1.4
	Total	158.99	158	157.6	-0.6	-0.9

Table B-54. Patient Plan

Beam Name	MU	Pinnacle Dose (cGy)	RadCalc Dose (cGy)	% Difference
200	49	29.7	29.6	-0.3
260	38	31.2	31.4	0.6
280	53	28.9	28.7	-0.7
330	93	60.8	62.2	2.3
0	113	49.2	49.0	-0.4
	Total	199.8	200.9	0.6

Plan 28

Table B-55. Phantom plan

Beam Name	MU	Measured Dose (cGy)	RadCalc Dose (cGy)	Pinnacle Dose (cGy)	RadCalc vs Measured % Difference	Pinnacle vs Measured % Difference
0	91	36.76	36.2	36.87	-1.5	0.3
30	66	33.38	33.3	33.126	-0.2	-0.8
80	47	18.25	18.1	17.88	-0.8	-2.0
100	51	19.82	19.8	19.726	-0.1	-0.5
160	59	30.508	29.6	30.07	-3.0	-1.4
	Total	138.718	137	137.672	-1.2	-0.8

Table B-56. Patient Plan

Beam Name	MU	Pinnacle Dose (cGy)	RadCalc Dose (cGy)	% Difference
0	91	44.4	43.3	-2.5
30	66	57.7	58.8	1.9
80	47	39.5	40.1	1.5
100	51	39.9	40.2	0.8
160	59	18.5	18.0	-2.7
	Total	200.0	200.4	0.2

Plan 29

Table B-57. Phantom plan

Beam Name	MU	Measured Dose (cGy)	RadCalc Dose (cGy)	Pinnacle Dose (cGy)	RadCalc vs Measured % Difference	Pinnacle vs Measured % Difference
0	93	38.6	41.2	39.6	6.7	2.6
30	126	24	22.9	24	-4.6	0.0
60	92	15.8	15.1	15.7	-4.4	-0.6
90	72	22.1	22.7	22.3	2.7	0.9
110	91	21.7	22.5	22.4	3.7	3.2
170	108	44.5	45.9	45.1	3.1	1.3
	Total	166.7	170.3	2.2	2.2	1.4

Table B-58. Patient Plan

Beam Name	MU	Pinnacle Dose (cGy)	RadCalc Dose (cGy)	% Difference
0	93	44.7	44.0	-1.6
30	126	35.6	37.2	4.5
60	92	24.1	22.5	-6.6
90	72	43.3	44.2	2.1
110	91	29.8	29.5	-1.0
170	108	42.2	42.3	0.2
	Total	219.7	219.7	0.0

Plan 30

Table B-59. Phantom plan

Beam Name	MU	Measured Dose (cGy)	RadCalc Dose (cGy)	Pinnacle Dose (cGy)	RadCalc vs Measured % Difference	Pinnacle vs Measured % Difference
20	107	27.47	27.1	27.1	-1.3	-1.3
60	76	21.33	21.0	20.8	-1.5	-2.5
85	106	18.93	19.0	18.3	0.4	-3.3
155	130	34.27	34.5	34.2	0.7	-0.2
180	182	32.27	31.5	32.2	-2.4	-0.2
205	114	16.13	15.9	15.8	-1.4	-2..0
275	69	11.47	11.4	11.3	-0.6	-1.5
300	93	15.47	16.2	14.5	4.7	-6.3
340	134	29.2	29.7	29.2	1.7	0.0
	Total	206.54	206.3	203.4	-0.1	-1.5

Table B-60. Patient Plan

Beam Name	MU	Pinnacle Dose (cGy)	RadCalc Dose (cGy)	% Difference
20	107	34.7	34.4	-0.9
60	76	31.2	29.6	-5.1
85	106	26.4	26.1	-1.1
155	130	29.6	30.0	1.4
180	182	26.7	28.6	7.1
205	114	13.7	13.8	0.7
275	69	20.7	20.5	-1.0
300	93	21.5	21.5	0.0
340	134	35.5	36.7	3.4
	Total	240.0	241.2	0.5

Plan 31

Table B-61. Phantom plan

Beam Name	MU	Measured Dose (cGy)	RadCalc Dose (cGy)	Pinnacle Dose (cGy)	RadCalc vs Measured % Difference	Pinnacle vs Measured % Difference
30	81	33.3	32.9	32.7	-1.2	-1.8
82	135	25.9	25.2	25	-2.7	-3.5
140	71	24.3	24.1	24.1	-0.8	-0.8
180	143	35.7	35.7	34.7	0.0	-2.8
210	83	32.8	35.1	35.3	7.0	7.6
275	65	7.3	6.9	7	-5.5	-4.1
310	31	12.9	13.0	12.7	0.8	-1.6
	Total	172.2	172.9	171.5	0.4	-0.4

Table B-62. Patient Plan

Beam Name	MU	Pinnacle Dose (cGy)	RadCalc Dose (cGy)	% Difference
30	81	36.1	36.9	2.2
82	135	58.7	57.9	-1.4
140	71	27.0	28.0	3.7
180	143	42.6	41.9	-1.6
210	83	21.4	21.9	2.3
275	65	6.0	6.1	1.7
310	31	10.9	10.9	0.0
	Total	202.7	203.6	0.4

Plan 32

Table B-63. Phantom plan

Beam Name	MU	Measured Dose (cGy)	RadCalc Dose (cGy)	Pinnacle Dose (cGy)	RadCalc vs Measured % Difference	Pinnacle vs Measured % Difference
180	64	28.6	28.1	28.3	-1.7	-1.0
195	20	10.7	10.6	10.5	-0.9	-1.9
275	75	19.8	19.4	19.2	-2.0	-3.0
300	77	24.7	24.4	24.1	-1.2	-2.4
340	110	51.5	50.6	50.5	-1.7	-1.39
20	4	2.4	2.0	2	-16.7	-16.7
60	21	7.5	7.5	7.3	0.0	-2.7
85	57	10.8	10.6	10.5	-1.9	-2.8
155	70	21.3	21.3	21.2	0.0	-0.5
	Total	177.3	174.5	173.6	-1.6	-2.1

Table B-64. Patient Plan

Beam Name	MU	Pinnacle Dose (cGy)	RadCalc Dose (cGy)	% Difference
180	64	36.9	37.2	0.8
195	20	13.6	13.7	0.7
275	75	29.0	29.1	0.3
300	77	33.3	34.3	3.0
340	110	43.5	43.9	0.9
20	4	1.4	1.4	0.0
60	21	4.3	4.1	-4.7
85	57	11.1	10.7	-3.6
155	70	27.0	28.0	3.7
	Total	200.1	202.4	1.1

Appendix C: IMRT phantom measurement reproducibility and precision data

Table C-1. Charge readings given in nC for each beam angle for an IMRT plan delivered five times consecutively, without shifting the phantom. Also shown is the total charge for each plan, a charge reading for a standard field, the mean charge reading, the standard deviation and the percentage error.

	Beam Angle								
	30	82	140	180	210	275	310	Total	Std
Measurement 1 (nC)	1.235	0.94	0.935	1.295	1.33	0.26	0.465	6.46	3.78
Measurement 2 (nC)	1.245	0.93	0.94	1.315	1.335	0.255	0.465	6.485	3.78
Measurement 3 (nC)	1.235	0.93	0.93	1.315	1.34	0.255	0.46	6.465	3.78
Measurement 4 (nC)	1.24	0.935	0.935	1.3	1.335	0.25	0.455	6.45	3.78
Measurement 5 (nC)	1.24	0.93	0.935	1.3	1.33	0.255	0.465	6.455	3.775
Mean (nC)	1.239	0.933	0.935	1.305	1.334	0.255	0.462	6.463	
Std Dev (nC)	0.0042	0.0045	0.0035	0.0094	0.0042	0.0035	0.0045	0.0135	
Std Dev (%)	0.3	0.5	0.4	0.7	0.3	1.4	1.0	0.2	

Table C-2. Charge readings given in nC for each beam angle for an IMRT plan delivered five times consecutively, where the phantom was moved and repositioned between measurements. Also shown is the total charge for each plan, a charge reading for a standard field, the mean charge reading, the standard deviation and the percentage error.

	Beam Angle								
	30	82	140	180	210	275	310	Total	Std
Measurement 1 (nC)	1.23	0.935	0.925	1.3	1.305	0.26	0.48	6.435	3.77
Measurement 2 (nC)	1.24	0.94	0.91	1.295	1.305	0.26	0.48	6.43	3.77
Measurement 3 (nC)	1.23	0.935	0.915	1.31	1.31	0.255	0.465	6.42	3.775
Measurement 4 (nC)	1.23	0.935	0.905	1.3	1.325	0.255	0.47	6.42	3.77
Measurement 5 (nC)	1.23	0.935	0.91	1.305	1.3	0.255	0.47	6.405	3.765
Mean (nC)	1.232	0.936	0.913	1.302	1.309	0.257	0.473	6.422	
Std Dev (nC)	0.0045	0.0022	0.0076	0.0057	0.0096	0.0027	0.0067	0.0115	
Std Dev (%)	0.4	0.2	0.8	0.4	0.7	1.1	1.4	0.2	